Measurement and Analysis of Pressure Profile for Nozzle Based Single Screw Extrusion Systems

A Thesis Presented for the

Master of Science

Degree

The University of Tennessee, Knoxville

Jake Fielder Dvorak
December 2020

To Meredith and everyone who supports me

ACKNOWLEDGMENTS

Many persons were key in the completion of this work. Dr. Chad Duty, my research advisor, provided invaluable suggestions and methods when needed the most. His perspective was key in outlining this pursuit for me and keeping me on the right path. Dr. Young, Dr. Compton, and Dr. Kunc all provided key insight into tying this work together and ensuring its ability to move into future work.

My lab mates, Tyler Smith and Christine Ajinjeru were key in supporting experimental efforts on the BAAM and answering questions I had along the way. Eli Charles and Carson Helton, both undergraduate research assistants in Dr. Duty's lab, made the vast experimental efforts on the Microtruder possible. Without them I am certain the results of this work would be nowhere near as comprehensive. Their willingness to learn and process data was refreshing.

Thank you to the Manufacturing Demonstration Facility at Oak Ridge National Lab, sponsored by the US Department of Energy, for providing the BAAM system for testing.

Many peoples at the Manufacturing Demonstration Facility were key in getting this work started, John Lindahl, Seokpum Kim, Christopher Hershey, and Vidya Kishore, all provided key information for properly characterizing the BAAM system and other suggestions for methods and theory. Alan Franc at Techmer PM was of extreme help in manufacturing and providing all materials for this work.

ABSTRACT

Most large-scale material-extrusion (MatEx) AM systems utilize a single screw extruder. Simulating flow rate and operating pressures of extrusion systems is notoriously difficult without resorting to full finite element analysis due to the phase change and non-Newtonian nature of relevant polymers. This study characterized two machines of interest: a Big Area Additive Manufacturing (BAAM) system and a Randcastle Microtruder. A custom nozzle adapter was fabricated to gather pressure data within the nozzle and mimic the die design of the BAAM on the Microtruder system. Several theories were tested for overall machine output and max pressure. Feed and compression zone theories were added to generate a pressure map throughout the system. The data was related to theory to observe extrusion, screw, and machine issues. Overall, this work provides and tests theory for simulating single screw extruder output and pressure throughout the system.

TABLE OF CONTENTS

CHAPTER 1: INTRODUCTION 1

1.1 MOTIVATION 1

1.2 SINGLE SCREW EXTRUSION 1

1.3 RESEARCH APPROACH 4

CHAPTER 2: SYSTEMS AND MATERIALS 5

2.1 MACHINE INTRODUCTION 5

2.2 BIG AREA ADDITIVE MANUFACTURING 5

2.3 RANDCASTLE MICROTRUDER 7

2.4 BUILT-IN SENSORS 7

2.5 ADDITIONAL NOZZLE SENSORS 7

2.6 MATERIALS AND MATERIAL PROPERTIES 11

2.7 TEMPERATURE PROFILES 16

CHAPTER 3: ANALYTICAL APPROACH TO PRESSURE PROFILE 19

3.1 INTRODUCTION 19

3.2 MODIFIED NEWTONIAN MODEL FOR THE METERING ZONE 19

3.3 THE FEED ZONE 22

3.4 THE COMPRESSION ZONE – FOUR ZONE MODEL 24

3.5 HAGEN-POISEUILLE PRESSURE FLOW 29

CHAPTER 4: EXPERIMENTAL APPROACH TO PRESSURE PROFILE 31

4.1 INTRODUCTION 31

4.2 DAQ SYSTEM AND MELT PRESSURE SENSOR 31

4.3 BAAM Experimental Procedure 32
4.4 Microtruder Experimental Procedure 34
4.5 BAAM Experimental Results & Discussion 36
4.6 Microtruder Experimental Results & Discussion 36
4.7 BAAM Experimental Results Compared to Analytical Model 42
4.8 Microtruder Experimental Results Compared to Analytical Model 46
CHAPTER 5: SUMMARY AND CONCLUSIONS 54
5.1 Summary of Research Work 54
5.2 Conclusions 54
5.3 Future Work 55
REFERENCES 56
APPENDIX 58
A1. Material Product Information 59
A2. LCR Tabulated Test Data 60
A3. Microtruder Die Constant Plots 65
A4. Microtruder Data Plots 76
A5. Microtruder Tabulated Data 97
VITA 107

LIST OF TABLES

TABLE 1: BAAM AND MICROTRUDER GEOMETRICAL CONSTANTS. 6

TABLE 2: POWER LAW PARAMETERS FOR ALL MATERIALS IN THIS STUDY. 15

TABLE 3: MATERIAL THERMAL PROPERTIES OBTAINED FROM LITERATURE (RAUWENDAAL 2014. 249). 15

TABLE 4: MELT, BULK, AND SOLID DENSITIES FOR ALL MATERIALS. 17

TABLE 5: PELLET SIZES FOR ALL MATERIALS AND MACHINE SUGGESTED PELLET SIZE LIMITS 17

TABLE 6: TEMPERATURE SETTINGS FOR ALL MATERIALS AND BOTH MACHINES 18

TABLE 7: PRINT SPEEDS FOR ALL RPMS TESTED. 33

TABLE 8: SCOPE OF TESTS COMPLETED ON THE MICROTRUDER SYSTEM. 35

LIST OF FIGURES

FIGURE 1: DIAGRAM OF A TYPICAL SINGLE SCREW EXTRUDER SYSTEM (CAMPBELL AND SPALDING 2013, 2). 2

FIGURE 2: STANDARD SCREW ZONES (CAMPBELL AND SPALDING 2013, 7). 3

FIGURE 3: RELEVANT SCREW GEOMETRY AND COORDINATE SYSTEM (CAMPBELL AND SPALDING 2013, 8). 3

FIGURE 4: BAAM SYSTEM AT THE MANUFACTURING DEMONSTRATION FACILITY. PHOTO COURTESY OF OAK RIDGE NATIONAL LABORATORY, US DEPT. OF ENERGY. 6

FIGURE 5: MICROTRUDER SETUP AND CONTROL SYSTEM (LEFT) AND MICROTRUDER SECTIONED VIEW WITH NOTABLE FEATURES (RIGHT) ("WHAT IS A MICROTRUDER?" 2020). 8

FIGURE 6: SCREW PRESSURE SENSOR IN MICROTRUDER CIRCLED IN RED. 9

FIGURE 7: SCREW PRESSURE SENSOR IN BAAM END CAP CIRCLED IN RED. 9

FIGURE 8: NEW NOZZLE ADAPTER AND PRESSURE SENSOR ATTACHED TO BAAM END CAP. 10

FIGURE 9: NEW NOZZLE ADAPTER WITHOUT PRESSURE SENSOR AND DIE BLOCK ATTACHED TO THE MICROTRUDER. 10

FIGURE 10: SCHEMATIC OF PRESSURE SENSOR MOUNTING PORT ("TRANSDUCER MOUNTING HOLE MACHINING TOOL KIT MANUAL" 2020). 12

FIGURE 11: SECTIONED VIEW OF MICROTRUDER THROAT, DIE BLOCK, NOZZLE ADAPTER, AND NOZZLE. 12

FIGURE 12: DYNISCO LCR 7000 USED TO OBTAIN THE POWER LAW PARAMETERS. 13

FIGURE 13: FORCES ON POLYMER IN THE FEED ZONE (CAMPBELL AND SPALDING 2013, 708). 23

FIGURE 14: CROSS SECTION OF RESIN IN COMPRESSION ZONE FROM A SOLIDIFICATION EXPERIMENT (CAMPBELL AND SPALDING 2013, 193). 25

FIGURE 15: CROSS SECTION OF RESIN IN COMPRESSION ZONE AXIALLY DOWN THE COMPRESSION ZONE (CAMPBELL AND SPALDING 2013, 197). 25
FIGURE 16: SCHEMATIC OF FOUR ZONE MELTING MODEL (CAMPBELL AND SPALDING 2013, 204). 27
FIGURE 17: SCHEMATIC OF SOLID BED WIDTH (TOP) AND HEIGHT (BOTTOM) DOWN THE COMPRESSION CHANNEL (CAMPBELL AND SPALDING 2013, 210). 27
FIGURE 18: BAAM PRINTING SINGLE BEADS FOR EXPERIMENT. PHOTO COURTESY OF OAK RIDGE NATIONAL LABORATORY, US DEPT. OF ENERGY. 33
FIGURE 19: PRESSURE DATA FROM NOZZLE SENSOR FOR ONE BEAD OF CF-ABS AT 50 RPM. 34
FIGURE 20: SAMPLE DATA FOR SCREW PRESSURE WITH CF PLA, 0.1" NOZZLE AT 110 RPM. 35
FIGURE 21: MASS FLOW RATE RESULTS FOR BAAM TESTING FOR CF ABS AT ALL NOZZLE SIZES AND RPMS..... 37
FIGURE 22: NOZZLE PRESSURE RESULTS FOR BAAM TESTING FOR CF ABS AT ALL NOZZLE SIZES AND RPMS..... 37
FIGURE 23: SCREW PRESSURE RESULTS FOR BAAM TESTING FOR CF ABS AT ALL NOZZLE SIZES AND RPMS..... 38
FIGURE 24: MASS FLOW RATE RESULTS FOR MICROTRUDER TESTING FOR ALL MATERIALS AND NOZZLE SIZES AT 70 RPM. 39
FIGURE 25: SCREW PRESSURE RESULTS FOR LLDPE ON MICROTRUDER SYSTEM AT ALL NOZZLE SIZES. 39
FIGURE 26: SCREW PRESSURE RESULTS FOR PLA ON MICROTRUDER SYSTEM AT ALL NOZZLE SIZES. 40
FIGURE 27: SCREW PRESSURE RESULTS FOR CF-PLA ON MICROTRUDER SYSTEM AT ALL NOZZLE SIZES. 40

FIGURE 28: SCREW AND NOZZLE PRESSURE RESULTS FOR ABS ON MICROTRUDER SYSTEM AT ALL NOZZLE SIZES. 41
FIGURE 29: SCREW AND NOZZLE PRESSURE RESULTS FOR CF-ABS ON MICROTRUDER SYSTEM AT ALL NOZZLE SIZES. 41
FIGURE 30: DIE CONSTANTS FROM BAAM 0.2 NOZZLE TESTS. 43
FIGURE 31: DIE CONSTANTS FROM BAAM 0.3 NOZZLE TESTS. 43
FIGURE 32: DIE CONSTANTS FROM BAAM 0.4 NOZZLE TESTS. 44
FIGURE 33: FLOW RATE AND PRESSURE RESULTS FOR BAAM 0.2 NOZZLE TESTS AND CODE. 44
FIGURE 34: FLOW RATE AND PRESSURE RESULTS FOR BAAM 0.3 NOZZLE TESTS AND CODE. 45
FIGURE 35: FLOW RATE AND PRESSURE RESULTS FOR BAAM 0.4 NOZZLE TESTS AND CODE. 45
FIGURE 36: PRESSURE MAP RESULTS FOR BAAM 0.2 NOZZLE. 47
FIGURE 37: PRESSURE MAP RESULTS FOR BAAM 0.3 NOZZLE. 47
FIGURE 38: PRESSURE MAP RESULTS FOR BAAM 0.4 NOZZLE. 48
FIGURE 39: DIE CONSTANTS FOR CF-ABS MICROTRUDER 0.1 NOZZLE TESTS. 48
FIGURE 40: FLOW RATE AND PRESSURE RESULTS FOR MICROTRUDER 0.1 NOZZLE AND CF-ABS TESTS AND CODE. 49
FIGURE 41: FLOW RATE AND PRESSURE RESULTS FOR MICROTRUDER 0.15 NOZZLE AND CF-ABS TESTS AND CODE. 49
FIGURE 42: FLOW RATE AND PRESSURE RESULTS FOR MICROTRUDER 0.2 NOZZLE AND CF-ABS TESTS AND CODE. 50
FIGURE 43: FLOW RATE AND PRESSURE RESULTS FOR MICROTRUDER 0.25 NOZZLE AND CF-ABS TESTS AND CODE. 50

FIGURE 44: FLOW RATE AND PRESSURE RESULTS FOR MICROTRUDER 0.1 NOZZLE AND ABS TESTS AND CODE. 51
FIGURE 45: FLOW RATE AND PRESSURE RESULTS FOR MICROTRUDER 0.1 NOZZLE AND LLDPE TESTS AND CODE. 51
FIGURE 46: FLOW RATE AND PRESSURE RESULTS FOR MICROTRUDER 0.1 NOZZLE AND CF-PLA TESTS AND CODE. 52
FIGURE 47: FLOW RATE AND PRESSURE RESULTS FOR MICROTRUDER 0.1 NOZZLE AND PLA TESTS AND CODE. 52

Chapter 1: Introduction

1.1 Motivation

Extrusion systems are notoriously difficult to model and troubleshoot (Campbell and Spalding 2013; Vlachopoulos and Wagner 2001). The extrusion process includes a phase change, rotational and pressure flow, complex geometry, and Non-Newtonian flow. To simulate extrusion without resorting to costly finite element analysis, many assumptions must be made. This work explores several assumptions for the varying theories in the extrusion process and compares them to physical data from multiple machines, materials, nozzle sizes, and print settings. The BAAM was of primary interest for this study, as the ability to simulate pressures and output have large potential for future studies and supporting the large scope of research surrounding the system. The simulations provide preliminary information for testing of new materials, screw geometries, and machine settings. Ultimately, this work leads to more accurate print parameters, testing of new materials and settings computationally, and built a base simulation code for expansion from future research.

1.2 Single Screw Extrusion

Single screw extruders have become increasingly common in industry over the past several decades (Campbell and Spalding 2013, 1). Single screw extruders share several characteristics that will be explained and studied individually: the screw, the barrel, a motor-drive system, and control systems for heaters and the motor speed (Figure 1). In the case of machines used in this study, the extruders are gravity fed pellets via the hopper into the feed section. The screw contains

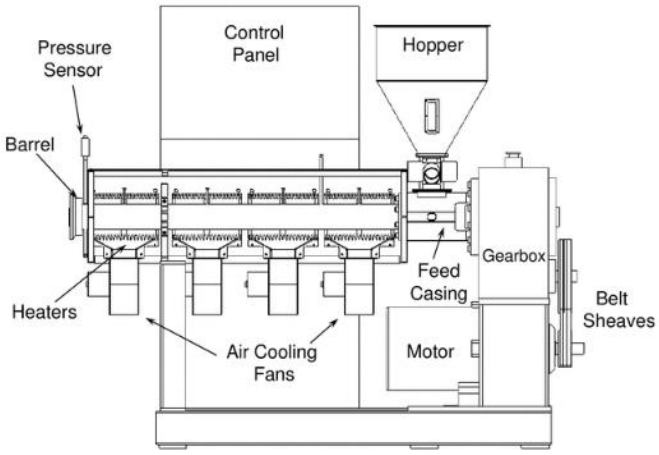

Figure 1: Diagram of a typical single screw extruder system (Campbell and Spalding 2013, 2).

three characteristics zones: the feed zone where pellets are brought together but not melted, the compression zone where the solid bed is melted and compressed, and the metering zone where the melt is pressurized and pushed through any systems after the screw, typically, a die. A diagram of a standard screw is shown in Figure 2.

Due to the physical complexity of a screw, its geometry is broken down further. The flight and channel of a screw is helical and is typically unwound to simplify calculations (Middleman 1977, 125). All screws utilized in this study were single flighted. There is a small clearance between the flights of the screw and the barrel that allow molten polymer to flow between flights and center the screw (Campbell and Spalding 2013, 7). Several geometrical constants are identified in Figure 3: lead length, L, screw diameter, D, barrel diameter, D_b, flight width, e, and channel depth, H. For the coordinate system, x is the direction perpendicular to the flights, y is normal to the barrel surface, and z is in the down-channel direction. Typically, the channel depth is constant in the feed zone, decreasing in the compression zone, and constant in the metering zone. Channel depth and core diameter, D_c, are related in Equation 1.

$$D_c = D_b - 2H \qquad Eq.(1)$$

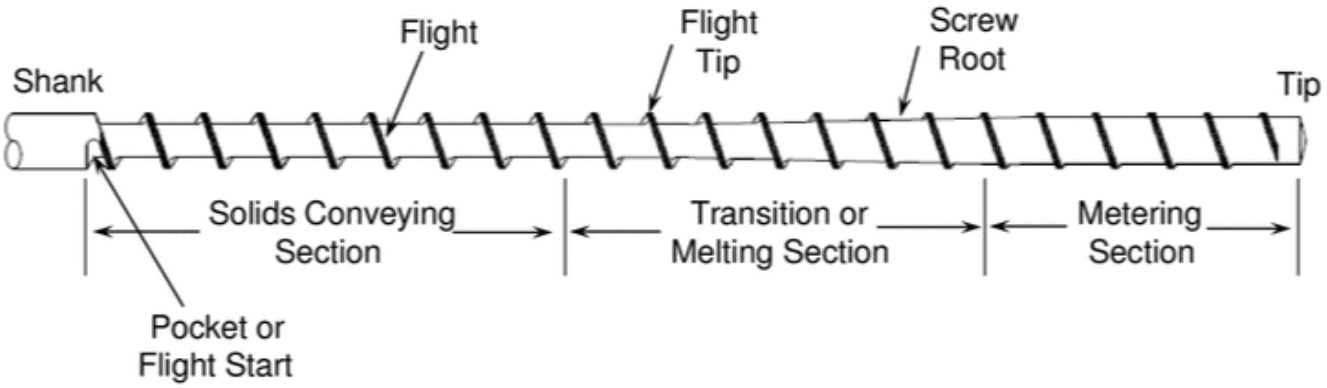

Figure 2: Standard screw zones (Campbell and Spalding 2013, 7).

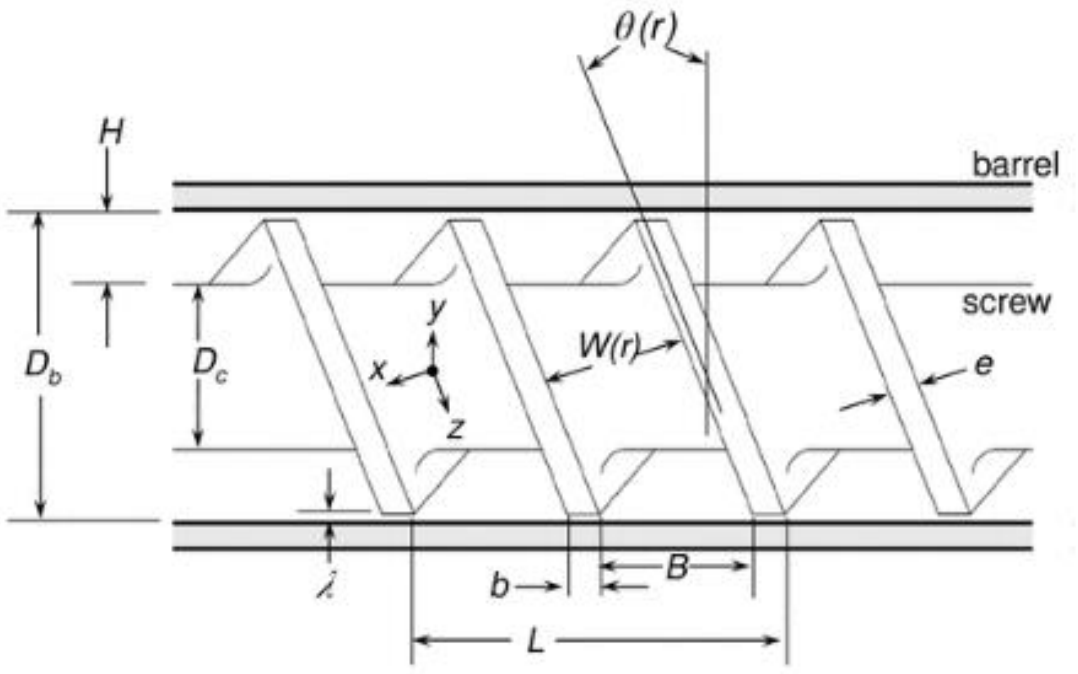

Figure 3: Relevant screw geometry and coordinate system (Campbell and Spalding 2013, 8).

The helix angle, θ, and channel width, W, are both a function of the radius of the screw. As a result, they are calculated at radii of interest at the barrel and core of the screw (Equation 2 through 5).

$$\theta_b = \arctan\left(\frac{L}{\pi D_b}\right) \qquad Eq.(2)$$

$$W_b = Lcos\theta_b - e \qquad Eq.(3)$$

$$\theta_c = \arctan\left(\frac{L}{\pi D_c}\right) \qquad Eq.(4)$$

$$W_c = Lcos\theta_c - e \qquad Eq.(5)$$

1.3 Research Approach

To properly evaluate theories and code a wide range of data had to be collected that covered the entire range of practical extrusion situations. The scope of independent variables in these experiments included, but were not limited to, nozzle size, material, and zone temperatures. The primary dependent variable was RPM in each run. It was also necessary to gather data from multiple machines to better verify the theory and code.

Chapter 2: Systems and Materials

2.1 Machine Introduction

In this work, two machines were employed for study: the BAAM at the Manufacturing Demonstration Facility in Oak Ridge National Lab and a Randcastle Microtruder at University of Tennessee, Knoxville. In order to be able to differentiate characteristics between machines, they have been divided into subsections for comparison. This work has done the literature standard of separating the screw and the die as much as possible (Campbell and Spalding 2013; Middleman 1977; Tadmor and Gogos 2006). The screw used in each machine will be broken down and compared.

2.2 Big Area Additive Manufacturing

The BAAM (Figure 4) is an extrusion system that utilizes a single screw extruder, vacuum fed hopper, and gantry to support Fused Filament Fabrication (FFF) on a large scale. Because of this setup, the BAAM is inherently different from typical extrusion systems. Its orientation is entirely vertical, it starts and stops extrusion rapidly, and a wide variety of materials and screws for differing print requirements are utilized. The BAAM was originally developed by the MDF in collaboration with Cincinnati Inc. A standard style compression screw found in most extrusion systems was utilized for this work (Campbell and Spalding 2013, 8-10).

The BAAM also uniquely features a “back pressure screw” located in the end cap. This screw allows for simple adjustments of the pressure profile in the machine. For these tests the back pressure screw was left at approximately 25%.



Figure 4: BAAM system at the Manufacturing Demonstration Facility. Photo courtesy of Oak Ridge National Laboratory, US Dept. of Energy.

Table 1: Microtruder geometrical constants.

Parameter	**Microtruder (in)**
Feed zone depth	0.125
Metering zone depth	0.041
Axial length of feed zone	4
Axial length of compression zone	5.6
Axial length of metering zone	4
Barrel diameter	0.5
Screw clearance	0.003
Lead length	0.5
Flight width	0.093
Throat	0.25
Throat length	3.68
Nozzle diameter	0.1,0.15,0.2,0.25
Nozzle length	0.425
Compression ratio	3.05
Compression rate	0.006254

2.3 Randcastle Microtruder

The Microtruder (Figure 5) is a specialty system designed and built by Randcastle Extrusion Systems aimed at being able to fit a variety of industrial needs. As suggested by its name, it is one of the smallest extrusion systems widely available in terms of screw and barrel size ("What is a Microtruder?" 2020). The relevant geometrical constants for this study are shown in Table 1, including compression rate and compression ratio. Randcastle offers a variety of dies for the system, and initially came with a slit die. The machine was retrofitted with a new die like that on the BAAM system, which is discussed in detail in the Additional Nozzle Sensors section below.

2.4 Built-In Sensors

Traditionally, extruders feature a pressure sensor towards the end of the screw for measuring discharge pressure (Campbell and Spalding 2013, 14). The Microtruder features a screw pressure sensor (Figure 6), however, the BAAM's screw pressure sensor is located just below the screw, slightly into the end cap (Figure 7). These screw pressure ports were utilized in this work since discharge pressure is relevant in screw modeling (Campbell and Spalding 2013; Tadmor and Gogos 2006).

2.5 Additional Nozzle Sensors

To meet experimental demands and mimic the flow of the BAAM on the Randcastle, a custom nozzle adapter with a sensor port was designed and constructed for both machines as shown in Figures 8 and 9. This nozzle adapter added the ability to rapidly change nozzle tip sizes and obtain pressure in the throat as close to the nozzle tip as feasibly possible. The nozzle adapters and tips were constructed out of brass due to its easy to machine nature and superior thermal



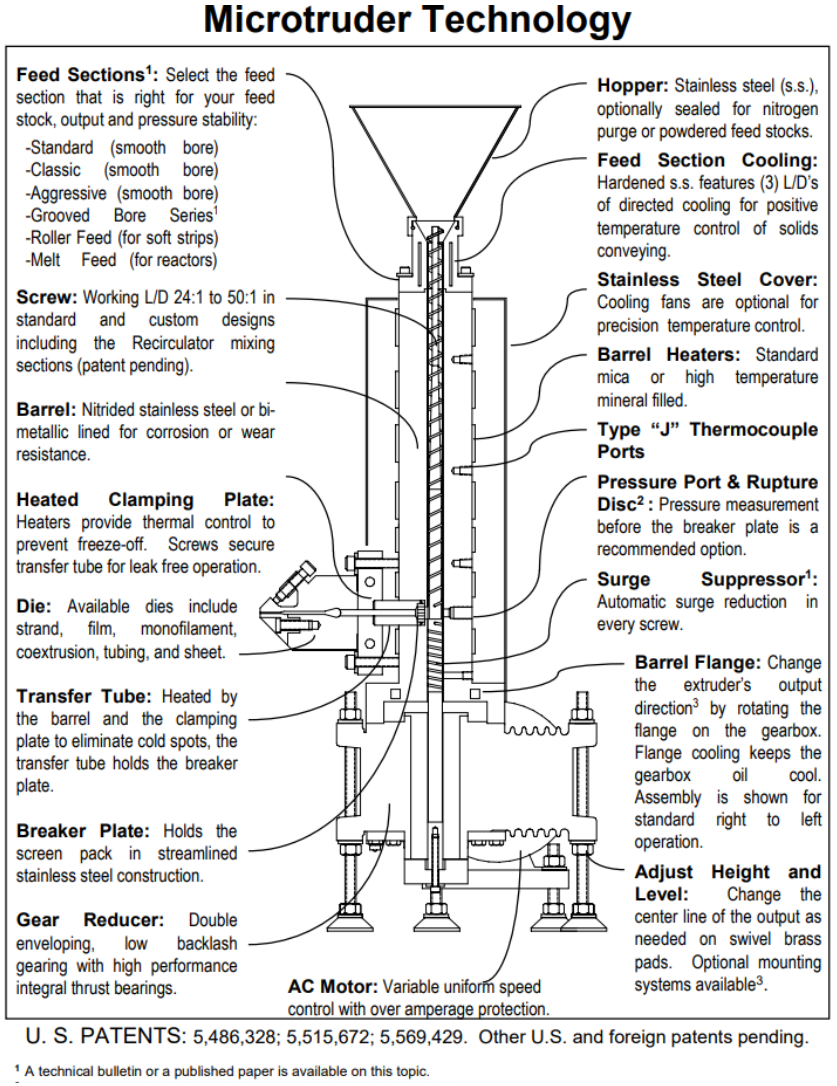

Figure 5: Microtruder setup and control system (left) and Microtruder sectioned view with notable features (right) ("What is a Microtruder?" 2020).



Figure 6: Screw pressure sensor in Microtruder circled in red.

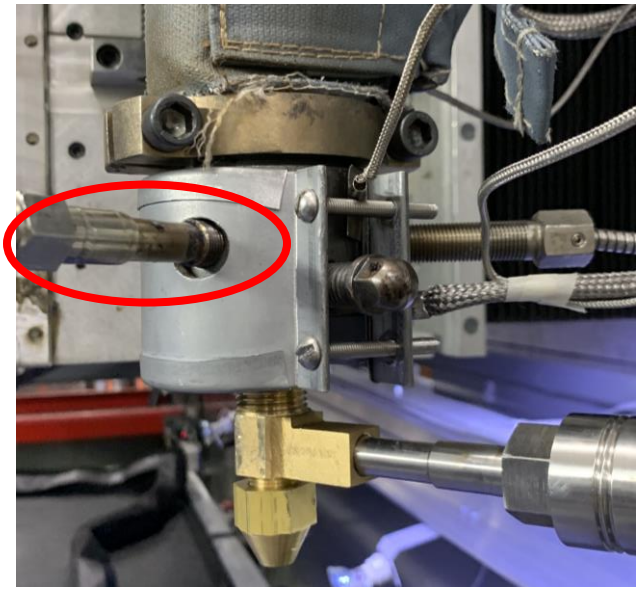

Figure 7: Screw pressure sensor in BAAM end cap circled in red.

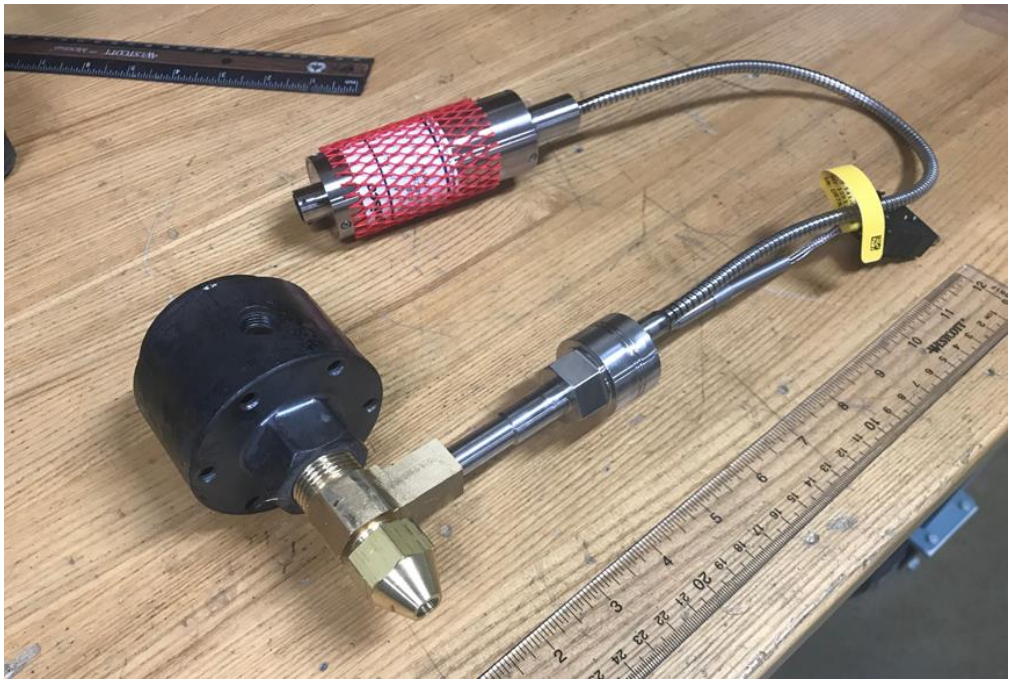

Figure 8: New nozzle adapter and pressure sensor attached to BAAM end cap.



Figure 9: New nozzle adapter without pressure sensor and die block attached to the Microtruder.

conductivity. While a different adapter was made for the BAAM and the Microtruder, their designs differ only slightly. As stated previously, the Microtruder's scale relative to the BAAM is roughly 50% in terms of its screw and flow paths. The nozzle adapter for the BAAM featured a 0.4" throat, whereas on the Microtruder the throat was 0.25". Smaller nozzle tips were constructed for the Microtruder as needed to meet back pressure demands of the machine, resulting in 0.1", 0.15", 0.2", and 0.25" nozzle tips. Both nozzle adapters featured the same pressure port design shown in Figure 10. This pressure port design is standard among Dynisco sensors ("Transducer Mounting Hole Machining Tool Kit Manual" 2020). The depth of the pressure port was adjusted during machining to minimalize flow interruption while still providing enough depth to accurately measure the melt pressure. Lastly, the BAAM's nozzle adapter featured 7/8"-14 UNF threads to fit into the end cap, and the Microtruder's nozzle adapter featured 1/2"-13 UNC threads to fit into the designed die block. The die block was constructed to house the die heaters, thermocouple, and provide threads to connect the nozzle adapter and throat. A sectioned view of this setup is shown in Figure 11.

2.6 Materials and Material Properties

In order to properly validate pressure models, a variety of materials were characterized and tested. On the Microtruder system neat PLA, 20% CF-PLA, neat ABS, 20% CF-ABS, and neat LLDPE were utilized. Only 20% CF-ABS was tested on the BAAM system due to availability and testing time; the broad scope of this research resulted in timely testing procedures in order to properly capture pressure at a variety of nozzle sizes, screw speeds, flow rates, and materials. The table of Techmer product numbers is provided in Appendix A1.

A variety of relevant material properties were gathered, namely, rheological properties. A Dynisco LCR7000 (Figure 12) capillary rheometer was utilized to obtain the Weissenberg-

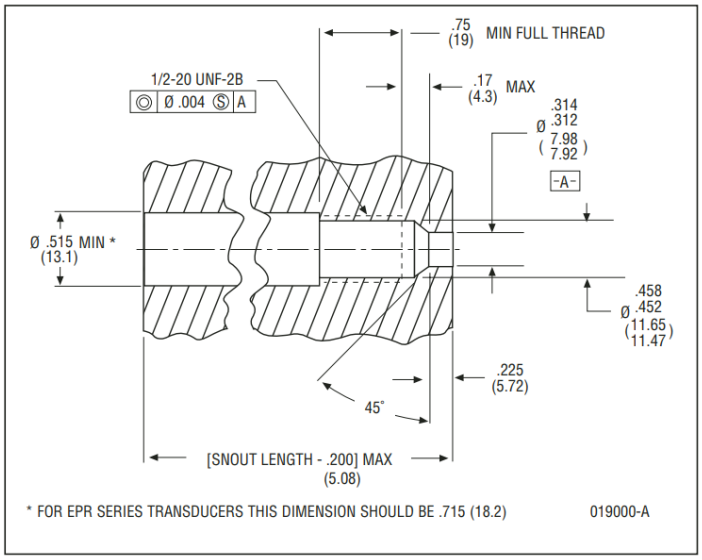

Figure 10: Schematic of pressure sensor mounting port ("Transducer Mounting Hole Machining Tool Kit Manual" 2020).

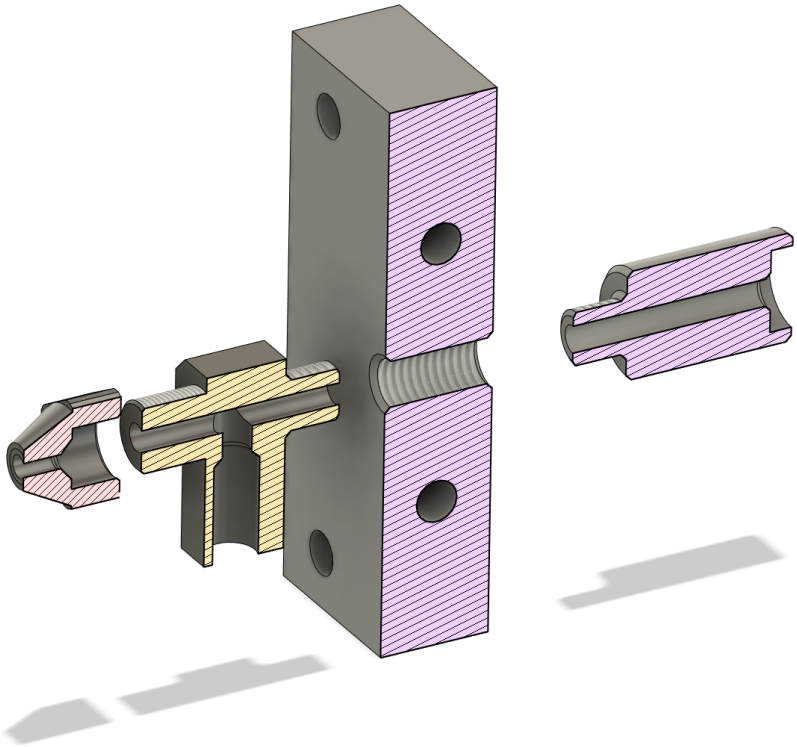

Figure 11: Sectioned view of Microtruder throat, die block, nozzle adapter, and nozzle.



Figure 12: Dynisco LCR 7000 used to obtain the power law parameters.

Rabinowitsch corrected power law parameters for all materials in this study (Table 2). The power law parameters, consistency index, m, and power law index, n, for these materials were obtained at their respective set die temperatures on each machine. This is a common practice in theory to account for non-Newtonian nature in the most relevant sections of the machine (Campbell and Spalding 2013, 14). The power law relating shear rate, $\dot{\gamma}$, and viscosity, μ, is shown in Equation 6.

$$\mu = m\dot{\gamma}^{n} \qquad Eq.(6)$$

The full data containing shear rate and viscosity data from the LCR tests is found in Appendix A2.

Several thermal properties were also needed as inputs to the compression zone theory where the phase change takes place. The thermal properties consisted of thermal conductivity, k_m, heat of fusion, λ, and specific heat, C_v. These properties were not directly measured; they were obtained from literature and are shown in Table 3. The thermal properties will only be used in the compression zone theory.

Melt, bulk, and solid density were also gathered to support theory. For the single screw extrusion process, the material begins at bulk density as loose pellets in the hopper, packs together in the feed zone, melts in the compression zone to reach its melt density, then finally extrudes and hardens back to its solid density. Melt density, ρ_d, which is relevant for melt flow in the machine, was gathered using the LCR7000 by extruding a set amount of material through the capillary rheometer at its set die temperature and taking its mass. A detailed description of the procedure for obtaining melt density is found in page 87 of the LCR7000 manual ("7000 Series Capillary Rheometers & LabKARS Software" 2020). Melt density is most relevant to the models proposed, and is used throughout calculations in the compression zone, feed zone, and die. Bulk density, ρ_b, is the density of loose pellets in the hopper. It was measured by placing pellet feedstock in a

Table 2: Power law parameters for all materials in this study.

LCR Power Law Results		
Material	**m (Consistency Index) (Pa*s^n)**	**n (Power Law Index)**
PLA (@ 190 C)	22985	-0.637
ABS (@ 220 C)	21363	-0.666
LLDPE (@ 245 C)	6799	-0.504
20% CF PLA (@ 210 C)	2785	-0.444
20% CF ABS (@ 240 C)	29356	-0.688
20% CF ABS (@ 250 C)	24459	-0.670

Table 3: Material thermal properties obtained from literature (Rauwendaal 2014. 249).

Material Thermal Properties			
Material	**Thermal Conductivity (J/ms°C)**	**Heat of Fusion (J/kg)**	**Specific Heat (J/kg°C)**
PLA	0.195	93600	1800
ABS	0.25	Amorphous	1400
LLDPE	0.2	215000	2300
20% CF PLA	0.195	93600	1800
20% CF ABS	0.25	Amorphous	1400

cylindrical container of known volume and taking its mass. The mass could then be divided by the known volume. Bulk density is used to calculate the weight of pellets in the hopper. Solid density, ρ_s, was measured using a Mettler Toledo XS204 analytical balance with a built-in density application using Archimedes principle. Beads from Microtruder testing were tested in the XS204 as shown in Table 4. It should be noted that due to extreme porosity in most materials, the solid density deviated wildly when testing different sections of each bead. Several measurements were taken at various sections of the beads and at differing RPMs for the result found in Table 4. Solid density is only used in the models proposed at the beginning of the compression zone, where the pellets are assumed to be compacted and near the solid density of the material.

Pellet size was also of interest, as it was discovered during testing that certain materials were above the recommended size for the Microtruder. Each material's pellet approximate shape, longest dimension, and shortest dimension were measured using calipers. To provide a sense of scale between materials, ten measurements were taken for each the longest and shortest dimension and averaged. These results as well as the BAAM and Microtruder max pellet size are shown in Table 5. The effect of pellet size on results will be discussed in the Chapter 4 Results section.

2.7 Temperature Profiles

As is standard with extrusion, temperature profiles were adjusted as needed. Temperature profiles from the BAAM system were initially used on the Microtruder and altered to achieve proper extrusion. Temperatures were typically increased as the shorter nature of the Microtruder compared to the BAAM required more heat for the material to melt properly at the faster rate. The temperature profile for CF-ABS on the BAAM was left to their standard values. The temperature profiles are shown in Table 6.

Table 4: Melt, bulk, and solid densities for all materials.

Material Densities			
Material	**Melt Density (g/cc)**	**Bulk Density (g/cc)**	**Solid Density (g/cc)**
PLA	1.104 (@ 190 C)	0.8711	1.242
ABS	0.9133 (@ 220 C)	0.7066	1.153
LLDPE	0.7305 (@ 245 C)	0.5955	0.792
20% CF PLA	1.1685 (@ 210 C)	0.6666	1.008
20% CF ABS	1.015 (@ 240 C)	0.6526	0.838

Table 5: Pellet sizes for all materials and machine suggested pellet size limits.

Material Pellet Sizes			
Material	**Pellet Style**	**Long Dimension (mm)**	**Short Dimension (mm)**
LLDPE	Ovoid	4.86	2.58
PLA	Ovoid	4.74	3.53
20% CF-PLA	Cylinder	2.88	2.52
ABS	Ovoid	4.63	2.10
20% CF-ABS	Cylinder	2.77	2.47
	BAAM Max pellet length	**Randcastle max pellet length**	
	7 mm	3.175 mm	

Table 6: Temperature settings for all materials and both machines.

Machine Set Temperatures In °C					
Machine	**Material**	**Temperature Zones**			
		Zone 1	**Zone 2**	**Zone 3**	**Die**
Microtruder	PLA	140	160	170	190
	ABS	160	200	220	220
	LLDPE	190	240	245	245
	20% CF PLA	160	180	190	210
	20% CF ABS	180	220	240	240
BAAM	20% CF ABS	175	205	250	250

Chapter 3: Analytical Approach to Pressure Profile

3.1 Introduction

In several works, a Newtonian model for the peak pressure (discharge pressure) and machine output is derived with varying modifications (Campbell and Spalding 2013, 11-15; Middleman 1977, 123-150; Tadmor and Gogos 2006, 247-259). By comparing their results to data, the model presented in section 3.2 was chosen for its balance between simplicity and accuracy. After this result, theories for the feed, compression zones, and nozzle were added to supplement the result and create a complete pressure map down the axis of the screw.

3.2 Modified Newtonian Model for the Metering Zone

When a single screw extruder is operating properly, the metering section can be assumed to be the rate controlling section of the system (Campbell and Spalding 2013, 247). This allows for estimation of discharge pressure and machine output using solely information from the metering zone and neglecting effects from the feed and compression zone. The following model was gathered from several works (Campbell and Spalding 2013, 11-15; Tadmor and Gogos 2006, 247-258, 450-452). The following assumptions are made:

(i) Flow is fully developed.

(ii) Flow channels are completely filled.

(iii) No slip at the boundary surfaces.

(iv) No leakage flow over the flight tips.

(v) All channel corners are square.

(vi) Flows are isothermal and Newtonian.

(vii) Channel dimensions are not changing in the metering section.

The overall flow rate, Q, is split into two terms, containing rotational flow, Q_d, and pressure flow, Q_p. Their relation is shown in Equation 7.

$$Q = Q_d - Q_p \qquad Eq.(7)$$

It should be noted that the average shear rate, $\dot{\gamma}$, is calculated using RPMs and the width of the channel in Equation 8 and then used in Equation 6 to find the shear viscosity. This is an attempt at account for non-Newtonian flow while still deriving expressions under the Newtonian assumption.

$$\dot{\gamma} = \frac{\pi D_c N}{H} \qquad Eq.(8)$$

Several velocities must first be established. As discussed in Chapter 1, there are several areas of interest along the screw radii, namely, at the screw core and barrel. Velocities in the X and Z directions are calculated at these locations as shown in Equations 9-11:

$$V_{cx} = \pi N D_c sin\theta_c \qquad Eq.(9)$$

$$V_{cz} = -\pi N D_c cos\theta_c \qquad Eq.(10)$$

$$V_{bz} = -\pi N D_b cos\theta_b \qquad Eq.(11)$$

where subscript c designates the screw core and b designates the screw barrel. Shape factors F_d and F_p are established to account for effects from shallow or deep channels, the screw's characteristic H/W. F_d is calculated in Equation 12 and F_p in Equation 13.

$$F_d = \frac{16W}{\pi^3 H} \sum_{i=1,3,5,\ldots}^{\infty} \frac{1}{i^3} \tanh\left(\frac{i\pi H}{2W}\right) \qquad Eq.(12)$$

$$F_p = 1 - \frac{192H}{\pi^5 W} \sum_{i=1,3,5,\ldots}^{\infty} \frac{1}{i^5} \tanh\left(\frac{i\pi W}{2H}\right) \qquad Eq.(13)$$

The shape factors are extremely important for deep channels (Tadmor and Gogos 2006, 254-255). The rotational flow can now be calculated as shown in Equation 14:

$$Q_d = \frac{pV_{bz}WHF_d}{2} \qquad Eq.(14)$$

where p is the number of flights of the screw. Similarly, the pressure flow term is calculated in Equation 15:

$$Q_p = \frac{pWH^3F_p}{12\mu}\left(\frac{\partial P}{\partial z}\right) \qquad Eq.(15)$$

where μ is the shear viscosity of the molten polymer as discussed in Chapter 2, and $\frac{\partial P}{\partial z}$ is the pressure gradient across the metering zone. For the purposes of this work, the pressure gradient is assumed to be at maximum as shown in Equation 16:

$$\frac{\partial P}{\partial z} = \frac{P_{dis}sin\theta_b}{l_m} \qquad Eq.(16)$$

where l_m is the length of the metering zone. The mass rate of the extruder can be calculated by combining Equations 7, 12, 13, 14, 15, and 16:

$$Q = \frac{pV_{bz}WHF_d}{2} - \frac{pWH^3F_p}{12\mu}\left(\frac{P_{dis}sin\theta_b}{l_m}\right) \qquad Eq.(17)$$

What has been neglected thus far is the effect the die has on the system. Equation 16 shows the relationship between pressure and flow rate for isothermal pressure flow for an incompressible Newtonian fluid through a die:

$$Q_D = \frac{K}{\mu}\Delta P_D \qquad Eq.(18)$$

where K is the die constant. The die constant is a term lumping together geometry of the die, for example, the die constant for a tubular die can be solved for:

$$K = \frac{\pi R_D^4}{8L_D} \qquad Eq.(19)$$

where L_D is the length of the die and R_D is the radius of the die. For more complex die geometry the die constant must be solved for experimentally (Tadmor and Gogos 2006, 451). The operating

point of the extruder is found by setting the flow rate through the screw and die equal and setting the pressure rise over the screw equal to the pressure drop over the die. The final flow rate and discharge pressure of the system can be calculated by setting the flow rate of the die and screw equal as shown in Equation 20 & 21:

$$Q = Q_s = Q_D = \frac{0.5\pi N D_b cos\theta_b W H F_d}{1 + \frac{W H^3 sin\bar{\theta} F_p}{12LK}} \qquad Eq.(20)$$

$$\Delta P = \Delta P_S = \Delta P_D = \frac{0.5\mu\pi \mathrm{N D_b} \cos\theta_\mathrm{b} W H \mathrm{F_d}}{\mathrm{K} + \frac{\mathrm{W H^3} \sin\bar{\theta} \mathrm{F_p}}{12\mathrm{L}}} \qquad Eq.(21)$$

where $\bar{\theta}$ is the average angle of the screw core and barrel. It is noteworthy that the viscosity term in Equation 20 is cancelled out. This work uses the viscosity calculated in the screw channel for all calculations allowing for the viscosity term to drop. These equations make the primary model for estimating machine output and discharge pressure.

3.3 The Feed Zone

The feed zone has historically been studied less than the metering and compression zones, as it is assumed to be operating properly. Under proper operation the metering zone is provided with adequate flow and is the rate-limiting part of the process (Campbell and Spalding 2013, 247). Air between pellets all the way up to a full melt in the compression zone is forced back through the screw and out of the hopper. When the feed zone is operating incorrectly, material can begin melting prematurely in the feed zone. This makes the metering zone no longer rate controlling, and flow rate and pressure consistency deteriorate as a result (Campbell and Spalding 2013, 131). Therefore, it is typical to have a water-cooled casing at the feed zone entry below the hopper. The

casing constricts the feed zone temperature to that section of the barrel and prevents heat from rising into the hopper (Campbell and Spalding 2013, 132). It should be noted that both machines, in this case, are smooth hopper and barrel style, as opposed to grooved systems.

The model used in this research was developed by Campbell and his students at Clarkson University (Campbell and Spalding 2013, 139-141). This was the first model to introduce the idea of the screw flight pushing the polymer bed. All similar models treat the polymer as a solid incompressible plug that travels down the screw. A force balance is made containing pressure and contact forces as shown in Figure 13.

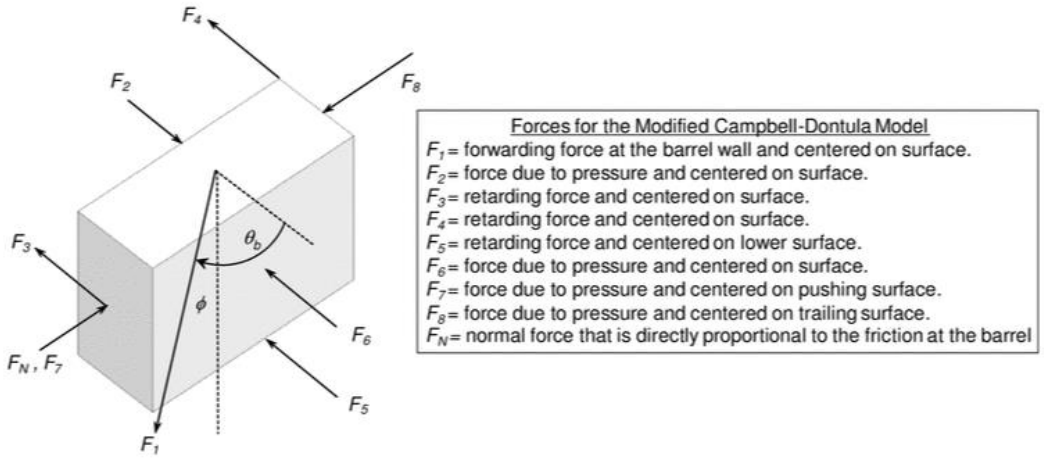

Figure 13: Forces on polymer in the feed zone (Campbell and Spalding 2013, 708).

A derivative relationship between angles is substituted in and integration is performed resulting in Equation 22:

$$sin\phi = cos\theta_b - \left(2\left(\frac{H}{W_b}\right)\left(\frac{f_H}{f_b}\right) + f_H + \left(\frac{W_c}{W_b}\right)\left(\frac{f_c}{f_b}\right)\right) sin\theta_b - \frac{HWsin\theta}{K_{xz}W_b f_b Z}\ln\left(\frac{P_z}{P_0}\right) \qquad Eq.(22)$$

where ϕ is the solids forwarding angle, K_{xz} is the lateral stress ratio in the x and y directions, P_0 is the pressure at the start of the solids conveying section, P_z is the pressure at the end of the solids

conveying section, and f_H, f_c, & f_b are dynamic coefficients of friction at the screw flights, screw core, and barrel, respectively. The solids conveying angle is the angle between the barrel velocity and the velocity difference between the barrel and plug and is typically in the range of 2-7 degrees (Campbell and Spalding 2013, 134). Equation 23 shows that the lateral stress ratio is a simple relationship between stress in the x and z directions.

$$K_{xz} = \frac{\sigma_x}{\sigma_z} \qquad Eq.(23)$$

Under the assumption that the hopper is sufficiently filled, the initial pressure is calculated using Equation 24 by calculating the weight of pellets on themselves:

$$P_0 = \frac{\rho_b g D}{4 f_w K_{xz}} \qquad Eq.(24)$$

where g is gravitational constant and D is the diameter of the hopper. By relating the velocity of the plug and its geometry Equation 25 is found:

$$Q = \pi^2 N H D_b (D_b - H) \left(\frac{tan\phi tan\theta_b}{tan\phi + tan\theta_b}\right)\left(\frac{W}{W + e}\right) \qquad Eq.(25)$$

Flow rate data or Equation 20 is used to find ϕ via Equation 25 and ϕ is plugged into Equation 22 to obtain pressure at the end of the feed zone.

3.4 The Compression Zone – Four Zone Model

The compression zone is increasingly difficult to characterize and simulate due to its complex nature. The material is undergoing a phase change, the channel depth is decreasing, and the melted material is flowing around the solid bed as the solid bed decreases in size. A photograph of solidified resin in a compression zone from a solidification experiment is shown in Figure 14. The melt pool gathers along the pushing flight and steadily increases in size as the solid bed melts. The cross section at multiple points along the compression zone is shown in Figure 15. It can be observed that melt films are forming and increasing all around the solid bed, leading to the four

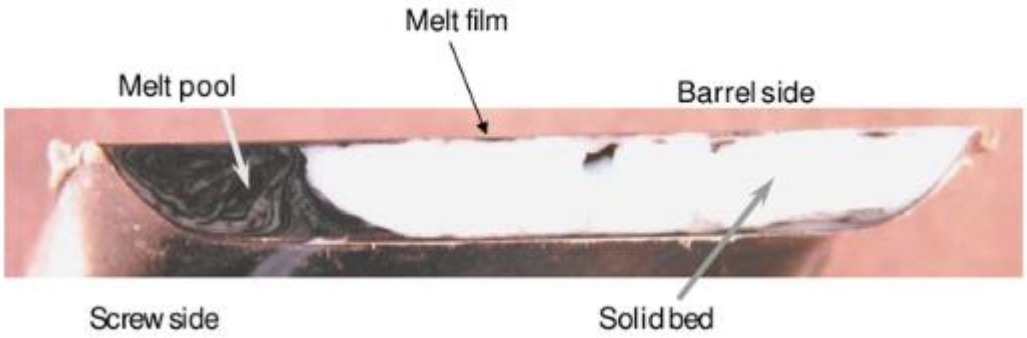

Figure 14: Cross section of resin in compression zone from a solidification experiment (Campbell and Spalding 2013, 193).

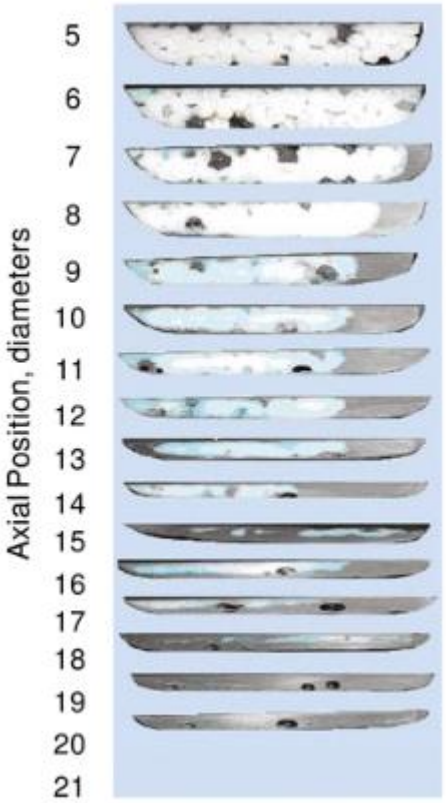

Figure 15: Cross section of resin in compression zone axially down the compression zone (Campbell and Spalding 2013, 197).

zone model proposed by Campbell and Spalding in Figure 16, where A is the solid bed, B is the film on the pushing flight, C is the film at the barrel, D is the film at the screw core, and E is the film at the trailing flight. Energy dissipation and melt pool velocities are used to iterate down the compression channel until full melt is reached. The expected profile for solid bed width, X, and height, Y, is shown in Figure 17. It should be noted that the melting is completed when Y is equal to zero, as the primary melting takes place directly from barrel heat into the top of the solid bed causing its height to decrease at a faster rate than its width.

The velocity of the solid bed at the beginning of the compression zone must first be established:

$$V_{sz} = \frac{Q}{\rho_s W H_f} \qquad Eq.(26)$$

where H_f is the depth of the feed section. Another diameter of interest is established at the surface of the solid bed and its interface with film C, D_f. The velocity at this location is calculated through Equation 27:

$$V_{sx} = \pi N D_f sin\theta_f \qquad Eq.(27)$$

Equations 8-10 will now need to be calculated at each increment since the diameter of the core is decreasing. The average z velocity is calculated by Equation 28:

$$\overline{V_{fz}} = \frac{V_{cz} + V_{bz}}{2} \qquad Eq.(28)$$

The vectorial velocity of each film, V_j, can now be calculated with Equation 29 through 32:

$$V_{j,C} = \sqrt{V_{sx}^2 + V_{sz}^2} \qquad Eq.(29)$$

$$V_{j,D} = |V_{cz}| + V_{sz} \qquad Eq.(30)$$

$$V_{j,E} = \left|\overline{V_{fz}}\right| + V_{sz} \qquad Eq.(31)$$

$$V_{j,B} = \left|\overline{V_{fz}}\right| + V_{sz} \qquad Eq.(32)$$

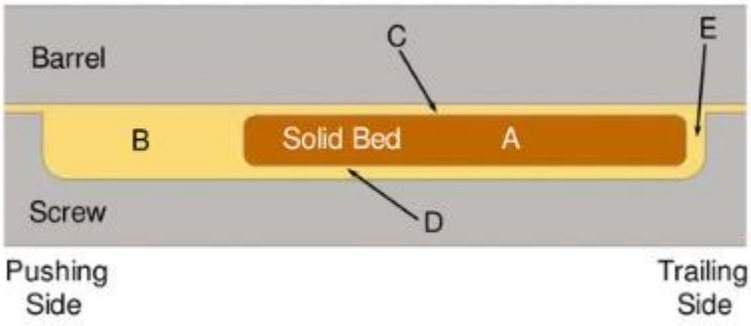

Figure 16: Schematic of four zone melting model (Campbell and Spalding 2013, 204).

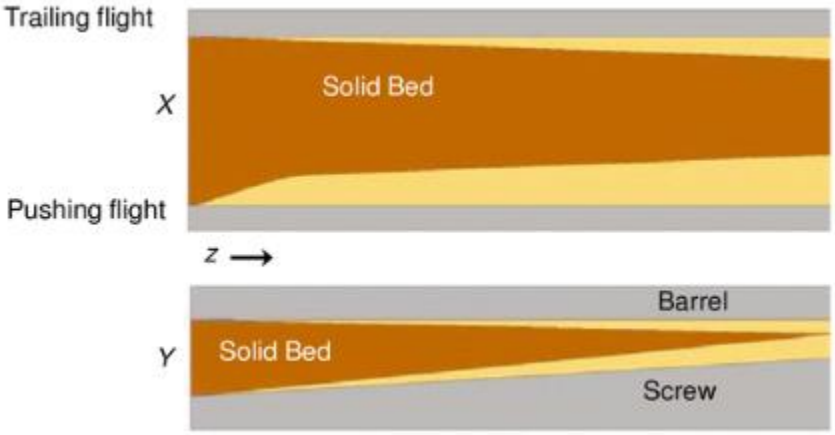

Figure 17: Schematic of solid bed width (top) and height (bottom) down the compression channel (Campbell and Spalding 2013, 210).

By completing an energy and material balance for the melting process melting velocities for the four films are established in Equations 33-36:

$$V_{sy,C} = \frac{\left[\frac{k_m}{\delta_C}(T_b - T_m) + \frac{\mu V_{j,C}^2}{2\delta_C}\right]}{\rho_s\lambda + \rho_s C_v(T_m - T_s)} \qquad Eq.(33)$$

$$V_{sy,D} = \frac{\left[\frac{k_m}{\delta_D}(T_{screw} - T_m) + \frac{\mu V_{j,D}^2}{2\delta_D}\right]}{\rho_s\lambda + \rho_s C_v(T_m - T_s)} \qquad Eq.(34)$$

$$V_{sx,B} = \frac{\left[\frac{k_m}{\delta_B}(T_b - T_m) + \frac{4\mu V_{j,B}^2}{2\delta_B}\right]}{\rho_s\lambda + \rho_s C_v(T_m - T_s)} \qquad Eq.(35)$$

$$V_{sx,E} = \frac{\left[\frac{k_m}{\delta_E}(T_b - T_m) + \frac{4\mu V_{j,E}^2}{2\delta_E}\right]}{\rho_s\lambda + \rho_s C_v(T_m - T_s)} \qquad Eq.(36)$$

where δ is each melt film thickness, T_b is the barrel temperature, T_m is the resin melt temperature, T_{screw} is the temperature of the screw, and T_s is the temperature of the solid bed. The thickness of melt film C is calculated via Equation 37:

$$\delta_C = \left[\frac{\left[2k_m(T_b - T_m) + \mu V_{j,C}^2\right]\left(\frac{X}{\alpha}\right)}{V_{sx}\rho_m(C_v(T_m - T_s) + \lambda)}\right]^{0.5} \qquad Eq.(37)$$

Where α is a fitting factor. Similarly, the thickness of zone E is calculated through Equation 38:

$$\delta_E = \left[\frac{\left[3k_m(T_b - T_m) + 6\mu V_{j,E}^2\right]Z}{\frac{2}{9}V_{j,E}\rho_m(C_v(T_m - T_s) + \lambda)}\right]^{0.5} \qquad Eq.(38)$$

The thicknesses of Zones B and D can be found by difference:

$$\delta_B = W - X - \delta_E \qquad Eq.(39)$$

$$\delta_D = H(z) - Y - \delta_C \qquad Eq.(40)$$

Where $H(z)$ is the channel depth at the current increment. The solid bed width and height are found by subtracting the reduction over a small distance, Δz, at each increment, i:

$$Y_{i+1} = Y_i - \left[V_{sy,C} + V_{sy,D}\right]\left(\frac{\Delta z}{V_{sz}}\right) \qquad Eq.(41)$$

$$X_{i+1} = X_i - \left[V_{sx,B} + V_{sx,E}\right]\left(\frac{\Delta z}{V_{sz}}\right) \qquad Eq.(42)$$

$$Z_{i+1} = Z_i + \Delta z \qquad Eq.(43)$$

The volumetric flow rate of melted material is calculated at each increment:

$$Q_{melt,i} = \left(WH_f - Y_i X_i\right)V_{sz} \qquad Eq.(44)$$

The pressure change at each increment based on rotational and pressure flow is calculated via Equation 45:

$$\Delta P_i = \left[\frac{Q_{melt,i} - \frac{\frac{1}{2}V_{bz}(W - X_i)(H_i H_{i+1})}{0.5(H_i + H_{i+1})}}{\frac{(W - X_i)(H_i H_{i+1})^2}{6\mu(H_i + H_{i+1})}}\right]\Delta z \qquad Eq.(45)$$

Finally, the pressure at each increment is calculated:

$$P_{i+1} = P_i + \Delta P_i \qquad Eq.(46)$$

3.5 Hagen-Poiseuille Pressure Flow

To bridge the gap between exit pressure and discharge pressure, non-Newtonian tubular pressure flow was assumed via the Hagen-Poiseuille equation:

$$Q = \frac{\pi R_n^3}{s+3}\left(\frac{R_n \Delta P_n}{2mL_n}\right)^s \qquad Eq.(47)$$

where $s = \frac{1}{n+1}$, and ΔP_n is the pressure drop across the nozzle tip. This enables the pressure between the end of the screw (discharge pressure) and exit to be more complex than just a linear drop.

Chapter 4: Experimental Approach to Pressure Profile

4.1 Introduction

In order to validate the analytical model, pressure data during normal operations was conducted. Data was gathered from both machines, the BAAM and the Microtruder, over a range of RPMs, nozzle sizes, pressure locations, and materials. A sensor and DAQ setup were purchased for testing separate from each machine's built in sensing systems. Testing procedures for each machine varied due to the nature of each system, as explained below.

4.2 DAQ System and Melt Pressure Sensor

To obtain pressure data at the new nozzle location, a DAQ and pressure sensor were purchased. The pressure sensor, a Dynisco TPT4634-5M-3/18-SIL2, featured a melt pressure sensor capable of up to 5,000 psi. The TPT4634 also came equipped with a Type J melt flow thermocouple that was used during tests done on the Microtruder. It should be noted that the TPT4634 is a transmitter and not a transducer.

A National Instruments (NI) DAQ was purchased to go alongside the TPT4634, a cDAQ-9174 chassis with a NI 9219 analog voltage input model and a NI 9207 combo voltage and current input module. The NI 9219 was utilized for the melt thermocouple, as it provides built in excitation. The NI 9207 was utilized for the pressure sensor due to its capability for mA input.

4.3 BAAM Experimental Procedure

To establish a base set of data for this study an experiment with 20% CF-ABS, the custom nozzle adapter and simple print parameters was conducted. The 20% CF-ABS was first dried at 85 °C for 4 hours. The back pressure screw was set to 25%. A single layer of linear beads measuring 30" x 0.3" x 0.15" were printed long enough for the machine to reach steady state as shown in Figure 18. A range of RPMs and print speeds were utilized in order to keep the bead's dimensions consistent (Table 7). The BAAM slicing software automatically determined print speeds for the various RPMs to maintain the bead's dimensions. This meant that the higher the RPM, the shorter the run time per bead. These beads were weighed, and pressure data was used to obtain the time it took to print each bead in order to calculate mass flow rate. Discharge pressure was obtained via the BAAM's built-in pressure sensor within the end cap and logged directly to its controller PC. Nozzle pressure was gathered from the Dynisco TPT4634 sensor combined with the NI DAQ and a laptop computer at 50 Hz. Drooled material was wiped off the nozzle before each test to ensure no extra material would be added to the result. The entire range of RPMs, 50-350 in 50 RPM increments, were ran for the 0.3" and 0.4" nozzle. The 0.2" nozzle was not ran at 200, 250, 300, and 350 RPM due to potential issues with pressures above the BAAM's capability. A sample of raw pressure data at the nozzle at 50 RPM is shown in Figure 19 with extrusion start and stop indicated. This sample demonstrates the need to remove data near the start and stop of each bead to obtain the steady state pressure that the model predicts.

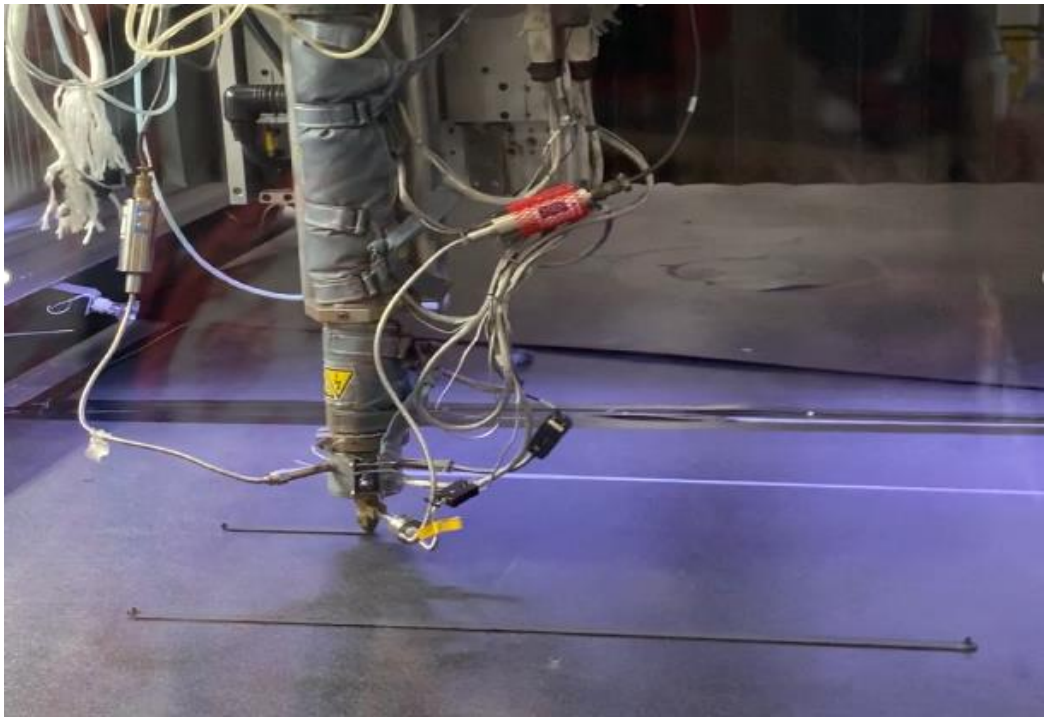

Figure 18: BAAM printing single beads for experiment. Photo courtesy of Oak Ridge National Laboratory, US Dept. of Energy.

Table 7: Print speeds for all RPMs tested.

Test RPM	Print Speed (mm/s)
50	39.06
100	78.11
150	117.17
200	156.23
250	195.28
300	234.34
350	278.98

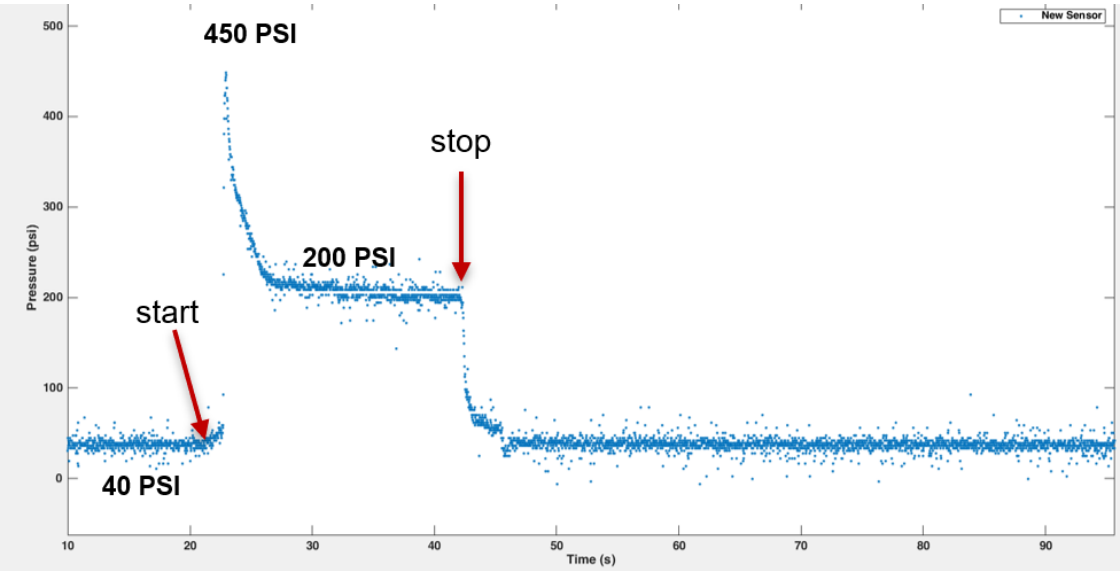

Figure 19: Pressure data from nozzle sensor for one bead of CF-ABS at 50 RPM.

4.4 Microtruder Experimental Procedure

A more extensive set of tests were conducted on the Randcastle Microtruder. A nozzle adapter was used as discussed in section 2.5. All materials covered in Chapter 2 were tested. Tests were done at 30-110 RPMs. Additionally, a wider variety of nozzle sizes were tested. The full scope of tests is shown in Table 8. Materials were dried before testing and the machine was allowed to achieve steady flow before each test was conducted by keeping the hopper full of material. As opposed to the BAAM system tests, each RPM was ran at the same amount of time of 1.5 minutes. This was more desirable as the extruder was allowed to reach steady state before tests, therefore eliminating the need to remove transient data later. A sample of screw pressure data for CF PLA at 110 RPM with a 0.1" nozzle is shown in Figure 20, that is noticeably more linear than that of Figure 19 due to reaching steady state before running each test. It should be noted that the sinusoidal nature of the screw pressure data is due to the rotation of the screw and is expected (Campbell and Spalding 2013, 546-548). Again, the time of the pressure data and

Table 8: Scope of tests completed on the Microtruder System.

Scope of Microtruder Testing					
Material	**Nozzle Diameter**				**Sensor Location**
	0.1	**0.15**	**0.2**	**0.25**	
PLA	■	■	■	■	Barrel
					Nozzle
20% CF PLA	■	■	■	■	Barrel
					Nozzle
LLDPE	■	■	■	■	Barrel
					Nozzle
ABS	■	■	■	■	Barrel
	■	■	■	■	Nozzle
20% CF ABS	■	■	■	■	Barrel
	■	■	■	■	Nozzle

Tested: ■

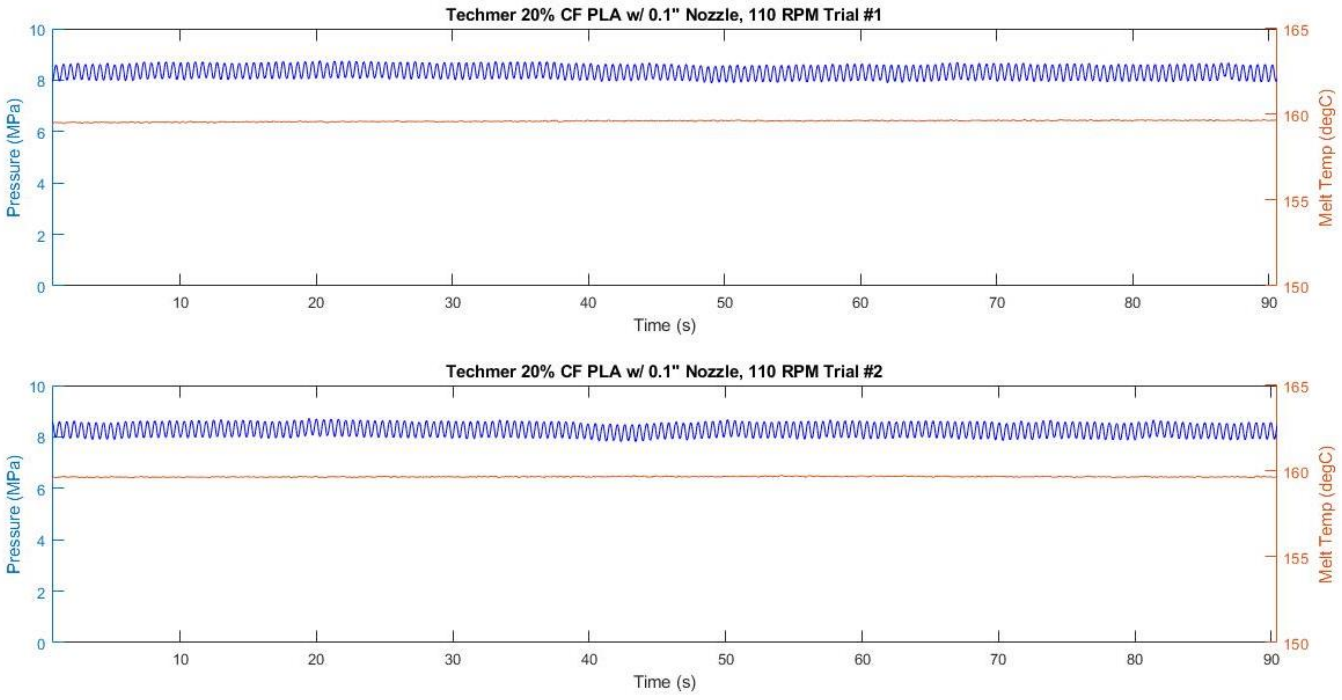

Figure 20: Sample data for screw pressure with CF PLA, 0.1" nozzle at 110 RPM.

weight of the resulting beads were used to calculate mass flow rate. The starts and stops of the bead were made by manually cutting the bead coming out of the nozzle during data start and data stop. The Dynisco TPT4634 with the NI DAQ at 25 Hz was used at two locations: the end of the screw and the nozzle tip to obtain discharge pressure and nozzle pressure, respectively. This meant that each "run" was done independently at each sensor location. This increased testing procedure resulted in nozzle pressure only gathered for ABS and CF ABS. Each run was done twice and their result average for the final results.

4.5 BAAM Experimental Results & Discussion

The results of mass flow rates from the BAAM testing are shown in Figure 21. It is clear that as nozzle size increases, flow rate increases, especially at higher RPM. Results for the nozzle pressure are shown in Figure 22, and the screw pressure in Figure 23. Interestingly, the nozzle pressure tapers off as RPM increases more so than at the screw sensor.

4.6 Microtruder Experimental Results & Discussion

Results for mass flow rates of all Microtruder tests are shown in Figure 24. Interestingly, ABS and CF-ABS seem to be the only materials where flow rate increases with nozzle size. This is likely due to several factors that will be discussed further. One of these factors is that there were extrusion issues with neat PLA due to pellet size. Table 5 tabulates the pellet size and the PLA pellets were exceeding the limit of the Microtruder recommended pellet size. This led to feed problems with the material and under extrusion. Another factor was how LLDPE, PLA, and CF-PLA all had flow surging issues. The full pressure results for all materials are shown in Figures 25 through 29. Figures 25-27 highlight some of the pressure inconsistencies visually. Figures 28

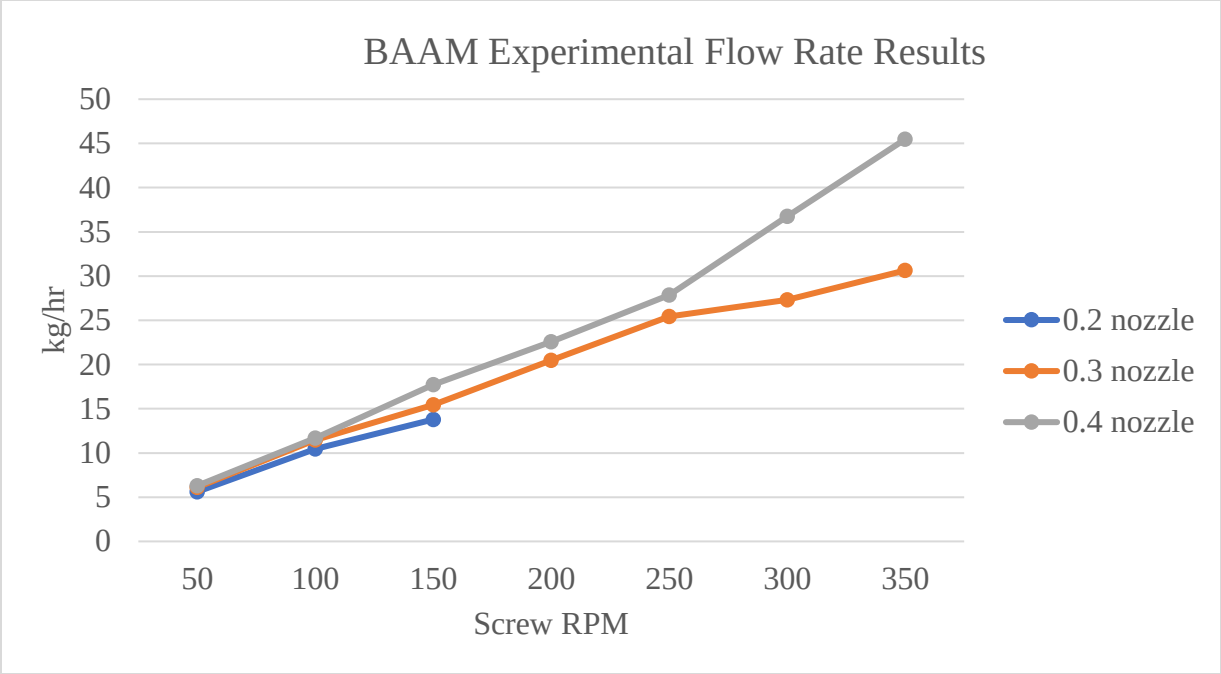

Figure 21: Mass flow rate results for BAAM testing for CF ABS at all nozzle sizes and RPMs.

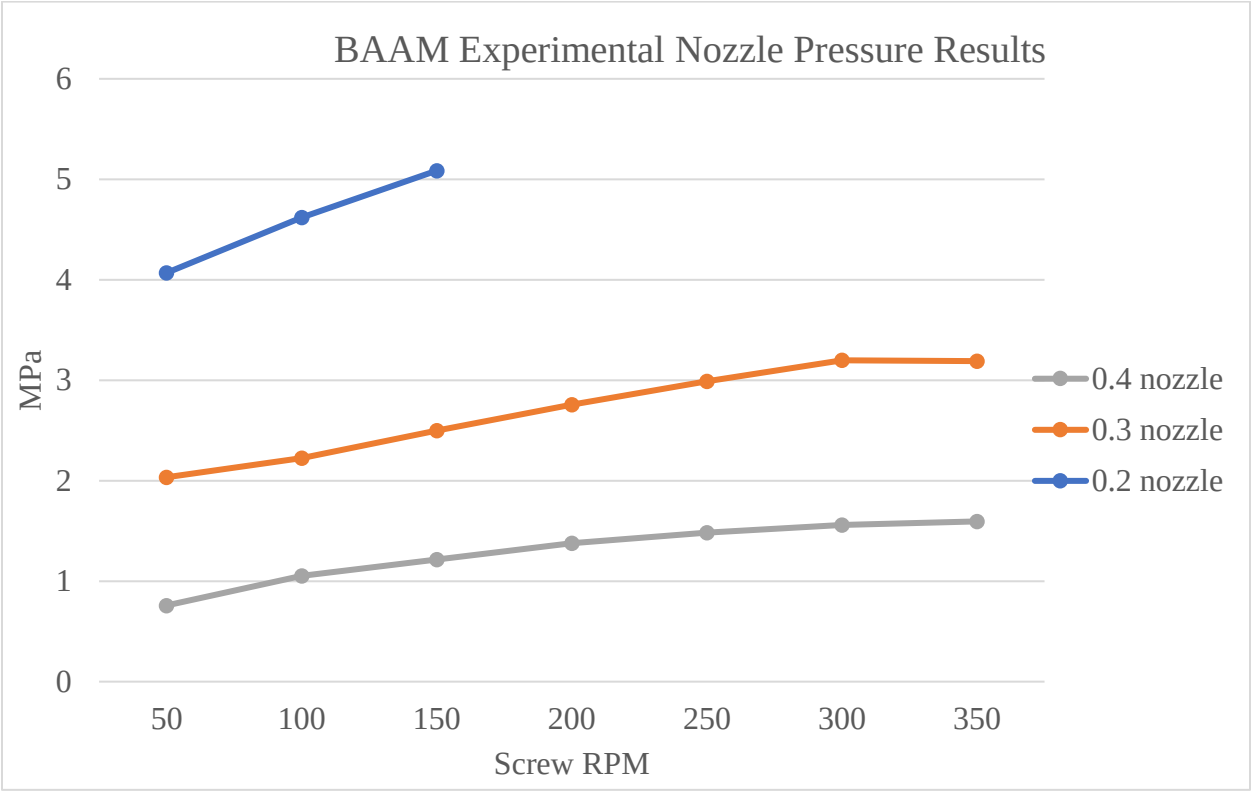

Figure 22: Nozzle pressure results for BAAM testing for CF ABS at all nozzle sizes and RPMs.

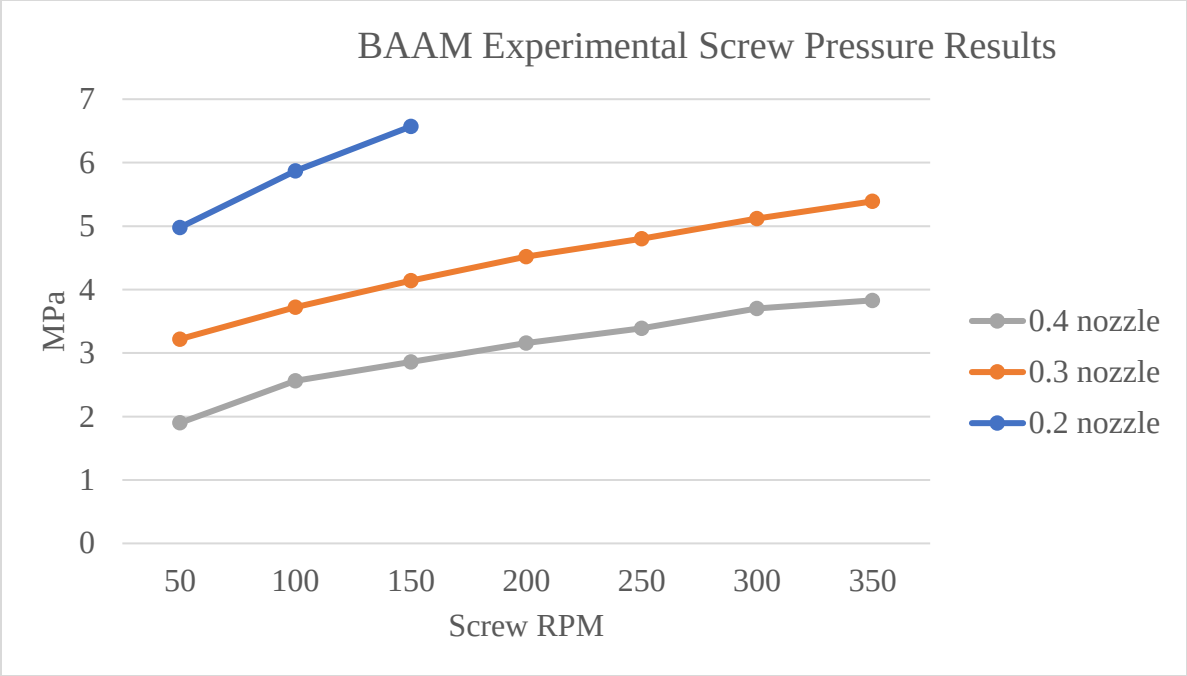

Figure 23: Screw pressure results for BAAM testing for CF ABS at all nozzle sizes and RPMs.

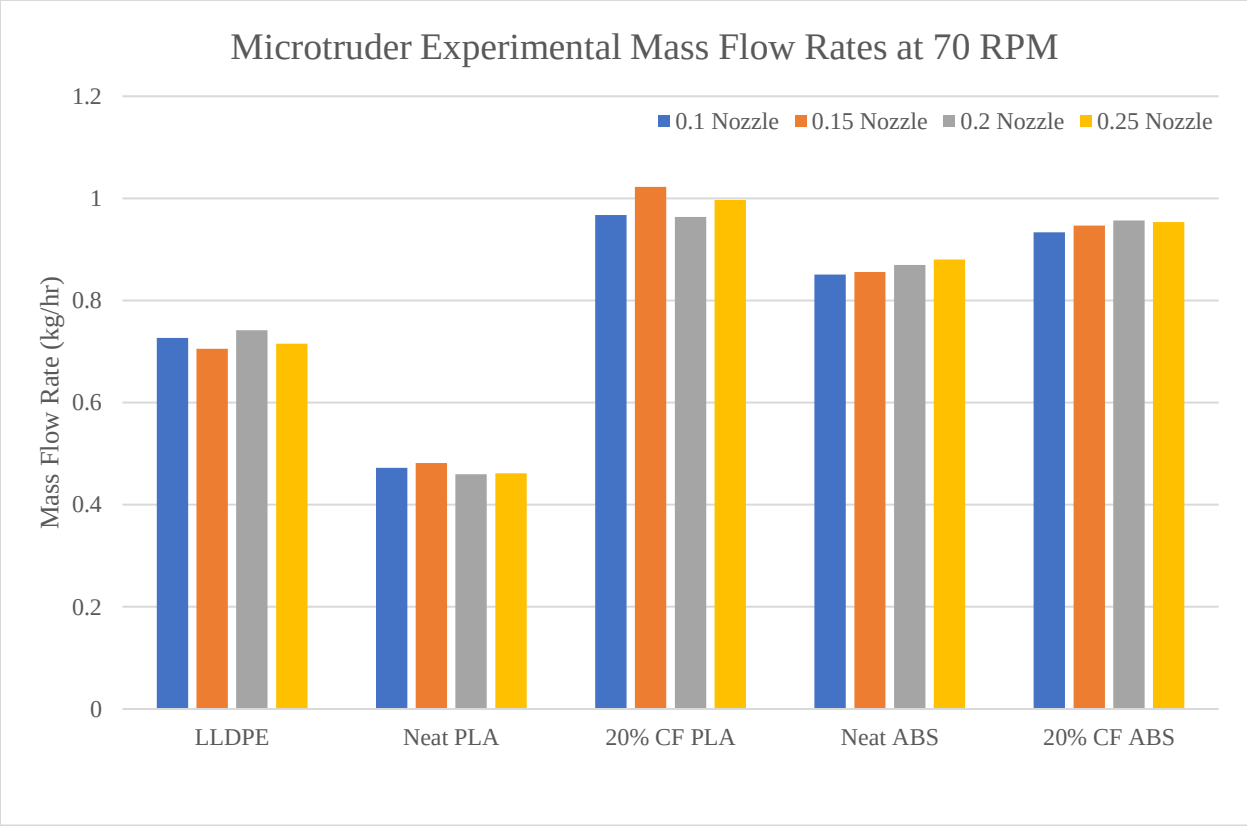

Figure 24: Mass flow rate results for Microtruder testing for all materials and nozzle sizes at 70 RPM.

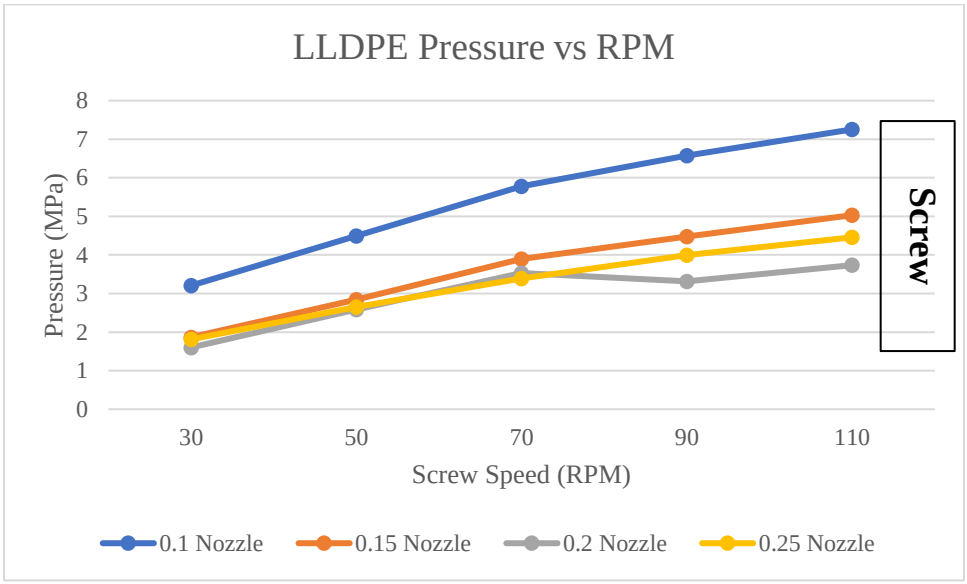

Figure 25: Screw pressure results for LLDPE on Microtruder system at all nozzle sizes.

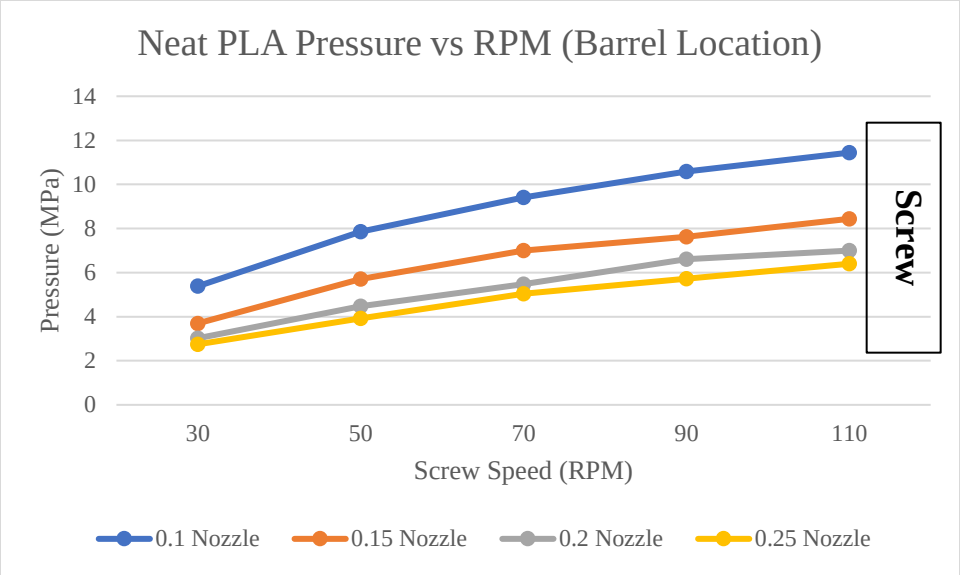

Figure 26: Screw pressure results for PLA on Microtruder system at all nozzle sizes.

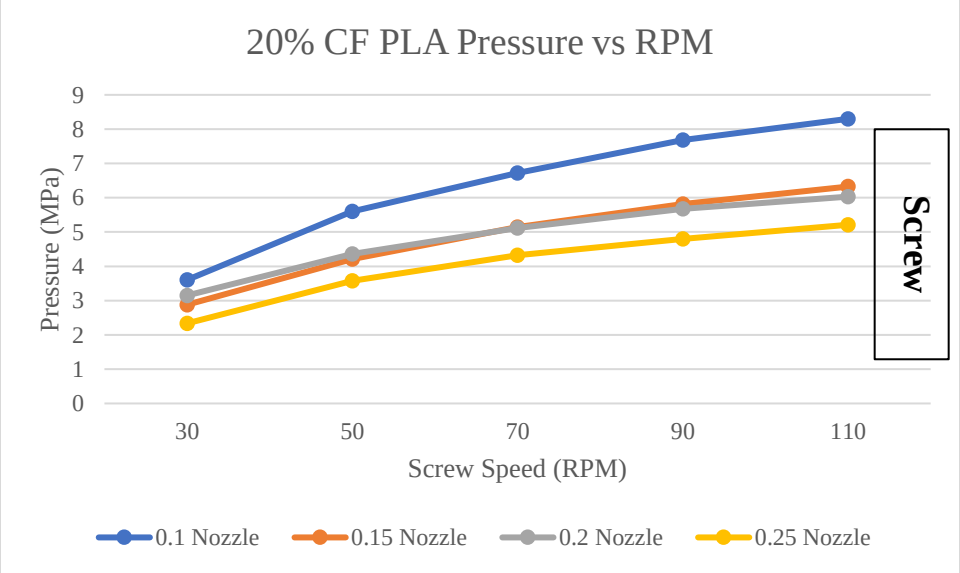

Figure 27: Screw pressure results for CF-PLA on Microtruder system at all nozzle sizes.

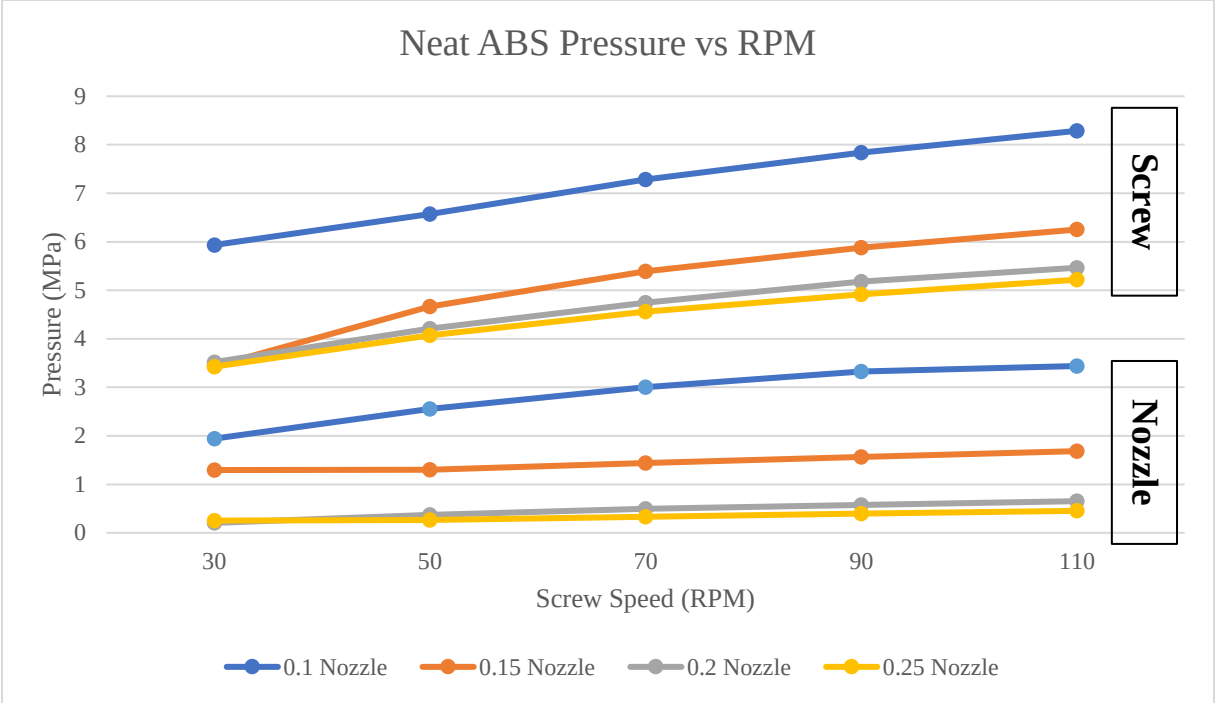

Figure 28: Screw and nozzle pressure results for ABS on Microtruder system at all nozzle sizes.

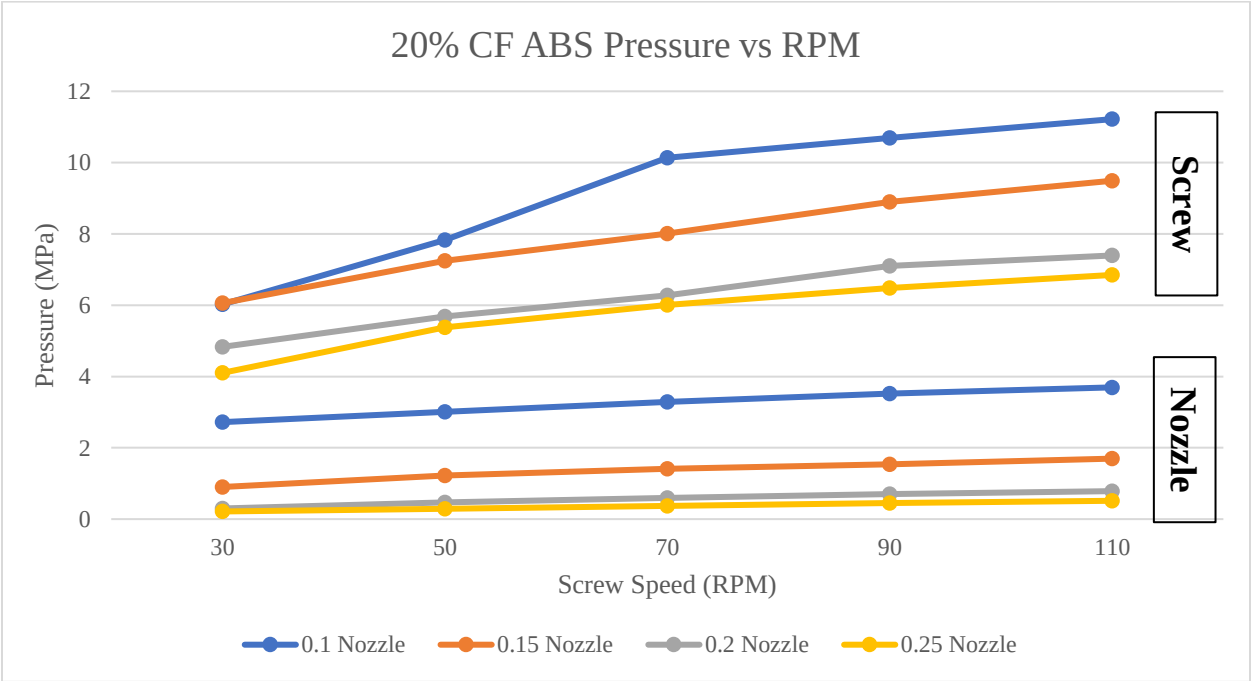

Figure 29: Screw and nozzle pressure results for CF-ABS on Microtruder system at all nozzle sizes.

and 29 show both the nozzle and screw pressure for neat ABS and CF-ABS. It is observed that at larger nozzle sizes of 0.2 and 0.25 inch, the pressure stays relatively constant. This was due to these nozzle sizes not providing ample back pressure proper for the machine. The 0.1 inch nozzle saw a steep increase in pressure relative to other nozzle sizes for all materials. The 0.1 inch nozzle size is close to what similar scale machines use.

4.7 BAAM Experimental Results Compared to Analytical Model

Before being able to review results of the model, the die constants had to be found. Initially, it was planned to gather data with nozzles the same sizes as the machine throat so that the die constant could be calculated analytically using Equation 19. However, issues with accuracy came from just using this result, and die constants were calculate from data as well.

The die constant calculation is the only direct interaction between data and the model. Since the die constants are a function of die geometry, it should remain constant across various pressures and materials for the same nozzle & throat. Die constants were calculated using pressure data, mass flow rate data, and Equation 18. The result for die constants of the BAAM are shown in Figures 30 through 32. These plots show die constants calculated directly from data, curves fit to the data, the Newtonian round tube assumption, the non-Newtonian tube assumption, and the die constant plugged into the model. The die constant plugged into the model was at the middle of RPMs tested using the curve fit to data. The die constants are increasing for increasing nozzle size as expected, and the die constants were found to be relatively non-constant across RPM. This was likely due to variations in data from the BAAM data testing itself.

Figures 33 through 35 show flow rate and pressure results. Interestingly, the model predicts accurately for the 0.2 and 0.3 inch nozzles, but less so on the 0.4 inch nozzle. Flow rate

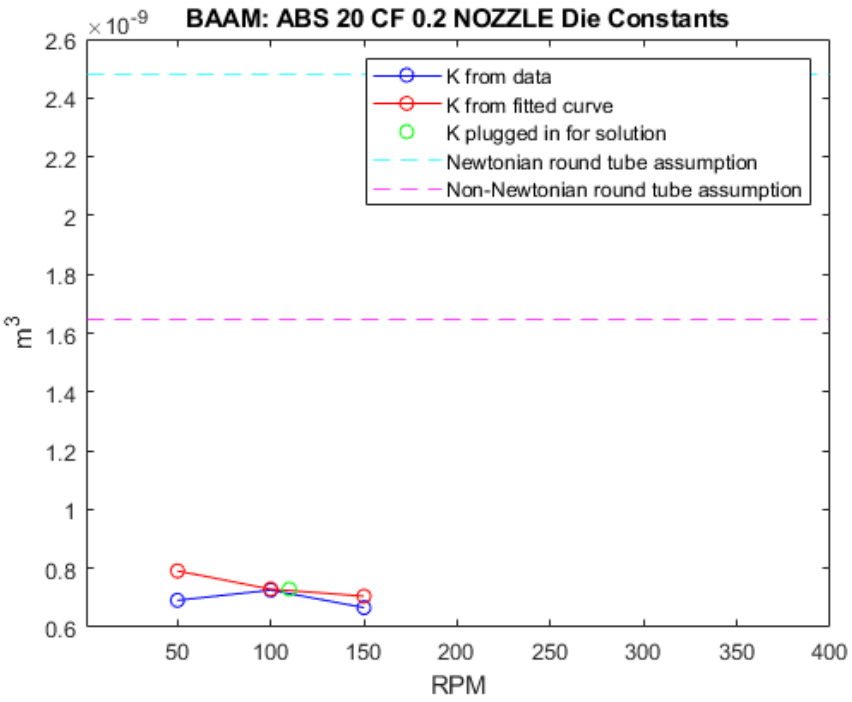

Figure 30: Die constants from BAAM 0.2 nozzle tests.

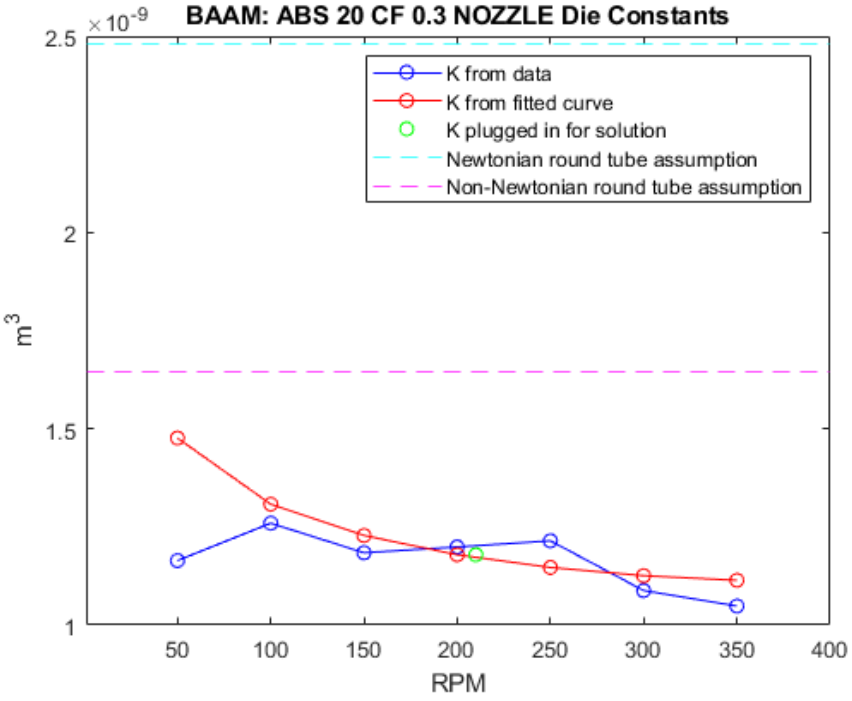

Figure 31: Die constants from BAAM 0.3 nozzle tests.

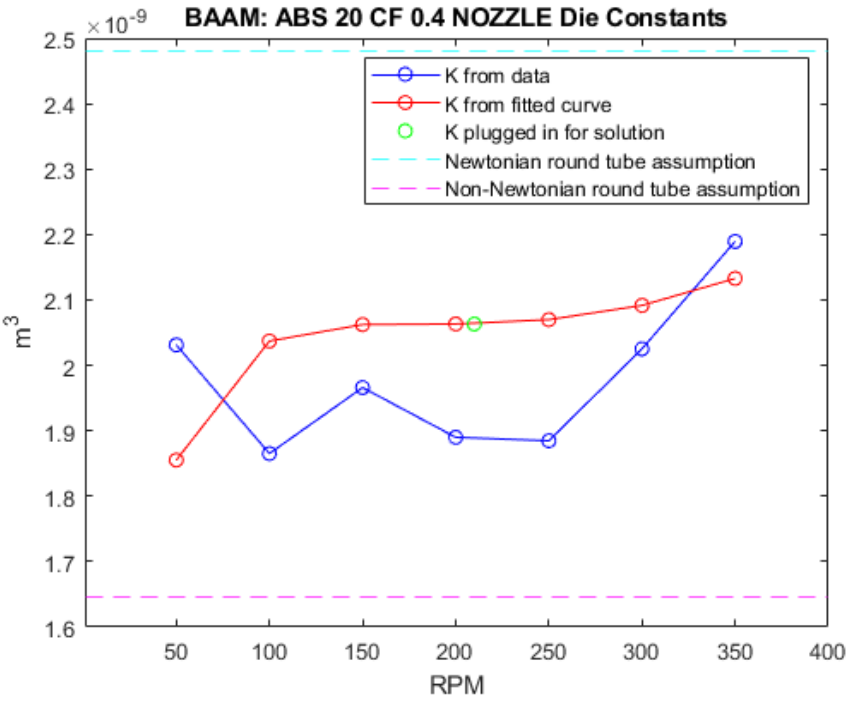

Figure 32: Die constants from BAAM 0.4 nozzle tests.

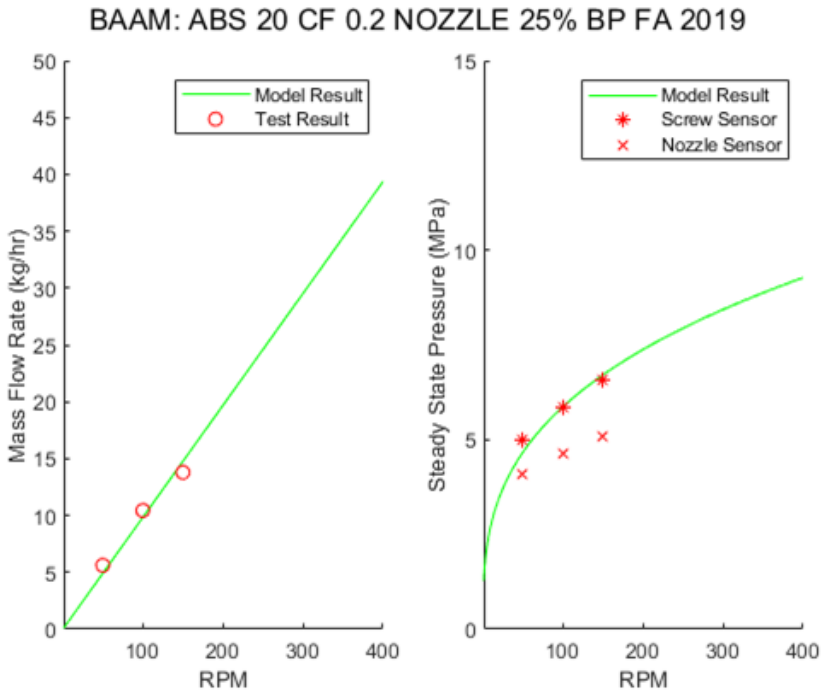

Figure 33: Flow rate and pressure results for BAAM 0.2 nozzle tests and code.

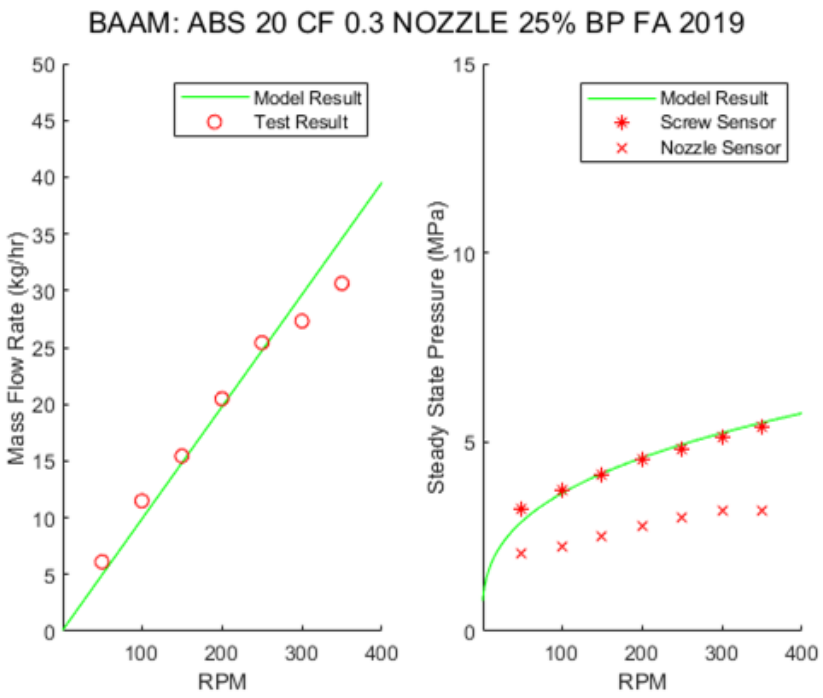

Figure 34: Flow rate and pressure results for BAAM 0.3 nozzle tests and code.

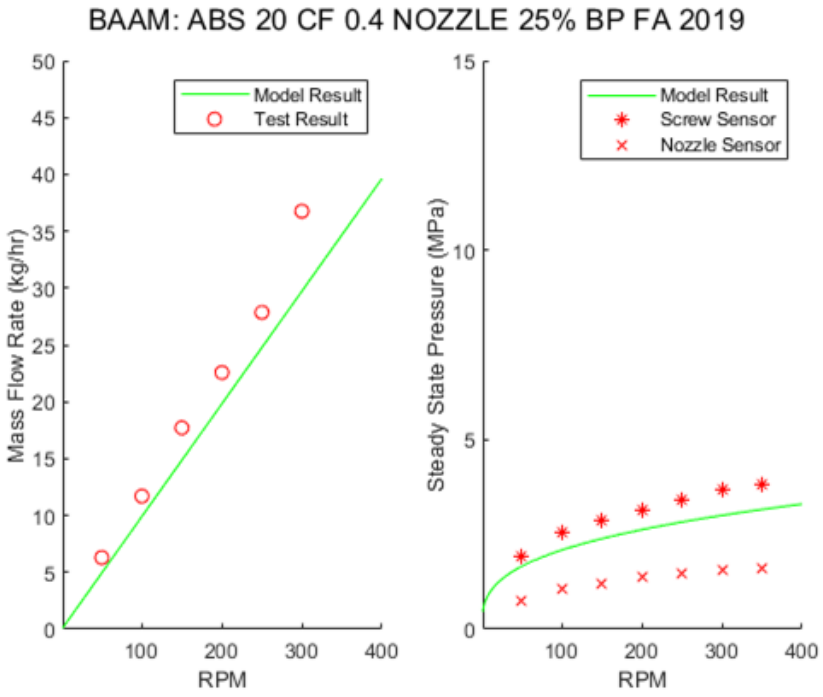

Figure 35: Flow rate and pressure results for BAAM 0.4 nozzle tests and code.

data for the 0.4 inch nozzle is trending above the analytical prediction. It is possible that this inaccuracy in only the 0.4 inch nozzle is due to it not providing proper back pressure to the machine, and the machine is over extruding as a result.

Lastly, Figures 36 through 38 show pressure map results for all the nozzle sizes. It is observed that as nozzle size increases the analytical model lines up more accurately with the nozzle data. This suggests the need for more rigorous flow theory in the nozzle than Hagen-Poiseuille.

4.8 Microtruder Experimental Results Compared to Analytical Model

The die constants for CF-ABS on the Microtruder with the 0.1 inch nozzle are shown in Figure 39. The die constants on the Microtruder were more linear than those on the BAAM. The full die constant plots are found in Appendix A3. Mass flow rate and pressure results for CF-ABS at all nozzle sizes are shown in Figures 40-43. It is observed that all analytical predictions are consistently below than the data. One explanation for the inaccurate result is the compression ratio of each screw. The Microtruder's compression ratio is 3.05, and the recommended range for ABS single screw extrusion is 2.25-2.7 (Campbell and Spalding 2013, 196).

The mass flow rate and pressure results for all other materials with the 0.1 inch nozzle are shown in Figures 44-47. The best fit is found to be CF-PLA, whereas neat PLA came out very poor. This result was actually expected, as the neat PLA's pellet size was much larger than Randcastle's recommended max as shown in Table 5. The CF-PLA pellet size was much smaller than the neat PLA and extruded properly, providing an accurate analytical prediction. The neat ABS's inaccuracy is again explained by the incorrect compression ratio for the material. The LLDPE result also came out inaccurate. This can be explained by the compression rate of the machine, as LLDPE requires a compression rate of less than 0.0055 without solid bed breakup

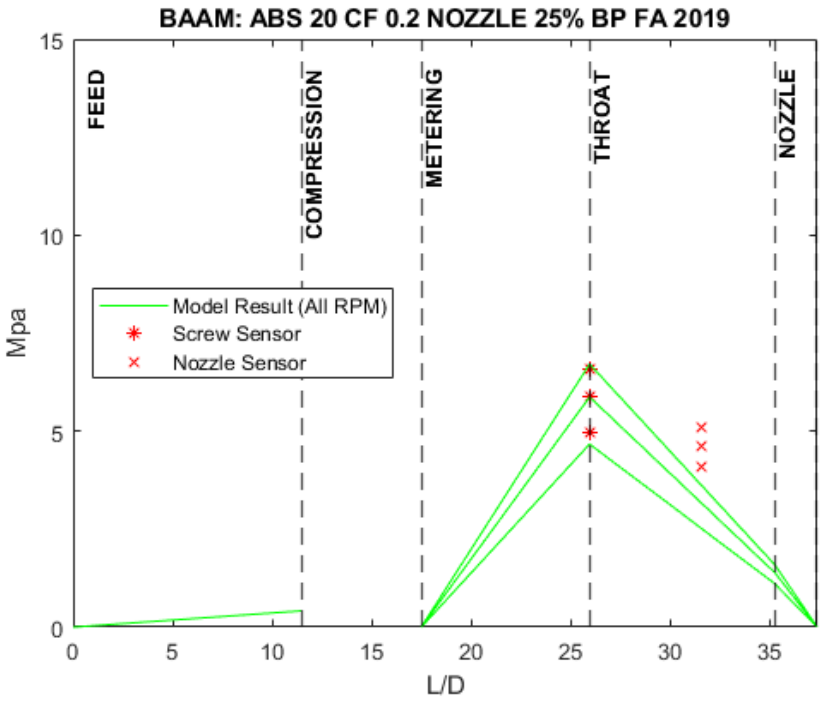

Figure 36: Pressure map results for BAAM 0.2 nozzle.

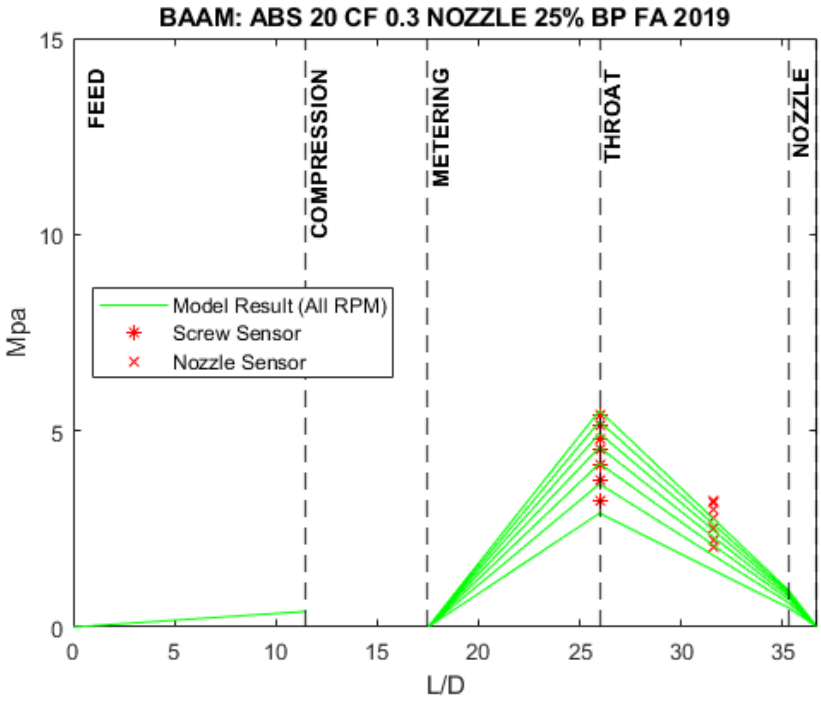

Figure 37: Pressure map results for BAAM 0.3 nozzle.

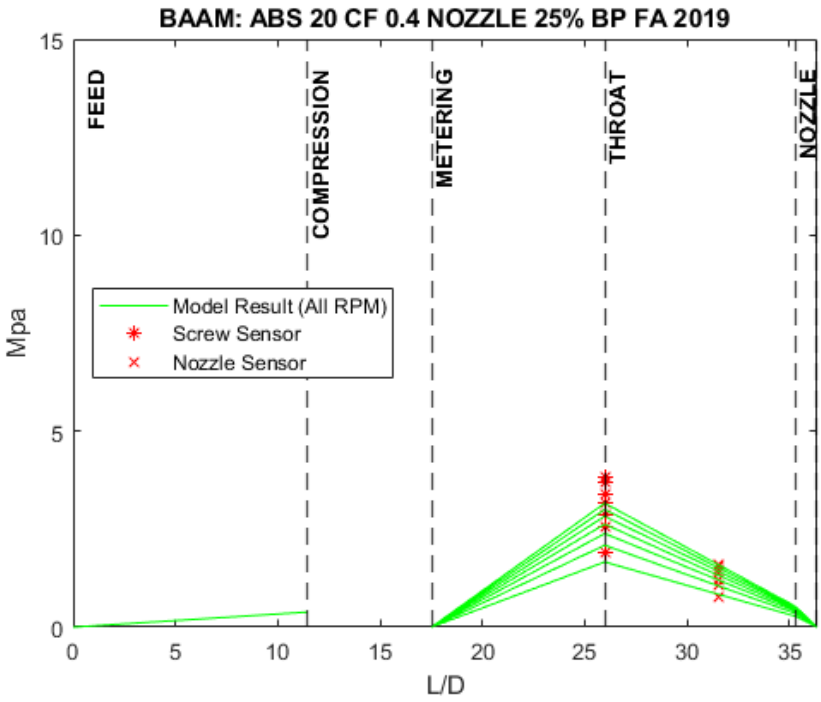

Figure 38: Pressure map results for BAAM 0.4 nozzle.

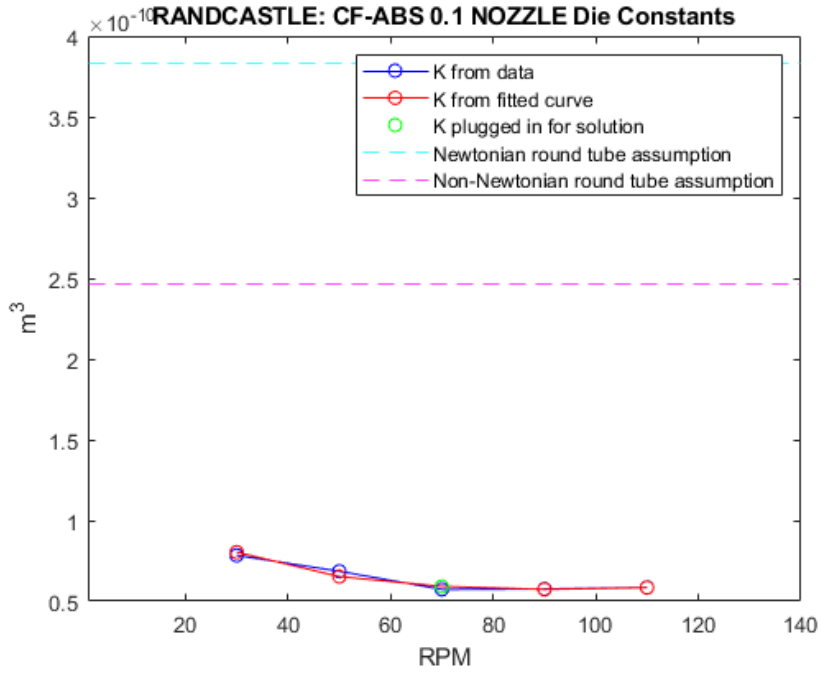

Figure 39: Die constants for CF-ABS Microtruder 0.1 nozzle tests.

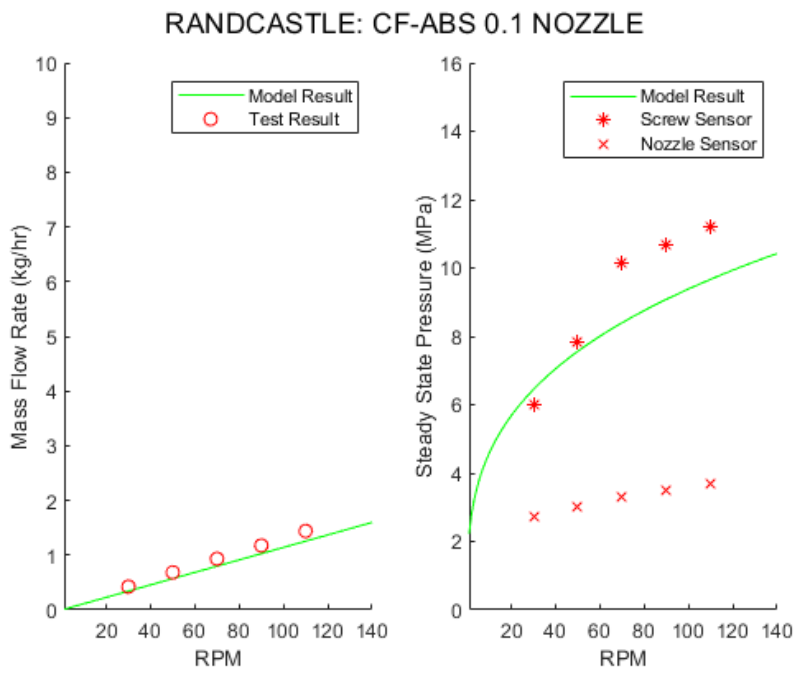

Figure 40: Flow rate and pressure results for Microtruder 0.1 nozzle and CF-ABS tests and code.

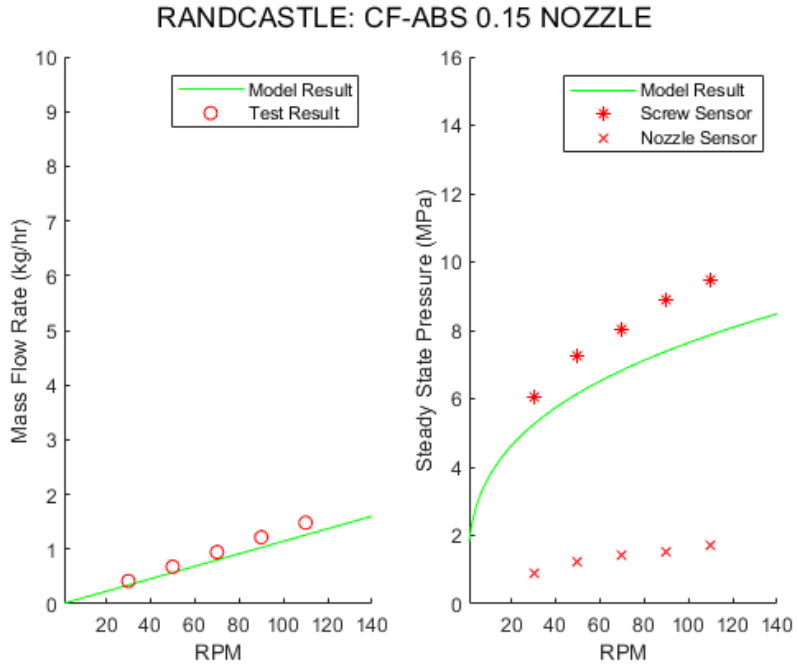

Figure 41: Flow rate and pressure results for Microtruder 0.15 nozzle and CF-ABS tests and code.

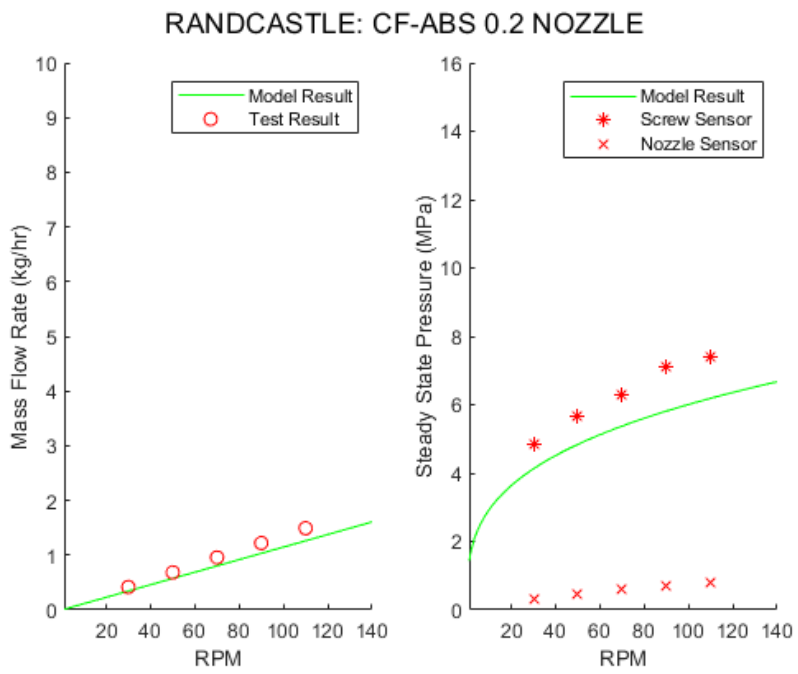

Figure 42: Flow rate and pressure results for Microtruder 0.2 nozzle and CF-ABS tests and code.

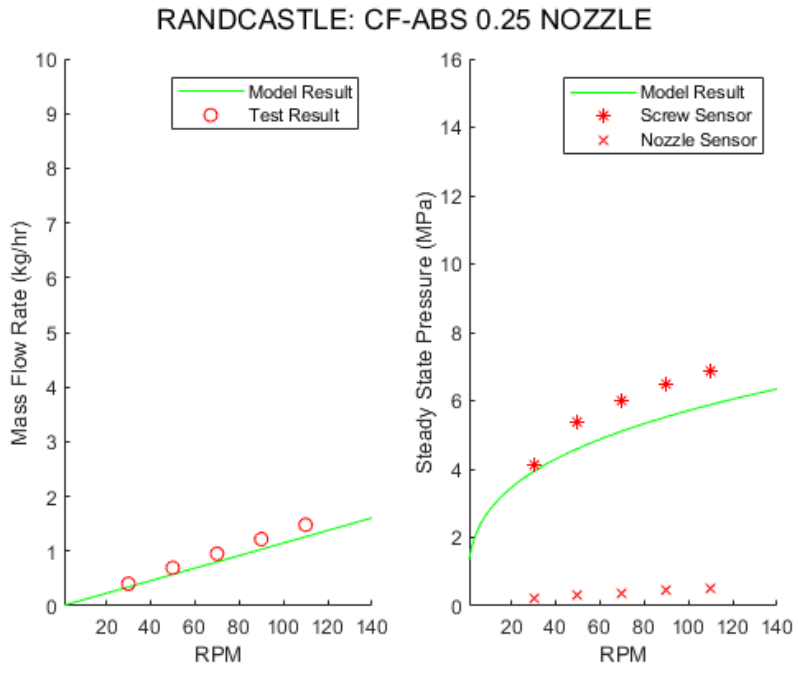

Figure 43: Flow rate and pressure results for Microtruder 0.25 nozzle and CF-ABS tests and code.

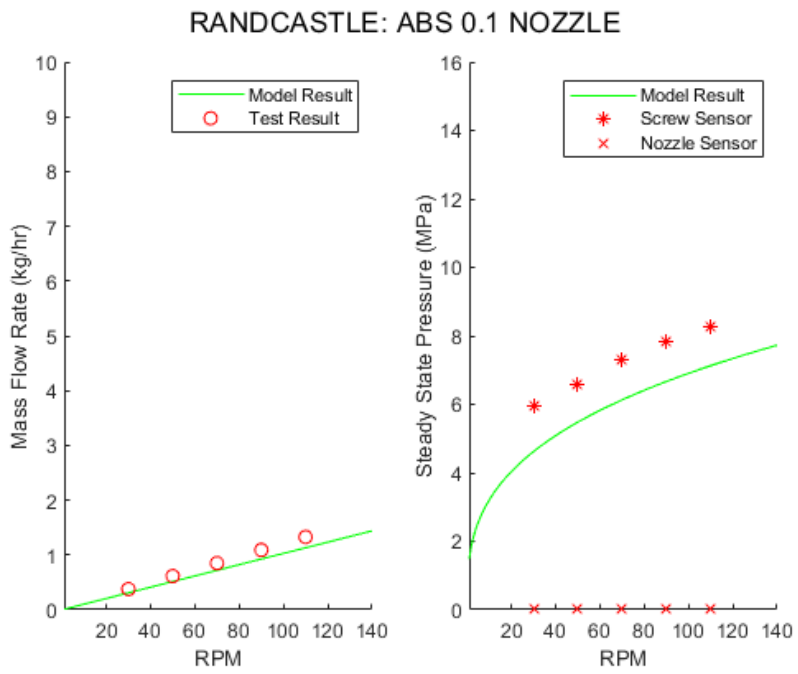

Figure 44: Flow rate and pressure results for Microtruder 0.1 nozzle and ABS tests and code.

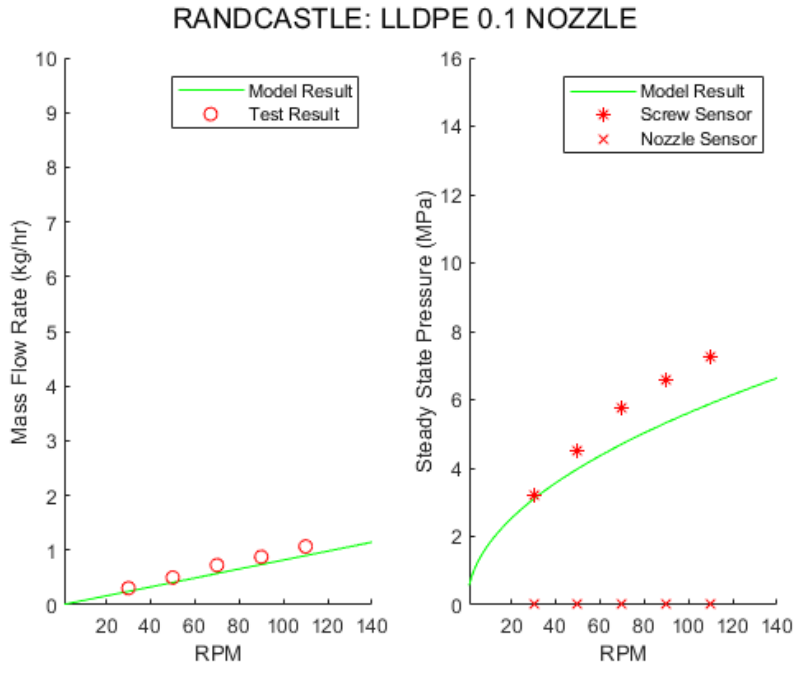

Figure 45: Flow rate and pressure results for Microtruder 0.1 nozzle and LLDPE tests and code.

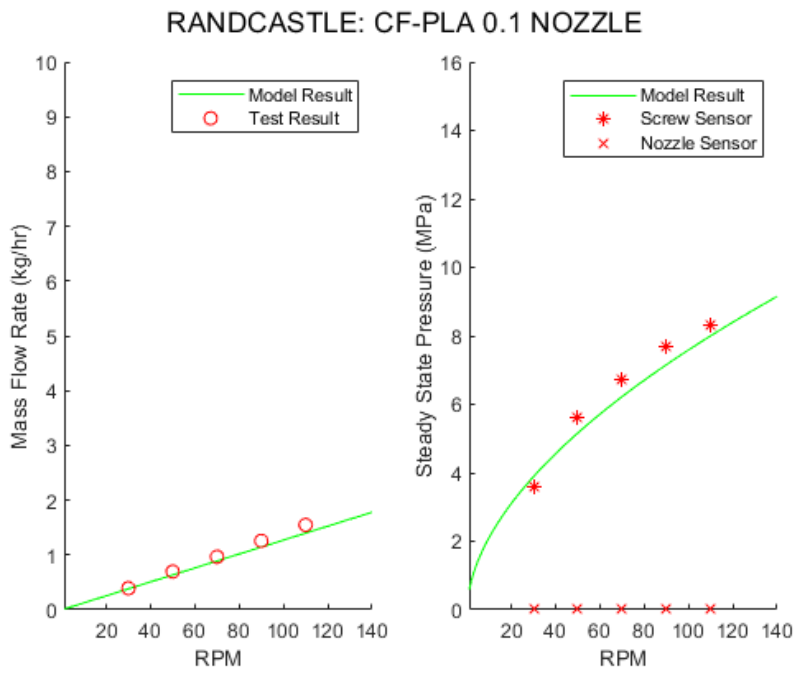

Figure 46: Flow rate and pressure results for Microtruder 0.1 nozzle and CF-PLA tests and code.

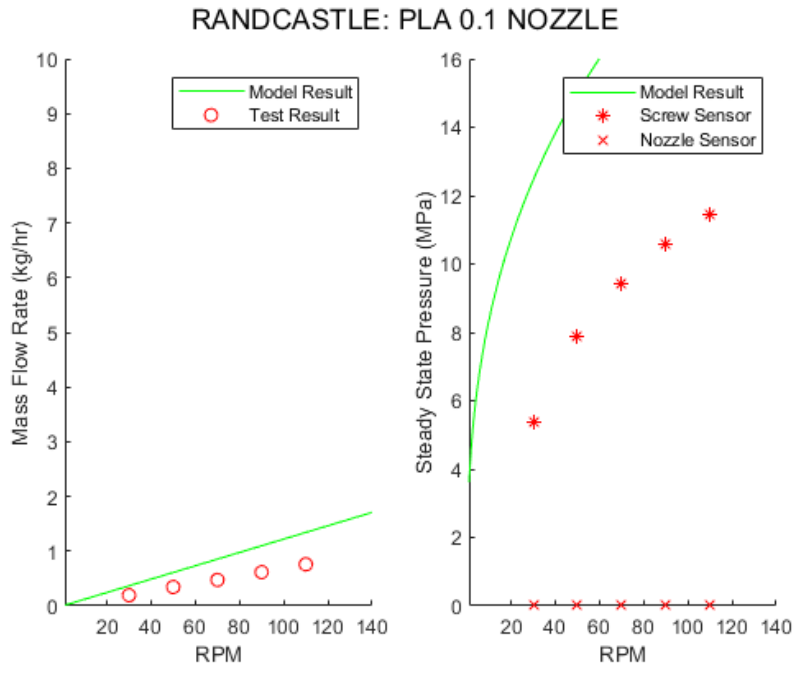

Figure 47: Flow rate and pressure results for Microtruder 0.1 nozzle and PLA tests and code.

issues (Campbell and Spalding 2013, 192), and the Microtruder has a compression rate of 0.00625. This is one example of why LLDPE is not seen in the additive extrusion field and is only used as a purge material with the BAAM. The complete set of Microtruder data plots can be found in Appendix A4, as well as tabulated data in Appendix A5.

Chapter 5: Summary and Conclusions

5.1 Summary of Research Work

This work stemmed from the goal of improving print quality through more accurate print settings. To meet this demand, predictions and simulations of single screw extrusion had to be made and tailored to the machines at hand: the BAAM at the MDF and the Microtruder at UT. Several models, methods, and traditions were explored before settling on Newtonian theory for a rate controlling metering zone to estimate discharge pressure and machine output. In addition to the theory for the metering zone, theories for the feed zone, compression zone, and nozzle were added to complete the pressure map down throughout each system. A Matlab code was developed to house these theories and was written in such a way that new machines, materials, data, and theory can be easily added on. A wide variety of pressure and flow rate data was gathered from both machines to ensure validity of theory. The result of this work allows for testing of new machine settings and materials without performing timely physical testing.

5.2 Conclusions

Several conclusions can be made from the results of this work:

(i) When nozzle size is equal to throat size of the machine, extrusion issues will appear due to low back pressure in the system. The BAAM accounts for this via the adjustable back pressure screw.

(ii) Die constants have a large impact theory accuracy. It is crucial to gather accurate data to properly encapsulate the die geometry into a die constant.

(iii) Non-Newtonian effects must be accounted for, for the materials and systems tested. In early testing using just the Newtonian assumption, the analytical pressures diverged wildly from reality.

(iv) Screw designs can be better tailored to material demands, namely, on the Microtruder system. Several extrusion issues arose in Microtruder testing, and the theory reinforced this idea.

5.3 Future Work

From the beginning it was known that this work should be done with future work in mind. Due to the broad scope of this research, there is a large area of potential for expansion and use. Direct use of this work includes improving print parameters through theory estimation, testing of new material grades and comparing to previous material grades, and finding machine limits for certain settings and materials.

The BAAM system is naturally of specific interest for future work. More data can be gathered, especially at more back pressure screw settings, and a full map of die constants for the system can be generated. The tests can be ran with the gantry in-air and not printing for more accurate pressure and flow rate data.

As a result of setup for this study, the Microtruder is now outfitted for quick testing in our laboratory with a die similar to that of the BAAM system. This removes the need to go through the MDF for certain data and adds a simpler direct source at UT.

Lastly, and potentially most important, the code is designed such that new models and theories can be tacked on. Certain research targets certain areas of the screw or new machine design can be united with the code resulting from this work.

References

Campbell, Gregory, and Mark Spalding. 2013. *Analyzing and Troubleshooting Single-Screw Extruders*. Munich: Hanser Publications.

Middleman, Stanley. 1977. *Fundamentals of Polymer Processing*. New York: McGraw-Hill.

Rauwendaal, Chris. 2014. *Polymer Extrusion.* 5th ed. Munich: Hanser Publications.

Tadmor, Zehev, and Costas Gogos. 2006. *Principles of Polymer Processing*. 2nd ed. Hoboken: John Wiley & Sons Incorporated.

Tadmor, Zehev, and Imrich Klein. 1970. *Engineering Principles of Plasticating Extrusion.* New York: Van Nostrand Reinhold Company.

“Transducer Mounting Hole Machining Tool Kit Manual”. 2020. Dynisco. https://www.dynisco.com/userfiles/files/Mounting%20Hole%20Machining%20Tool%20Kit.pdf.

Vlachopoulos, John, and John Wagner. 2001. *SPE Guide on Extrusion Technology and Troubleshooting*. Brookfield: Society for Plastic Engineers.

"What is a Microtruder?". 2020. Randcastle Extrusion Systems. http://www.randcastle.com/mcrtrdr.html.

“7000 Series Capillary Rheometers & LabKARS Software”. 2020. Dynisco. https://www.dynisco.com/userfiles/files/lcr7000_series_ver_2_4.pdf

Appendix

A1. Material Product Information

All materials were provided by Techmer PM LLC.

Material	Product Label
LLDPE	PF-0218-F
Neat PLA	Natureworks 4043D
CF-PLA	Electrafil® PLA 2007 3DP
Neat ABS	Hifill® ABS 1512 3DP
CF-ABS	Electrafil® ABS 1501 3DP

A2. LCR Tabulated Test Data

Laboratory Capillary Rheometer Readings and Relevant Info for PLA @ 175 °C - Trial 1									
Charge #:	506		Point	Sensor1 (N)	Pos (mm)	Ram (mm/min)	Time (sec)	Stress (Pa)	Rate (1/s)	Visc. (Pa-s)
Operator:	CDH		1	7499	132.3	345.51	65.65	1308569	9999.99	130.9
Material:	PLA		2	6223	138.3	231.59	67.17	1085926	6702.89	162
Machine:	7001		3	5039	142.2	155.23	68.69	879201	4492.86	195.7
Date:	5/29/2020 12:36		4	4536	146.7	104.05	71.27	791487	3011.5	262.8
Sample ID:	5.29.2020 Neat PLA - 175 C	Functional Form : PowerLaw	5	3775	153.2	69.74	76.88	658724	2018.57	326.3
Lot #:	Techmer	Viscosity = A * (Shear Rate)^B	6	3431	157.9	46.75	82.95	598624	1353.03	442.4
Die:	CX295-20	Sample ID: 5.29.2020 Neat PLA - 175 C [506]	7	3105	161.9	31.34	90.58	541772	906.91	597.4
Temperature (°C):	175		8	2814	165.5	21	100.78	490984	607.91	807.7
Start Position (mm):	100		9	2490	169.3	14.08	117.05	434565	407.45	1066.5
Melt Time (s):	60		10	2250	172.1	9.44	134.84	392549	273.13	1437.2
Rcal (%):	99.99		11	2011	174.5	6.33	158.25	350966	183.06	1917.2
Melt Pause (s):	0		12	1813	176.4	4.24	185.24	316313	122.72	2577.6
Sensor 1:	LC-103N	Parameters:	13	1594	178.3	2.84	225.95	278195	82.25	3382.1
Sensor 2:	PT-142BAR	A = 42473 (483.7)	14	1357	180	1.91	279.33	236829	55.14	4295.4
Program Name:	66:Neat PLA - 175	B = -0.649 (0.0018)	15	1127	181.4	1.28	342.43	196653	36.96	5320.8
Comment:	constant 12 mm/min	RMS Error = 18.880%	16	899	182.4	0.86	418.24	156911	24.77	6333.5
			17	709	183.1	0.57	491.02	123666	16.61	7444
			18	550	183.6	0.39	565.78	95944	11.14	8610.4
			19	395	184.3	0.26	725.06	68872	7.47	9223.3
			20	302	184.7	0.17	850.74	52737	5.01	10532.5

Laboratory Capillary Rheometer Readings and Relevant Info for PLA @ 175 °C - Trial 2									
Charge #:	507		Point	Sensor1 (N)	Pos (mm)	Ram (mm/min)	Time (sec)	Stress (Pa)	Rate (1/s)	Visc. (Pa-s)
Operator:	CDH		1	7357	126.1	345.51	64.61	1283771	9999.99	128.4
Material:	PLA		2	5538	132.2	231.59	66.18	966266	6702.89	144.2
Machine:	7001		3	4781	136.1	155.23	67.68	834261	4492.86	185.7
Date:	5/29/2020 13:05		4	4409	140.5	104.05	70.21	769396	3011.5	255.5
Sample ID:	5.29.2020 Neat PLA - 175 C #2	Functional Form : PowerLaw	5	3601	147	69.74	75.81	628403	2018.57	311.3
Lot #:	Techmer	Viscosity = A * (Shear Rate)^B	6	3335	151.4	46.75	81.44	581947	1353.03	430.1
Die:	CX295-20	Sample ID: 5.29.2020 Neat PLA - 175 C #2 [507]	7	3051	155.6	31.34	89.57	532459	906.91	587.1
Temperature (°C):	175		8	2759	159.2	21	99.75	481346	607.91	791.8
Start Position (mm):	100		9	2441	163	14.08	116.01	426010	407.45	1045.5
Melt Time (s):	60		10	2179	166	9.44	135.36	380204	273.13	1392
Rcal (%):	99.99		11	1961	168.7	6.33	160.78	342194	183.06	1869.3
Melt Pause (s):	0		12	1770	170.6	4.24	187.79	308841	122.72	2516.7
Sensor 1:	LC-103N	Parameters:	13	1550	172.5	2.84	229.48	270399	82.25	3287.3
Sensor 2:	PT-142BAR	A = 41417 (467.6)	14	1318	174.2	1.91	282.39	229898	55.14	4169.7
Program Name:	66:Neat PLA - 175	B = -0.652 (0.0018)	15	1085	175.8	1.28	357.2	189398	36.96	5124.5
Comment:	10000-5 /s shear rate	RMS Error = 21.883%	16	868	177.1	0.86	446.21	151389	24.77	6110.6
			17	685	177.7	0.57	515.41	119551	16.61	7196.3
			18	522	178.3	0.39	598.34	91071	11.14	8173.1
			19	379	178.8	0.26	733.2	66165	7.47	8860.8
			20	268	179.3	0.17	885.33	46781	5.01	9343

Laboratory Capillary Rheometer Readings and Relevant Info for 20% CF-PLA @ 210 °C - Trial 1									
Charge #:	531		**Point**	**Sensor1 (N)**	**Pos (mm)**	**Ram (mm/min)**	**Time (sec)**	**Stress (Pa)**	**Rate (1/s)**	**Visc. (Pa-s)**
Operator:	CDH		1	1757	111	172.76	63.85	306619	4999.99	61.3
Material:	20% CF PLA		2	1518	121.3	120.1	68.99	264813	3475.97	76.2
Machine:	7001		3	1354	127	83.49	73.09	236219	2416.47	97.8
Date:	########		4	1150	132.5	58.04	78.8	200586	1679.91	119.4
Sample ID:	6.22.2020 20% CF PLA 210 C #1	**Functional Form : PowerLaw**	5	977	137.3	40.35	86.02	170476	1167.86	146
Lot #:	Techmer	**Viscosity = A * (Shear Rate)^B**	6	804	148.6	28.05	110.22	140367	811.9	172.9
Die:	CX295-20	**Sample ID: 6.22.2020 20% CF PLA 210 C #1 [531]**	7	667	154	19.5	126.69	116323	564.41	206.1
Temperature (°C):	210		8	528	158	13.56	144.67	92062	392.37	234.6
Start Position (mm):	100		9	433	161.6	9.43	167.3	75491	272.78	276.7
Melt Time (s):	60		10	346	163.2	6.55	182.24	60327	189.63	318.1
Rcal (%):	99.97		11	276	164.7	4.55	201.71	48089	131.83	364.8
Melt Pause (s):	0		12	215	166.1	3.17	229.28	37475	91.66	408.8
Sensor 1:	LC-103N	**Parameters:**	13	163	168.1	2.2	282.66	28485	63.7	447.2
Sensor 2:	PT-142BAR	A = 2785 (33.5)	14	117	169.4	1.53	335.19	20470	44.28	462.3
Program Name:	77:20 CF PLA - 210 C	B = -0.444 (0.0021)	15	101	169.9	1.06	362.89	17546	30.79	569.8
Comment:	5000-5 /s	RMS Error = 10.528%	16	90	170.1	0.74	379.76	15705	21.42	733.3
			17	79	170.2	0.51	396.24	13863	14.88	931.9
			18	64	170.5	0.36	442.78	11156	10.33	1079.7
			19	58	170.7	0.25	476.19	10073	7.21	1397.7
			20	50	170.8	0.17	529.28	8665	5.01	1730.5

Laboratory Capillary Rheometer Readings and Relevant Info for 20% CF-PLA @ 210 °C - Trial 2									
Charge #:	532		**Point**	**Sensor1 (N)**	**Pos (mm)**	**Ram (mm/min)**	**Time (sec)**	**Stress (Pa)**	**Rate (1/s)**	**Visc. (Pa-s)**
Operator:	CDH		1	1375	117.5	172.76	66.11	239902	4999.99	48
Material:	20% CF PLA		2	1386	121.6	120.1	68.17	241851	3475.97	69.6
Machine:	7001		3	1314	127.3	83.49	72.29	229288	2416.47	94.9
Date:	########		4	1087	132.3	58.04	77.43	189647	1679.91	112.9
Sample ID:	6.22.2020 20% CF PLA 210 C #2	**Functional Form : PowerLaw**	5	873	137.4	40.35	85.16	152389	1167.86	130.5
Lot #:	Techmer	**Viscosity = A * (Shear Rate)^B**	6	736	141.5	28.05	93.92	128345	811.9	158.1
Die:	CX295-20	**Sample ID: 6.22.2020 20% CF PLA 210 C #2 [532]**	7	600	145.2	19.5	105.27	104625	564.41	185.4
Temperature (°C):	210		8	505	148.6	13.56	120.23	88163	392.37	224.7
Start Position (mm):	100		9	387	152.1	9.43	142.4	67584	272.78	247.8
Melt Time (s):	60		10	314	153.6	6.55	156.34	54804	189.63	289
Rcal (%):	99.97		11	244	154.8	4.55	173.26	42565	131.83	322.9
Melt Pause (s):	0		12	186	155.6	3.17	188.08	32384	91.66	353.3
Sensor 1:	LC-103N	**Parameters:**	13	143	156.5	2.2	210.67	24911	63.7	391
Sensor 2:	PT-142BAR	A = 1857 (21.5)	14	124	156.8	1.53	224.43	21662	44.28	489.2
Program Name:	77:20 CF PLA - 210 C	B = -0.402 (0.0020)	15	93	157.1	1.06	243.25	16246	30.79	527.6
Comment:	5000-5 /s	RMS Error = 20.106%	16	73	157.4	0.74	263.3	12780	21.42	596.7
			17	53	157.6	0.51	282.83	9206	14.88	618.8
			18	41	157.7	0.36	305.98	7148	10.33	691.8
			19	30	157.8	0.25	339.33	5307	7.21	736.4
			20	20	158	0.17	388.87	3466	5.01	692.2

Laboratory Capillary Rheometer Readings and Relevant Info for ABS @ 220 °C - Trial 1									
Charge #:	534		**Point**	**Sensor1 (N)**	**Pos (mm)**	**Ram (mm/min)**	**Time (sec)**	**Stress (Pa)**	**Rate (1/s)**	**Visc. (Pa-s)**
Operator:	CDH		1	2921	114	345.51	62.51	509697	9999.99	51
Material:	Neat ABS		2	2540	125.9	231.59	65.6	443196	6702.89	66.1
Machine:	7001		3	2364	133.5	155.23	68.7	412436	4492.86	91.8
Date:	########		4	2032	141.1	104.05	72.82	354491	3011.5	117.7
Sample ID:	6.22.2020 Neat ABS - 210 C	**Functional Form : PowerLaw**	5	1837	145.8	69.74	76.94	320483	2018.57	158.8
Lot #:	Techmer	**Viscosity = A * (Shear Rate)^B**	6	1594	149.8	46.75	82.06	278134	1353.03	205.6
Die:	CX295-20	**Sample ID: 6.22.2020 Neat ABS - 210 C [534]**	7	1469	153.6	31.34	89.29	256256	906.91	282.6
Temperature (°C):	220		8	1301	157.2	21	99.59	227013	607.91	373.4
Start Position (mm):	100		9	1162	160.8	14.08	115.1	202752	407.45	497.6
Melt Time (s):	60		10	1031	163.3	9.44	131.07	179899	273.13	658.7
Rcal (%):	99.97		11	912	165.3	6.33	149.56	159212	183.06	869.7
Melt Pause (s):	0		12	790	166.3	4.24	165.02	137876	122.72	1123.5
Sensor 1:	LC-103N	**Parameters:**	13	680	167.2	2.84	182.38	118705	82.25	1443.1
Sensor 2:	PT-142BAR	A = 21294 (245.2)	14	570	168.2	1.91	214.75	99535	55.14	1805.3
Program Name:	79:Neat ABS - 220 C	B = -0.665 (0.0018)	15	487	168.8	1.28	245.55	85022	36.96	2300.4
Comment:	10000-5 /s	RMS Error = 12.447%	16	399	169.4	0.86	285.57	69642	24.77	2811
			17	336	169.7	0.57	318.35	58703	16.61	3533.5
			18	264	170.2	0.39	400.15	46139	11.14	4140.7
			19	227	170.5	0.26	466.89	39641	7.47	5308.7
			20	172	170.8	0.17	575.39	30001	5.01	5991.8

Laboratory Capillary Rheometer Readings and Relevant Info for ABS @ 220 °C - Trial 2									
Charge #:	535		**Point**	**Sensor1 (N)**	**Pos (mm)**	**Ram (mm/min)**	**Time (sec)**	**Stress (Pa)**	**Rate (1/s)**	**Visc. (Pa-s)**
Operator:	CDH		1	2912	113.9	345.51	62.48	508072	9999.99	50.8
Material:	Neat ABS		2	2541	127.6	231.59	66.05	443304	6702.89	66.1
Machine:	7001		3	2260	132.9	155.23	68.11	394349	4492.86	87.8
Date:	########		4	2035	140.1	104.05	72.22	355033	3011.5	117.9
Sample ID:	.22.2020 Neat ABS - 210 C #2	**Functional Form : PowerLaw**	5	1835	144.2	69.74	75.83	320266	2018.57	158.7
Lot #:	Techmer	**Viscosity = A * (Shear Rate)^B**	6	1641	149	46.75	81.97	286258	1353.03	211.6
Die:	CX295-20	**Sample ID: 6.22.2020 Neat ABS - 210 C #2 [535]**	7	1469	153	31.34	89.71	256365	906.91	282.7
Temperature (°C):	220		8	1312	156.5	21	99.53	228963	607.91	376.6
Start Position (mm):	100		9	1164	160.1	14.08	114.96	203185	407.45	498.7
Melt Time (s):	60		10	1029	162.2	9.44	128.76	179574	273.13	657.5
Rcal (%):	99.97		11	899	164.1	6.33	146.76	156830	183.06	856.7
Melt Pause (s):	0		12	784	165.5	4.24	166.36	136793	122.72	1114.7
Sensor 1:	LC-103N	**Parameters:**	13	669	166.8	2.84	193.86	116756	82.25	1419.4
Sensor 2:	PT-142BAR	A = 21363 (245.8)	14	572	167.6	1.91	219.34	99860	55.14	1811.2
Program Name:	79:Neat ABS - 220 C	B = -0.666 (0.0018)	15	483	168.2	1.28	244.95	84263	36.96	2279.9
Comment:	10000-5 /s	RMS Error = 12.476%	16	404	168.7	0.86	281.53	70508	24.77	2846
			17	337	168.9	0.57	304.11	58811	16.61	3540.1
			18	274	169.2	0.39	343.66	47872	11.14	4296.2
			19	214	169.5	0.26	426.02	37366	7.47	5004.1
			20	176	169.7	0.17	494.3	30651	5.01	6121.6

Laboratory Capillary Rheometer Readings and Relevant Info for 20% CF-ABS @ 250 °C - Trial 1									
Charge #:	156		**Point**	**Sensor1 (N)**	**Pos (mm)**	**Ram (mm/min)**	**Time (sec)**	**Stress (Pa)**	**Rate (1/s)**	**Visc. (Pa-s)**
Operator:	CA		1	2936	110.7	345	81.92	512339	9985.17	51.3
Material:	ABS 20CF		2	2670	117.2	258.87	83.43	465980	7492.32	62.2
Machine:	7001		3	2450	122.1	194.24	84.94	427527	5621.82	76
Date:	2/24/2017 13:27		4	2267	128.4	145.75	87.53	395574	4218.29	93.8
Sample ID:	ABS 20 wt CF 250C high to low shear 1	**Functional Form : PowerLaw**	5	2167	133	109.36	90.04	378135	3165.18	119.5
Lot #:	Journal PPSU	**Viscosity = A * (Shear Rate)^B**	6	2046	138.6	82.06	94.1	357013	2374.97	150.3
Die:	CX295-20	**Sample ID: ABS 20 wt CF 250C high to low shear 1 [156]**	7	1955	142.2	61.57	97.69	341199	1782.05	191.5
Temperature (°C):	250		8	1881	146.9	46.2	103.79	328201	1337.14	245.4
Start Position (mm):	100		9	1810	150.7	34.67	110.42	315852	1003.32	314.8
Melt Time (s):	80		10	1726	154.9	26.01	120.07	301230	752.82	400.1
Rcal (%):	100		11	1610	158.2	19.52	130.24	280866	564.87	497.2
Melt Pause (s):	0		12	1412	162.1	14.64	146.02	246313	423.86	581.1
Sensor 1:	LC-103N	**Parameters:**	13	1270	165.6	10.99	165.35	221617	318.05	696.8
Sensor 2:	PT-142BAR	A = 40424 (498.8)	14	1119	169.4	8.24	192.9	195187	238.63	817.9
Program Name:	24:ABS 20CF	B = -0.737 (0.0019)	15	1004	171.3	6.19	212.2	175149	179.07	978.1
Comment:	high to low shear RATE	RMS Error = 6.085%	16	990	172.5	4.64	226.95	172766	134.35	1285.9
			17	870	173.6	3.48	246.29	151860	100.81	1506.5
			18	786	174.6	2.61	270.22	137238	75.66	1814
			19	750	175.1	1.96	284.47	130955	56.76	2307.3
			20	660	175.7	1.47	306.85	115141	42.6	2702.6
			21	613	176.1	1.1	332.27	106909	31.95	3345.9
			22	575	176.4	0.83	350.63	100410	23.96	4190
			23	536	176.6	0.62	374.53	93478	18	5192.6
			24	497	176.8	0.47	403.55	86654	13.49	6424.9
			25	471	177	0.35	427.41	82213	10.13	8115.9

Laboratory Capillary Rheometer Readings and Relevant Info for 20% ABS @ 250 °C - Trial 2									
Charge #:	157		**Point**	**Sensor1 (N)**	**Pos (mm)**	**Ram (mm/min)**	**Time (sec)**	**Stress (Pa)**	**Rate (1/s)**	**Visc. (Pa-s)**
Operator:	CA		4	2255	136.1	145.75	89.6	393407	4218.29	93.3
Material:	ABS 20CF		5	2157	140.7	109.36	92.11	376293	3165.18	118.9
Machine:	7001		6	2064	144.1	82.06	94.64	360154	2374.97	151.6
Date:	2/24/2017 13:57		7	1943	147.8	61.57	98.23	339032	1782.05	190.2
Sample ID:	ABS 20 wt CF 250C high to low shear 2	**Functional Form : PowerLaw**	8	1775	153.3	46.2	105.36	309678	1337.14	231.6
Lot #:	Journal PPSU	**Viscosity = A * (Shear Rate)^B**	9	1646	158	34.67	113.49	287257	1003.32	286.3
Die:	CX295-20	**Sample ID: ABS 20 wt CF 250C high to low shear 2 [157]**	10	1499	162.8	26.01	124.67	261477	752.82	347.3
Temperature (°C):	250		11	1365	166.4	19.52	135.89	238189	564.87	421.7
Start Position (mm):	100		12	1243	170.3	14.64	151.65	216959	423.86	511.9
Melt Time (s):	80		13	1154	172.9	10.99	165.92	201361	318.05	633.1
Rcal (%):	100		14	1115	175.2	8.24	183.19	194646	238.63	815.7
Melt Pause (s):	0		15	1048	176.8	6.19	197.95	182947	179.07	1021.7
Sensor 1:	LC-103N	**Parameters:**	16	984	177.8	4.64	211.7	171682	134.35	1277.9
Sensor 2:	PT-142BAR	A = 44332 (720.3)	17	922	178.8	3.48	228.98	160959	100.81	1596.7
Program Name:	24:ABS 20CF	B = -0.752 (0.0026)	18	859	179.6	2.61	246.86	149911	75.66	1981.5
Comment:	high to low shear RATE	RMS Error = 2.756	19	812	180.2	1.96	265.13	141679	56.76	2496.3
			20	759	180.8	1.47	289.55	132472	42.6	3109.4
			21	714	181.1	1.1	307.85	124673	31.95	3901.8
			22	665	181.4	0.83	329.72	116116	23.96	4845.3
			23	623	181.7	0.62	353.63	108642	18	6034.9
			24	587	181.9	0.47	381.12	102360	13.49	7589.4

Laboratory Capillary Rheometer Readings and Relevant Info for LLDPE @ 245 °C									
Charge #:	521		**Point**	**Sensor1 (N)**	**Pos (mm)**	**Ram (mm/min)**	**Time (sec)**	**Stress (Pa)**	**Rate (1/s)**	**Visc. (Pa-s)**
Operator:	CDH		1	3671	132.3	345.51	125.65	640641	9999.99	64.1
Material:	LLDPE		2	3283	136.2	231.59	126.67	572840	6702.89	85.5
Machine:	7001		3	2968	144.2	155.23	129.76	517820	4492.86	115.3
Date:	6/11/2020 14:45		4	2604	152.1	104.05	134.31	454460	3011.5	150.9
Sample ID:	6.11.2020 LLDPE 245 C Test 2	**Functional Form : PowerLaw**	5	2253	159.8	69.74	140.91	393049	2018.57	194.7
Lot #:	Techmer	**Viscosity = A * (Shear Rate)^B**	6	1918	165.7	46.75	148.55	334671	1353.03	247.3
Die:	CX295-20	**Sample ID: 6.11.2020 LLDPE 245 C Test 2 [521]**	7	1617	172.9	31.34	162.31	282142	906.91	311.1
Temperature (°C):	245		8	1357	177.1	21	174.5	236869	607.91	389.6
Start Position (mm):	100		9	1107	183.6	14.08	201.97	193113	407.45	474
Melt Time (s):	120		10	906	187.1	9.44	224.37	158129	273.13	579
Rcal (%):	100		11	731	189.2	6.33	244.74	127587	183.06	697
Melt Pause (s):	0		12	585	191.2	4.24	272.71	102134	122.72	832.3
Sensor 1:	LC-103N	**Parameters:**	13	464	192.5	2.84	300.68	80906	82.25	983.6
Sensor 2:	PT-142BAR	A = 6858 (77.1)	14	358	193.8	1.91	340.37	62494	55.14	1133.5
Program Name:	71:LLDPE-245 C-X295-20	B = -0.496 (0.0018)	15	278	194.5	1.28	376.5	48522	36.96	1312.8
Comment:	10000 - 5 /s	RMS Error = 22.463%	16	209	195.1	0.86	415.67	36500	24.77	1473.3
			17	163	195.3	0.57	437.55	28485	16.61	1714.6
			18	119	195.6	0.39	478.24	20687	11.14	1856.5
			19	92	195.7	0.26	518.44	16030	7.47	2146.7
			20	60	195.9	0.17	593.81	10398	5.01	2076.6

A3. Microtruder Die Constant Plots

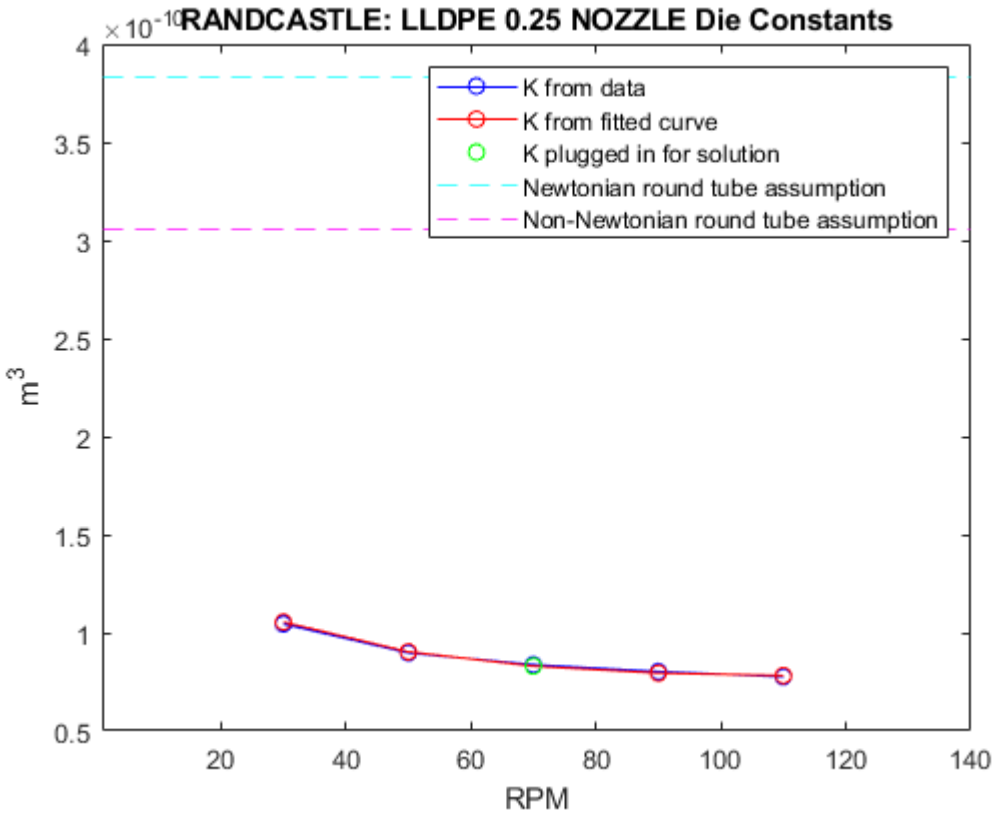

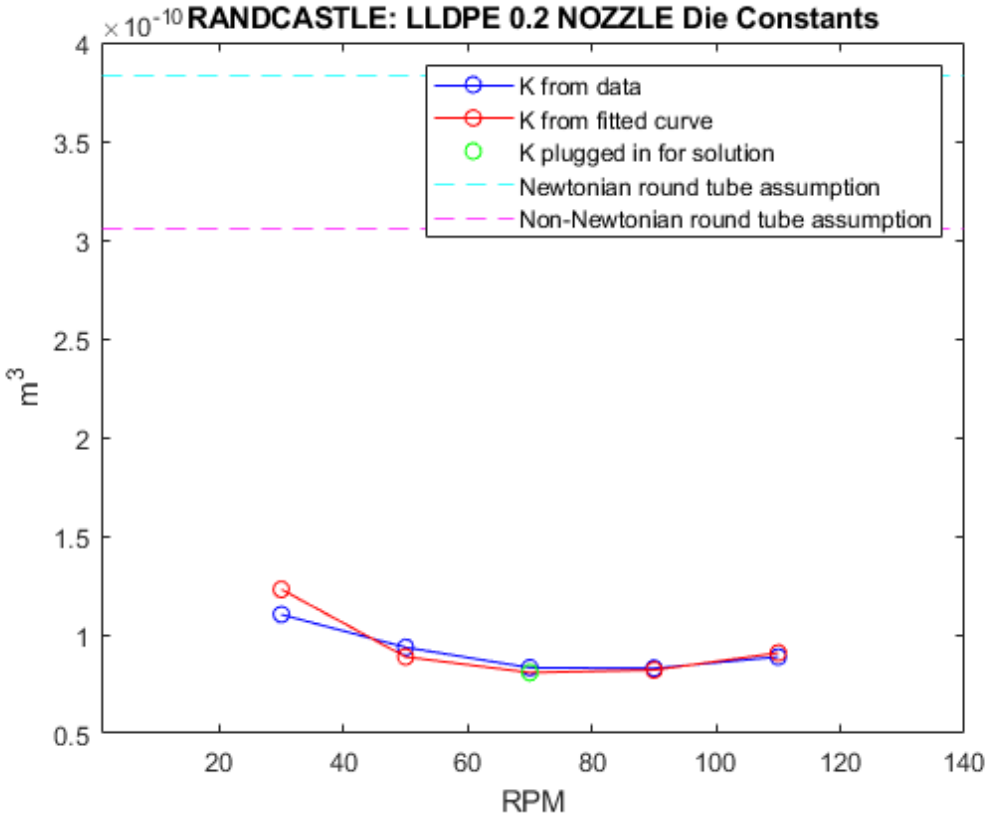
RANDCASTLE: LLDPE 0.2 NOZZLE Die Constants
×10^-10
K from data
K from fitted curve
K plugged in for solution
Newtonian round tube assumption
Non-Newtonian round tube assumption
m^3
RPM
4
3.5
3
2.5
2
1.5
1
0.5
20
40
60
80
100
120
140

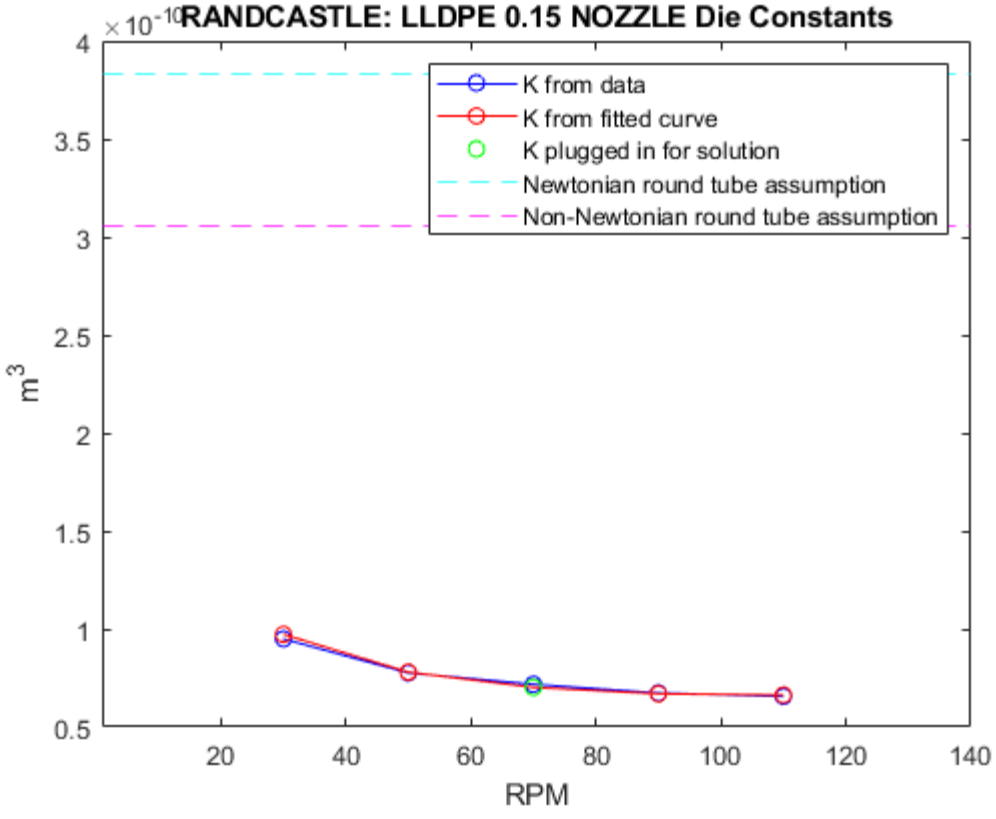
RANDCASTLE: LLDPE 0.15 NOZZLE Die Constants
×10^-10
K from data
K from fitted curve
K plugged in for solution
Newtonian round tube assumption
Non-Newtonian round tube assumption
m^3
RPM
4
3.5
3
2.5
2
1.5
1
0.5
20
40
60
80
100
120
140

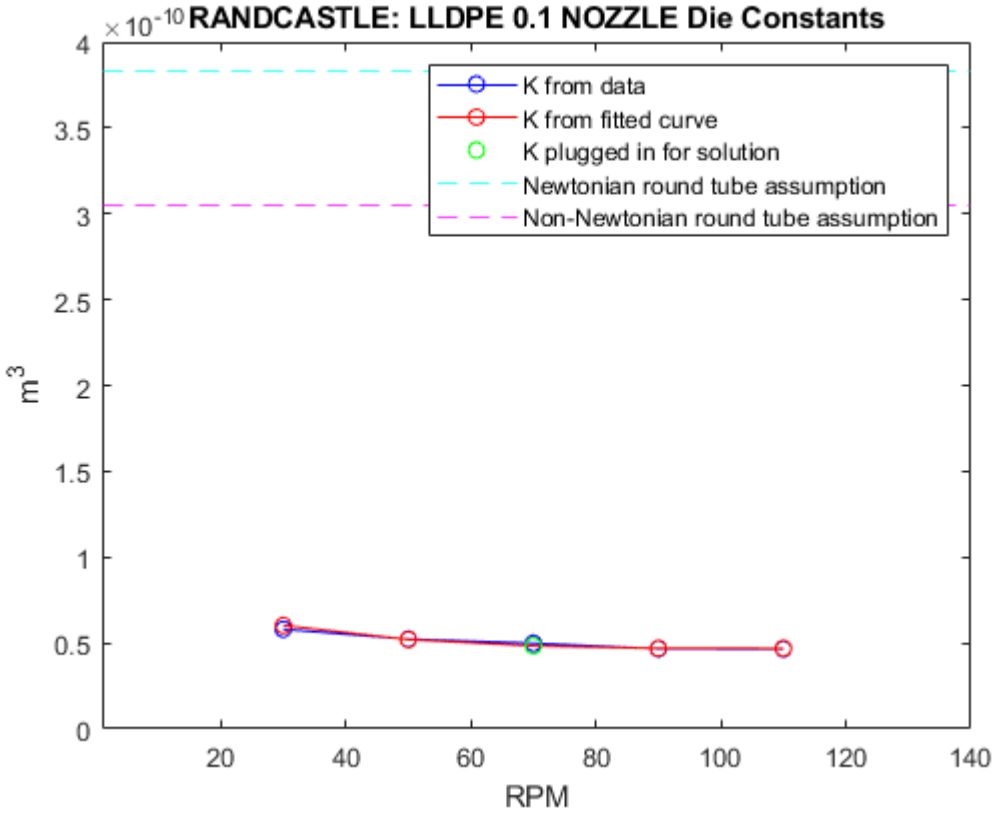
RANDCASTLE: LLDPE 0.1 NOZZLE Die Constants
×10^-10
K from data
K from fitted curve
K plugged in for solution
Newtonian round tube assumption
Non-Newtonian round tube assumption
m^3
RPM
0
0.5
1
1.5
2
2.5
3
3.5
4
20
40
60
80
100
120
140

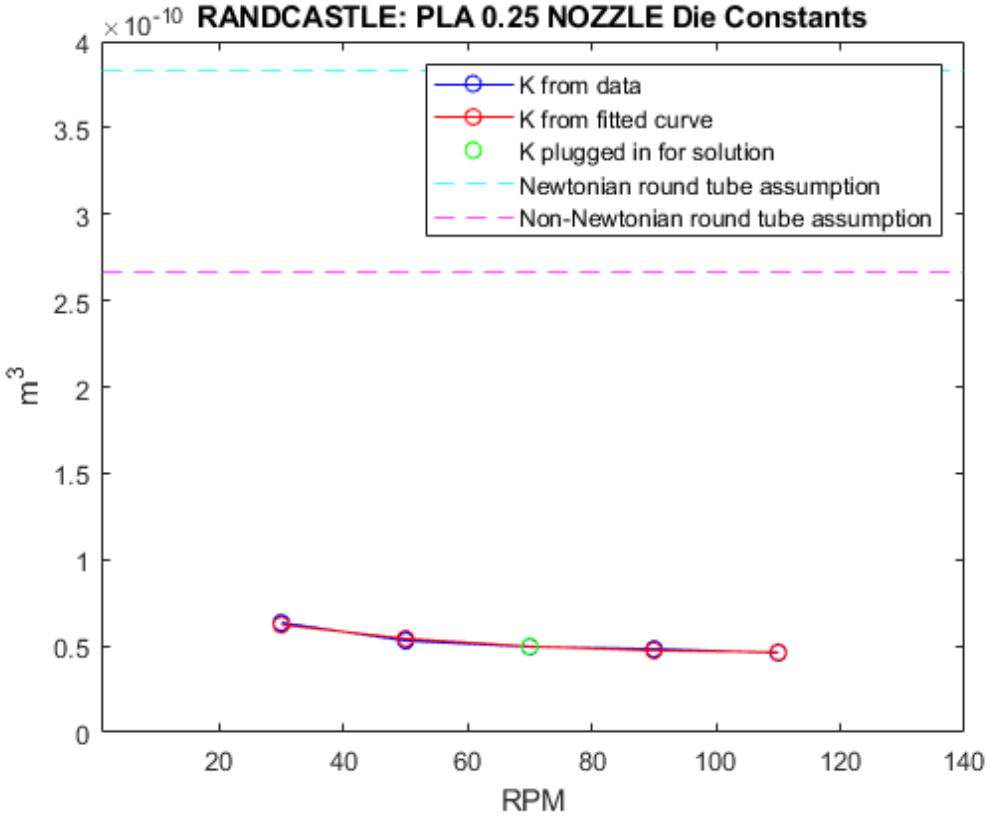
RANDCASTLE: PLA 0.25 NOZZLE Die Constants
×10^-10
K from data
K from fitted curve
K plugged in for solution
Newtonian round tube assumption
Non-Newtonian round tube assumption
m^3
RPM
0
0.5
1
1.5
2
2.5
3
3.5
4
20
40
60
80
100
120
140

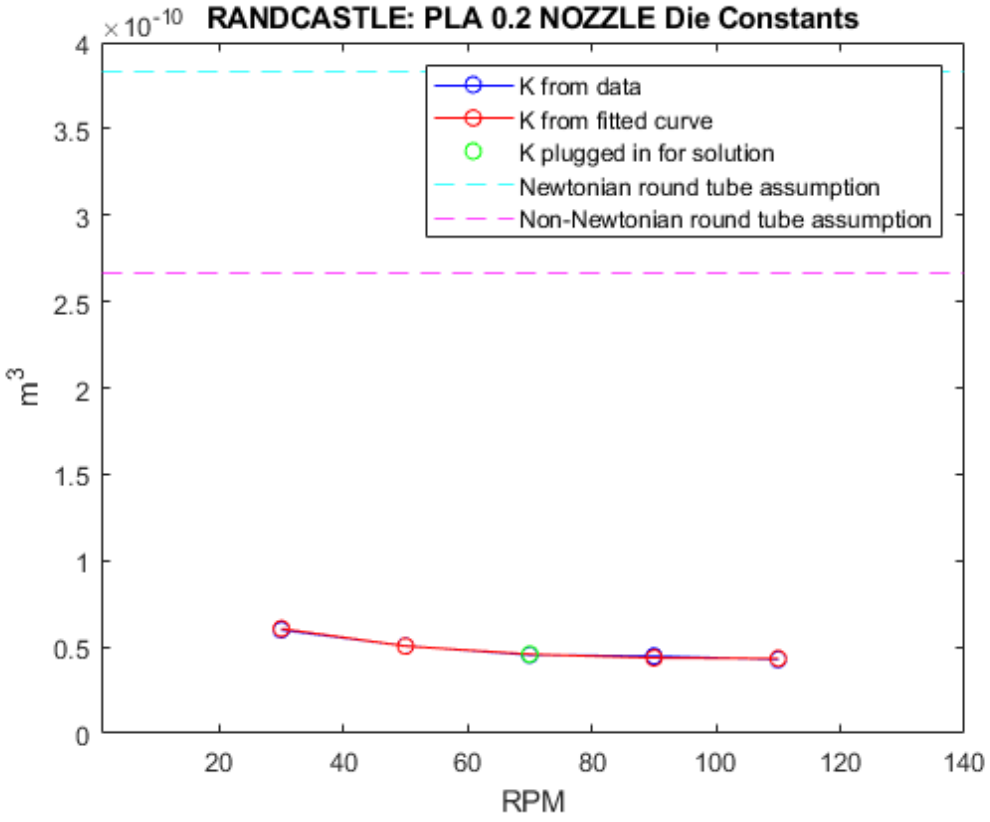
RANDCASTLE: PLA 0.2 NOZZLE Die Constants
×10^-10
4
3.5
3
2.5
2
1.5
1
0.5
0
m^3
20
40
60
80
100
120
140
RPM
K from data
K from fitted curve
K plugged in for solution
Newtonian round tube assumption
Non-Newtonian round tube assumption

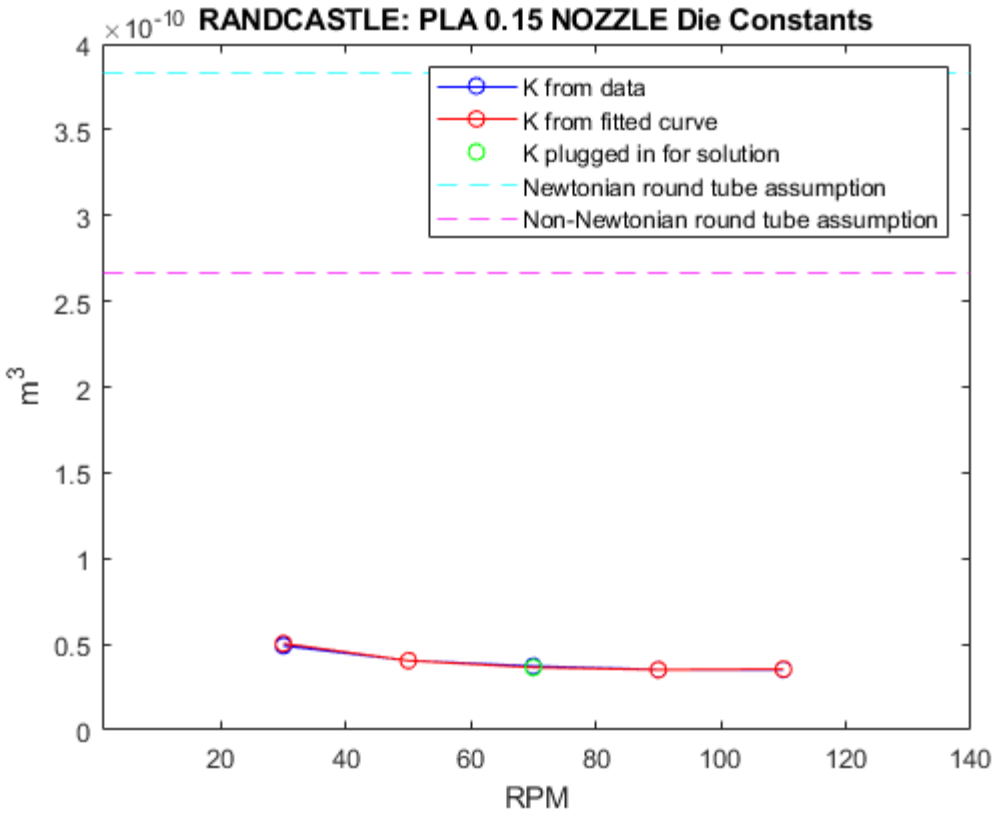
RANDCASTLE: PLA 0.15 NOZZLE Die Constants
×10^-10
4
3.5
3
2.5
2
1.5
1
0.5
0
m^3
20
40
60
80
100
120
140
RPM
K from data
K from fitted curve
K plugged in for solution
Newtonian round tube assumption
Non-Newtonian round tube assumption

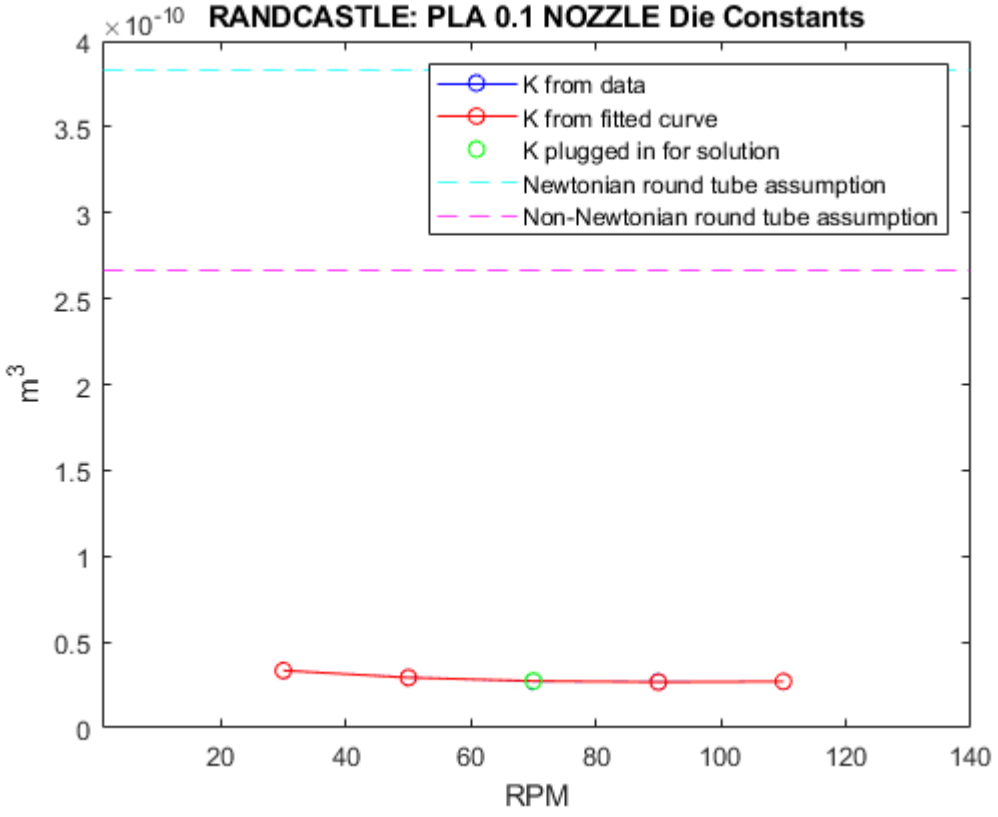
RANDCASTLE: PLA 0.1 NOZZLE Die Constants
×10^-10
K from data
K from fitted curve
K plugged in for solution
Newtonian round tube assumption
Non-Newtonian round tube assumption
m^3
RPM
0
0.5
1
1.5
2
2.5
3
3.5
4
20
40
60
80
100
120
140

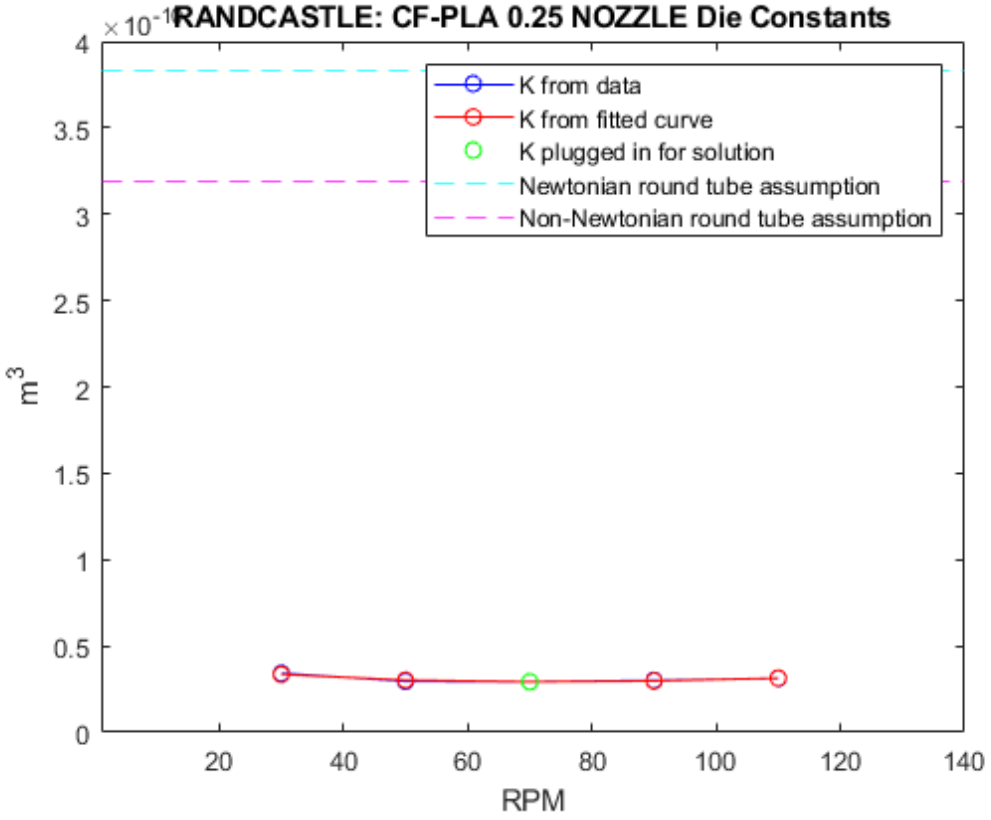
RANDCASTLE: CF-PLA 0.25 NOZZLE Die Constants
×10^-10
K from data
K from fitted curve
K plugged in for solution
Newtonian round tube assumption
Non-Newtonian round tube assumption
m^3
RPM
0
0.5
1
1.5
2
2.5
3
3.5
4
20
40
60
80
100
120
140

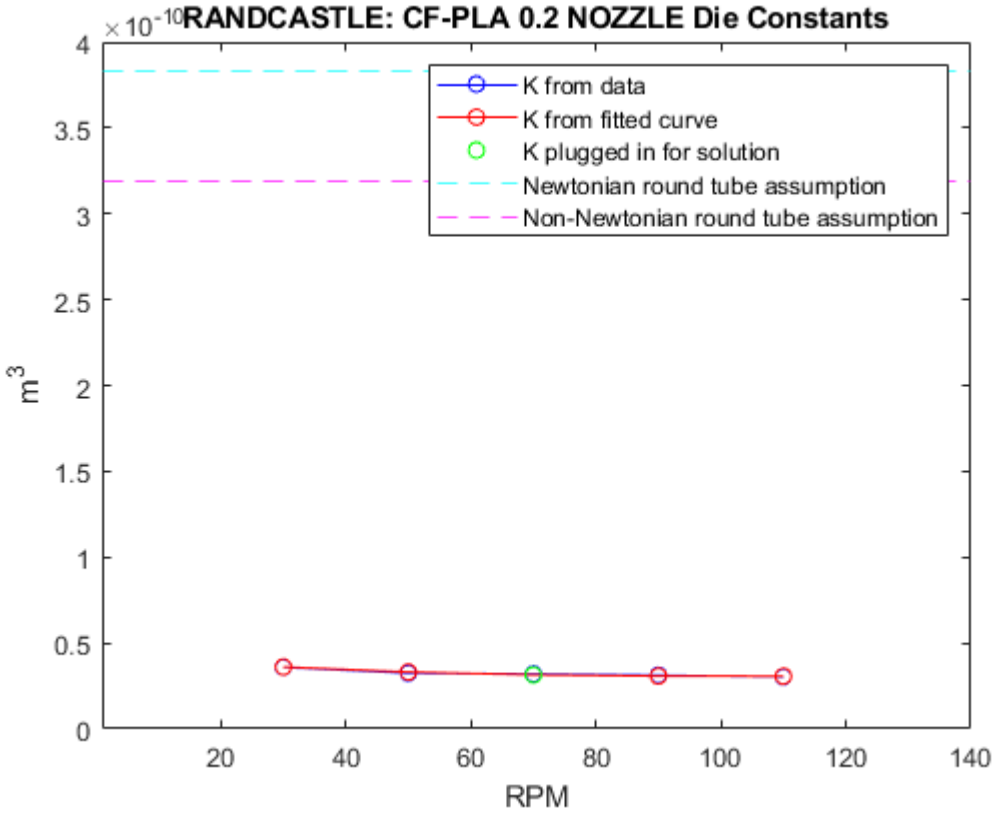
RANDCASTLE: CF-PLA 0.2 NOZZLE Die Constants
×10^-10
K from data
K from fitted curve
K plugged in for solution
Newtonian round tube assumption
Non-Newtonian round tube assumption
m^3
RPM
0
0.5
1
1.5
2
2.5
3
3.5
4
20
40
60
80
100
120
140

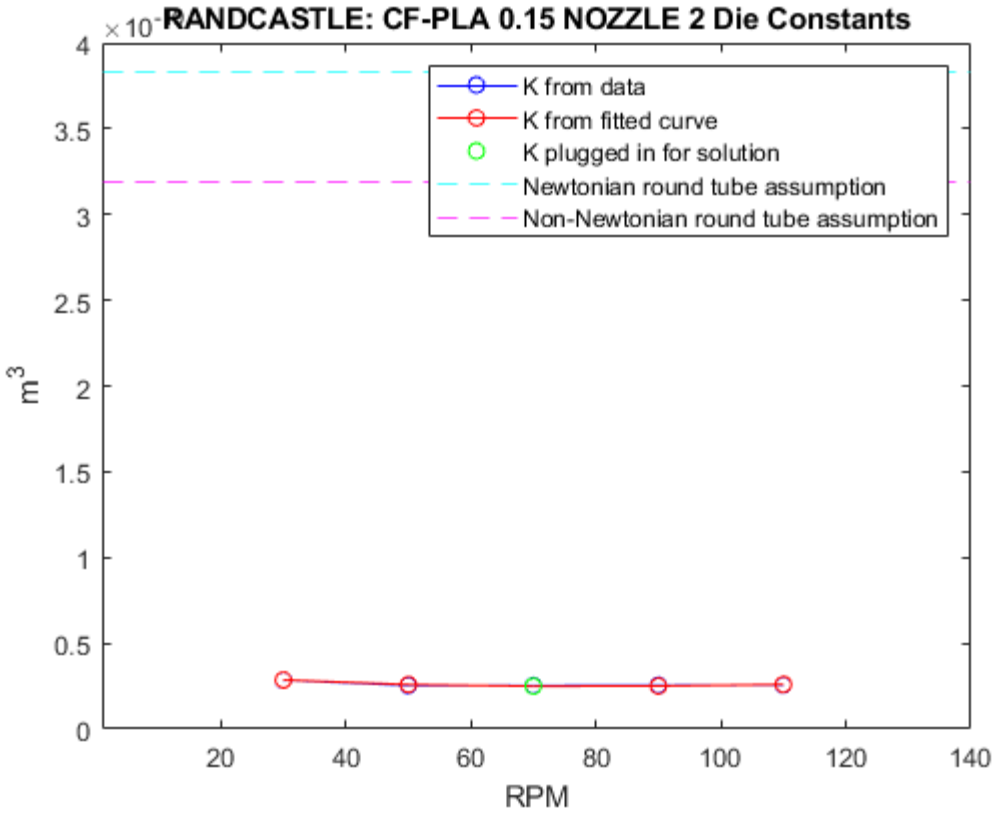
RANDCASTLE: CF-PLA 0.15 NOZZLE 2 Die Constants
×10^-10
K from data
K from fitted curve
K plugged in for solution
Newtonian round tube assumption
Non-Newtonian round tube assumption
m^3
RPM
0
0.5
1
1.5
2
2.5
3
3.5
4
20
40
60
80
100
120
140

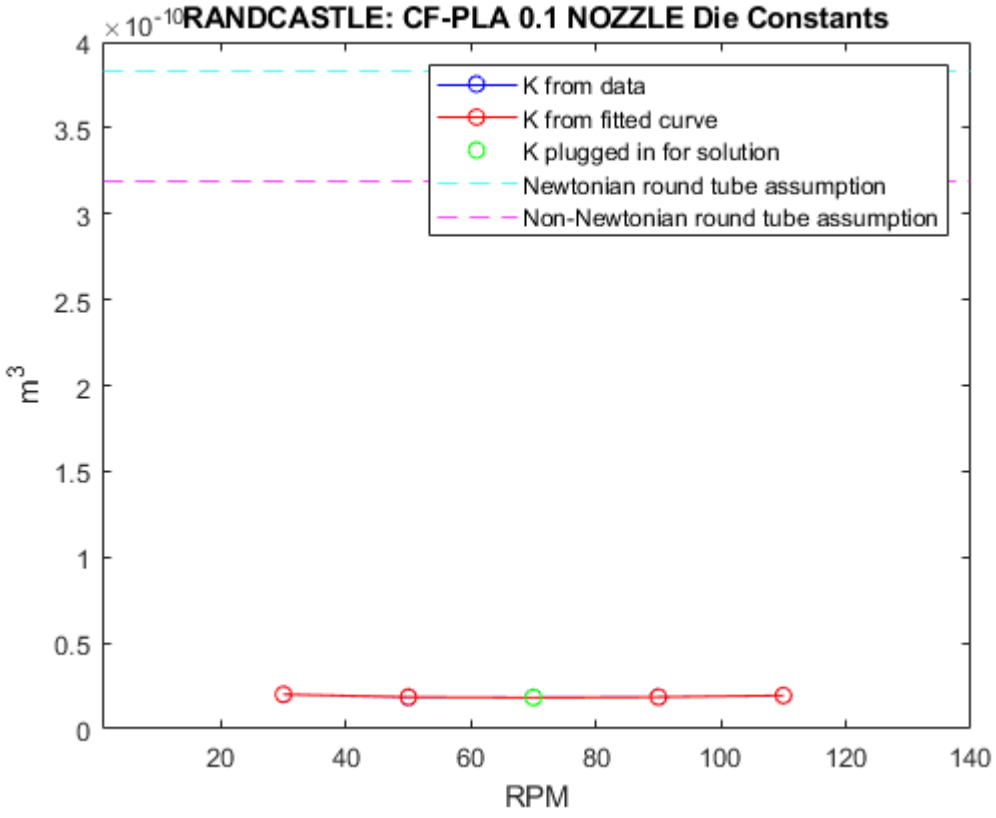
RANDCASTLE: CF-PLA 0.1 NOZZLE Die Constants
×10^-10
K from data
K from fitted curve
K plugged in for solution
Newtonian round tube assumption
Non-Newtonian round tube assumption
m^3
RPM
0
0.5
1
1.5
2
2.5
3
3.5
4
20
40
60
80
100
120
140

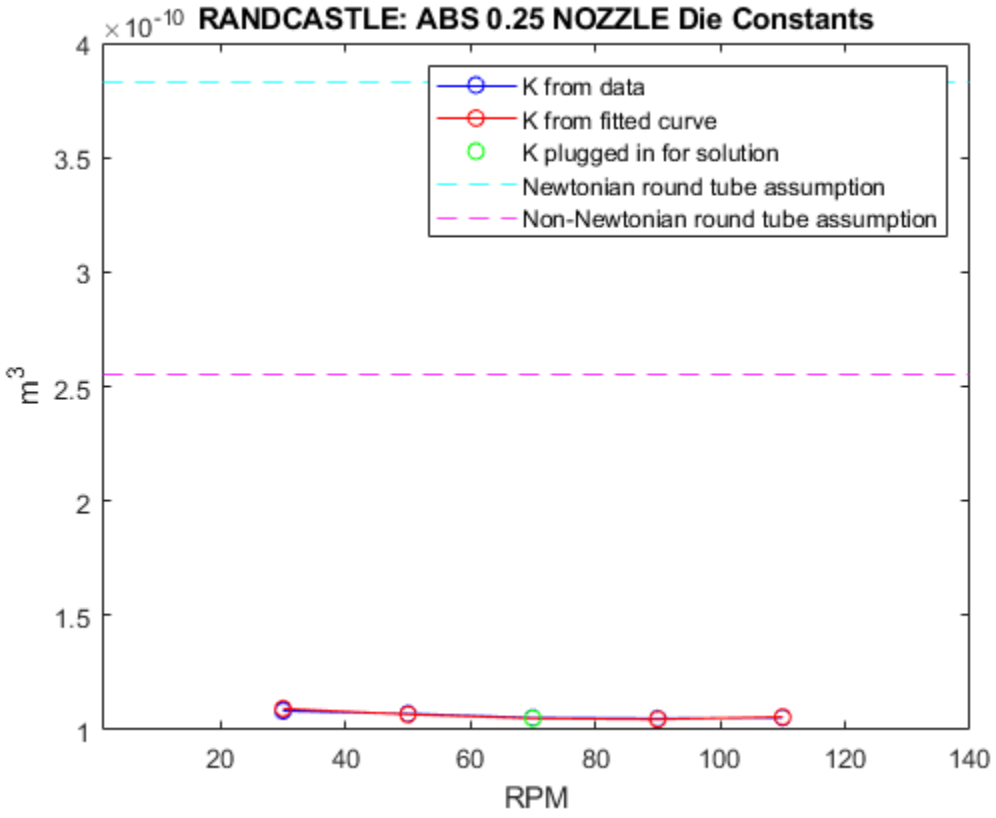
RANDCASTLE: ABS 0.25 NOZZLE Die Constants
×10^-10
K from data
K from fitted curve
K plugged in for solution
Newtonian round tube assumption
Non-Newtonian round tube assumption
m^3
RPM
1
1.5
2
2.5
3
3.5
4
20
40
60
80
100
120
140

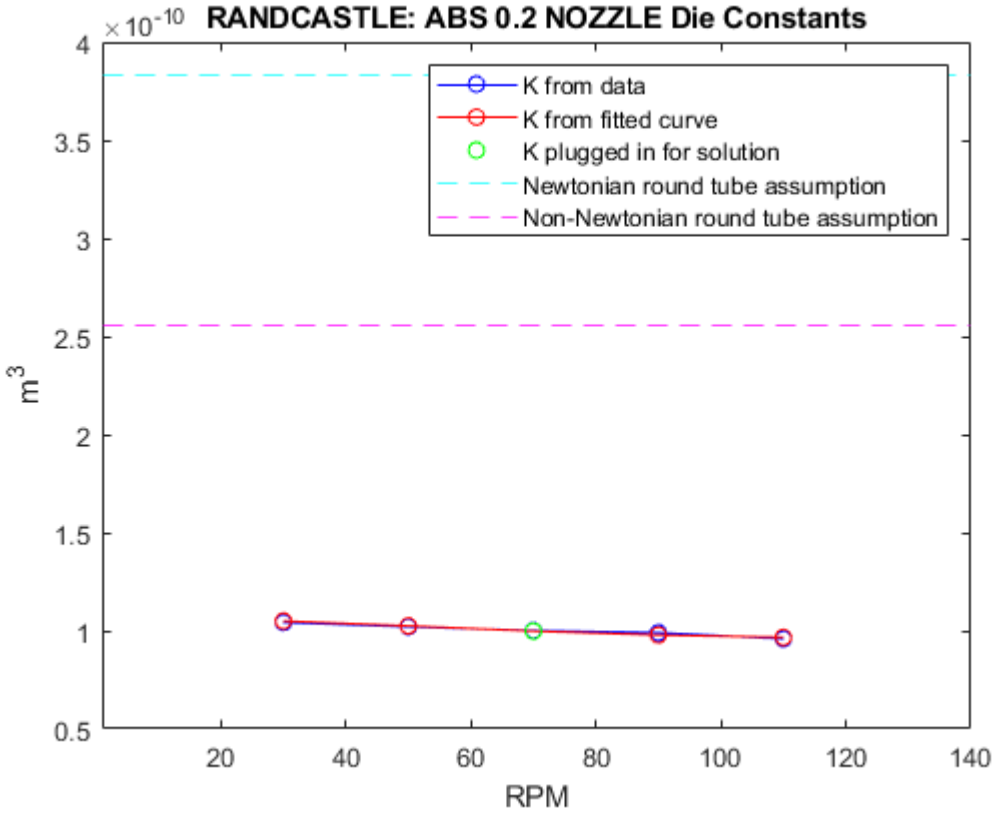
RANDCASTLE: ABS 0.2 NOZZLE Die Constants
×10^-10
4
3.5
3
2.5
2
1.5
1
0.5
m^3
20
40
60
80
100
120
140
RPM
K from data
K from fitted curve
K plugged in for solution
Newtonian round tube assumption
Non-Newtonian round tube assumption

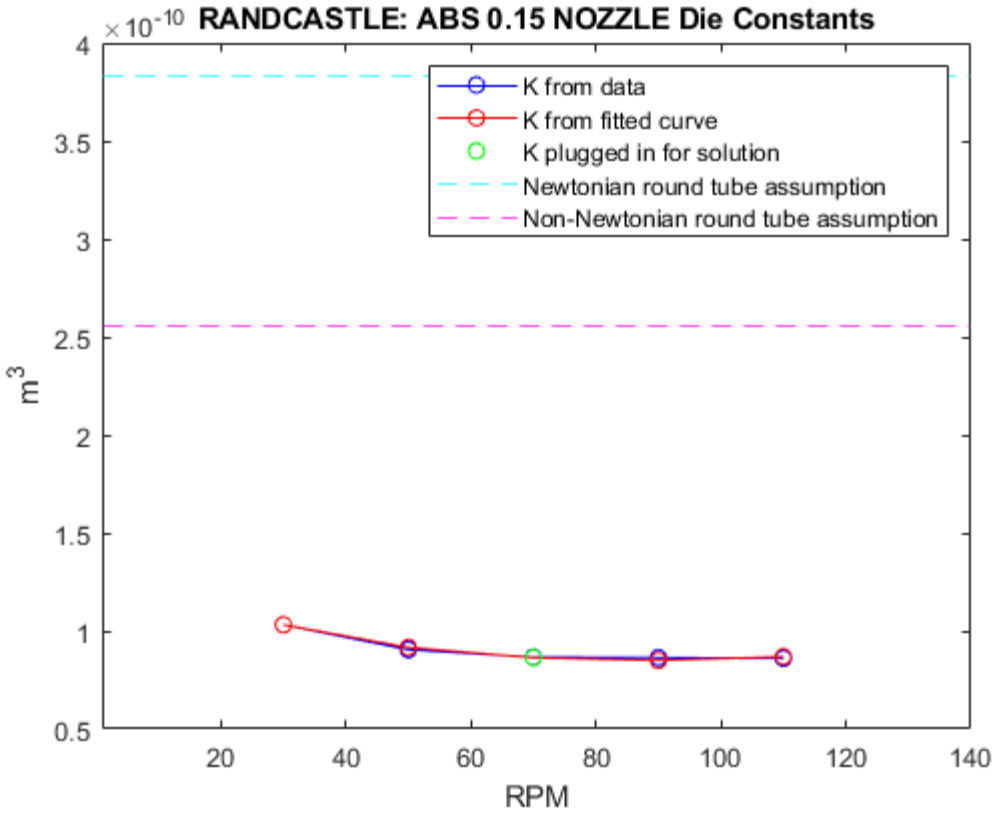
RANDCASTLE: ABS 0.15 NOZZLE Die Constants
×10^-10
4
3.5
3
2.5
2
1.5
1
0.5
m^3
20
40
60
80
100
120
140
RPM
K from data
K from fitted curve
K plugged in for solution
Newtonian round tube assumption
Non-Newtonian round tube assumption

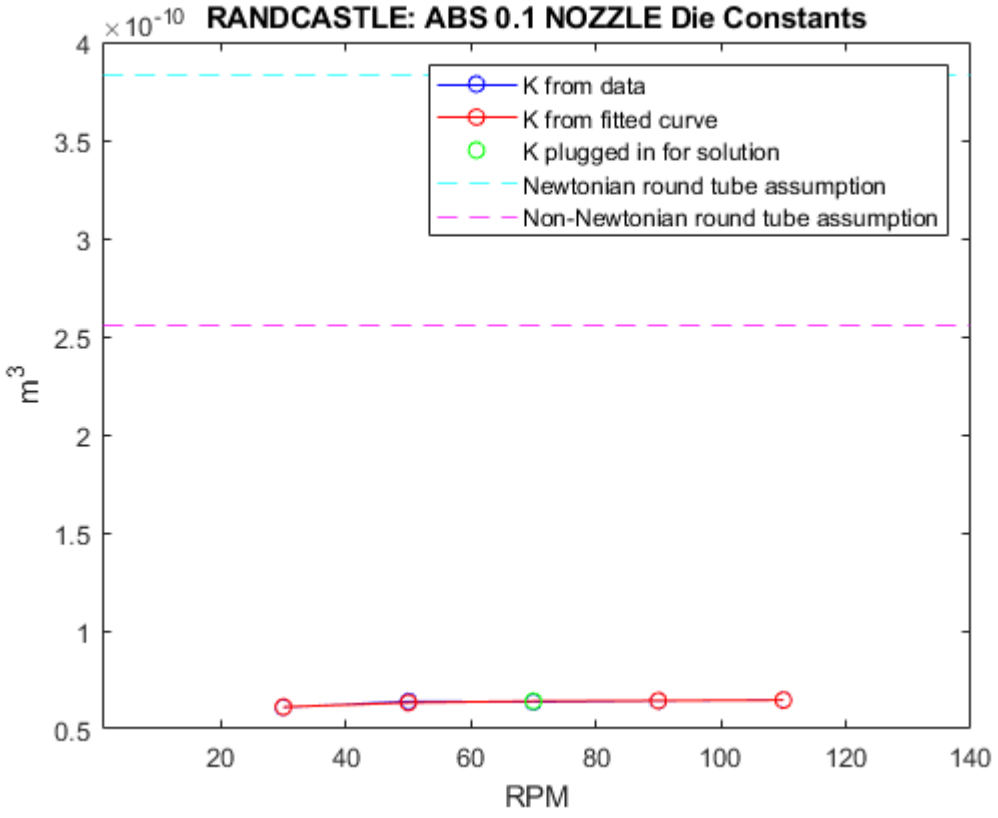
RANDCASTLE: ABS 0.1 NOZZLE Die Constants
×10^-10
4
3.5
3
2.5
2
1.5
1
0.5
m^3
20
40
60
80
100
120
140
RPM
K from data
K from fitted curve
K plugged in for solution
Newtonian round tube assumption
Non-Newtonian round tube assumption

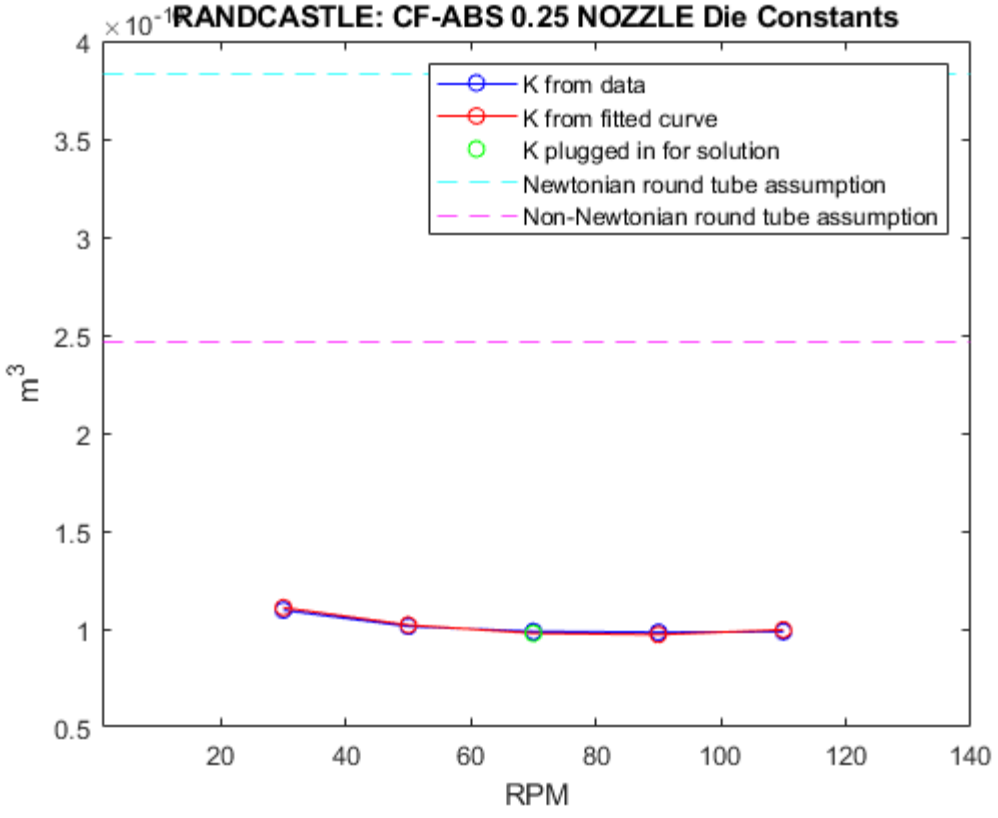
RANDCASTLE: CF-ABS 0.25 NOZZLE Die Constants
×10^-10
4
3.5
3
2.5
2
1.5
1
0.5
m^3
20
40
60
80
100
120
140
RPM
K from data
K from fitted curve
K plugged in for solution
Newtonian round tube assumption
Non-Newtonian round tube assumption

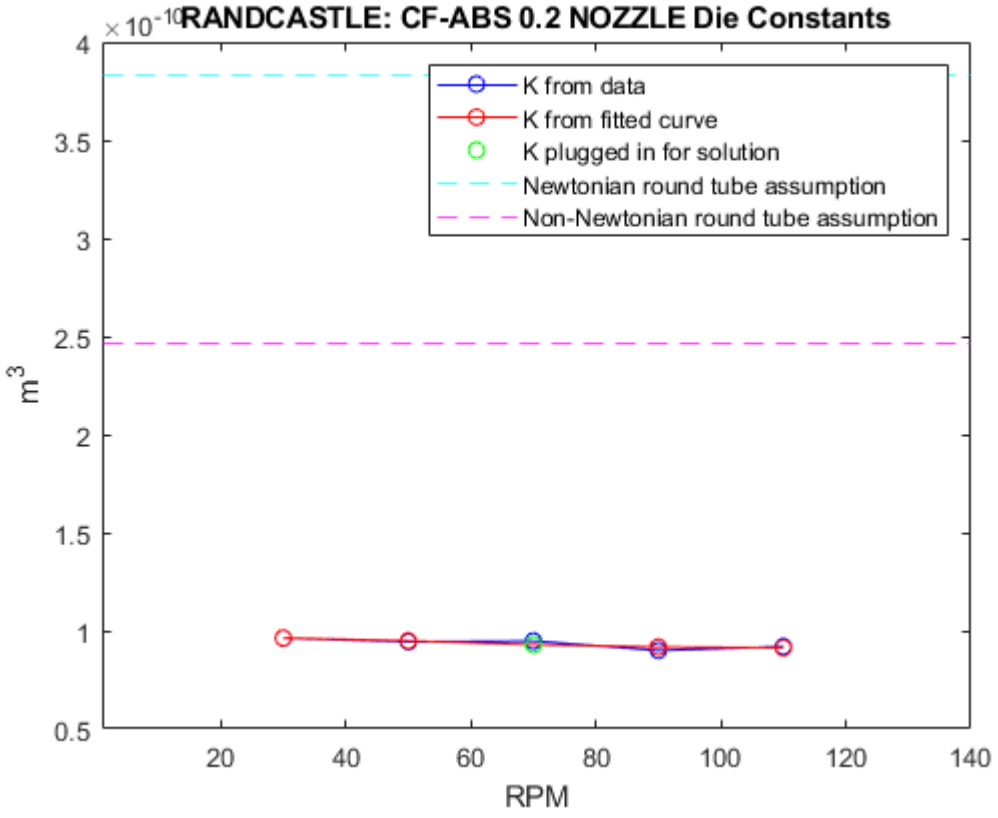
BRANDCASTLE: CF-ABS 0.2 NOZZLE Die Constants
×10^-10
4
3.5
3
2.5
2
1.5
1
0.5
m^3
20
40
60
80
100
120
140
RPM
K from data
K from fitted curve
K plugged in for solution
Newtonian round tube assumption
Non-Newtonian round tube assumption

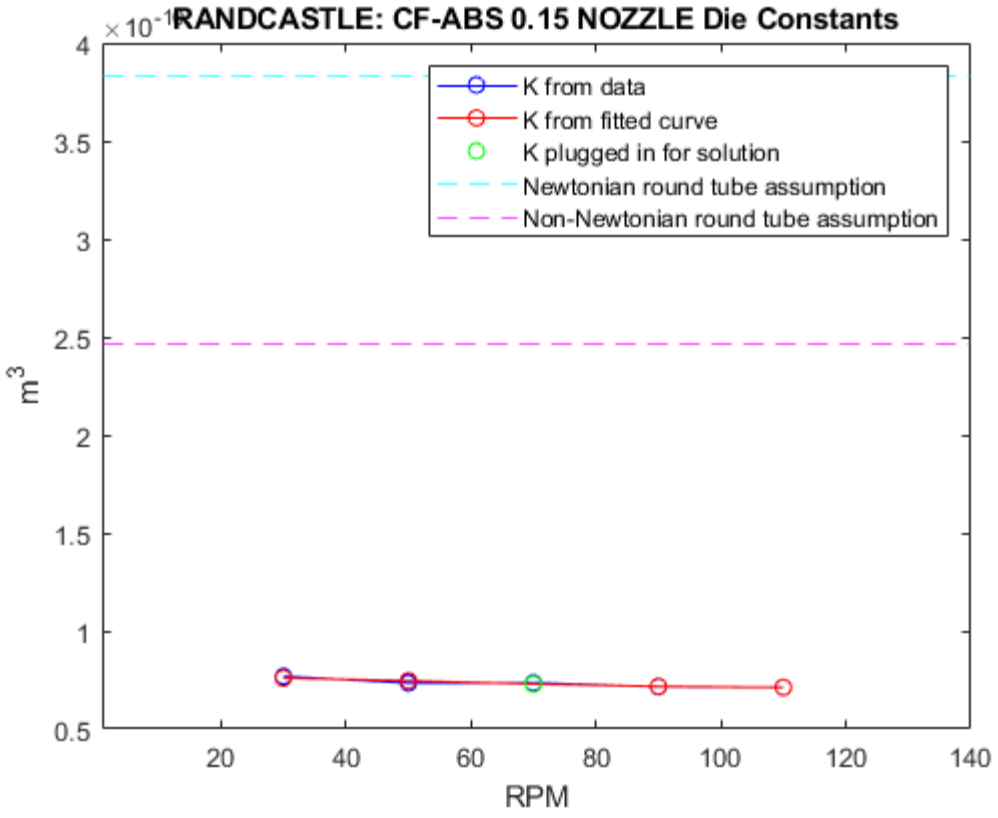
BRANDCASTLE: CF-ABS 0.15 NOZZLE Die Constants
×10^-10
4
3.5
3
2.5
2
1.5
1
0.5
m^3
20
40
60
80
100
120
140
RPM
K from data
K from fitted curve
K plugged in for solution
Newtonian round tube assumption
Non-Newtonian round tube assumption

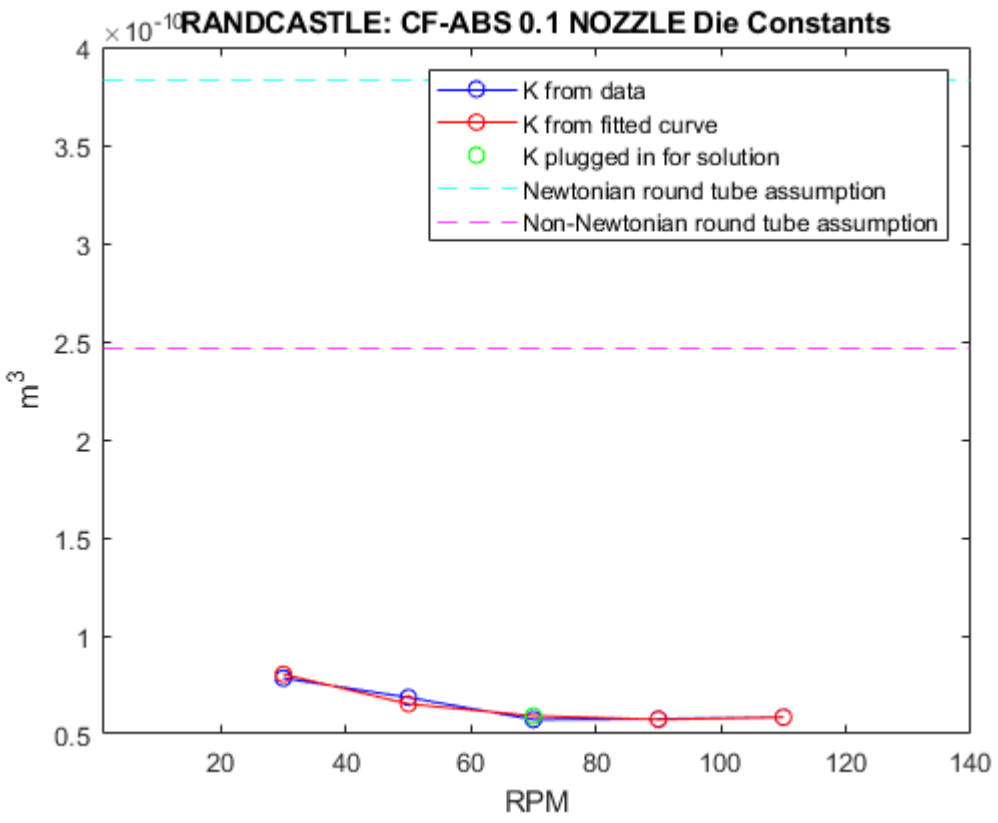
RANDCASTLE: CF-ABS 0.1 NOZZLE Die Constants
×10^-10
4
3.5
3
2.5
2
1.5
1
0.5
m^3
20
40
60
80
100
120
140
RPM
K from data
K from fitted curve
K plugged in for solution
Newtonian round tube assumption
Non-Newtonian round tube assumption

A4. Microtruder Data Plots

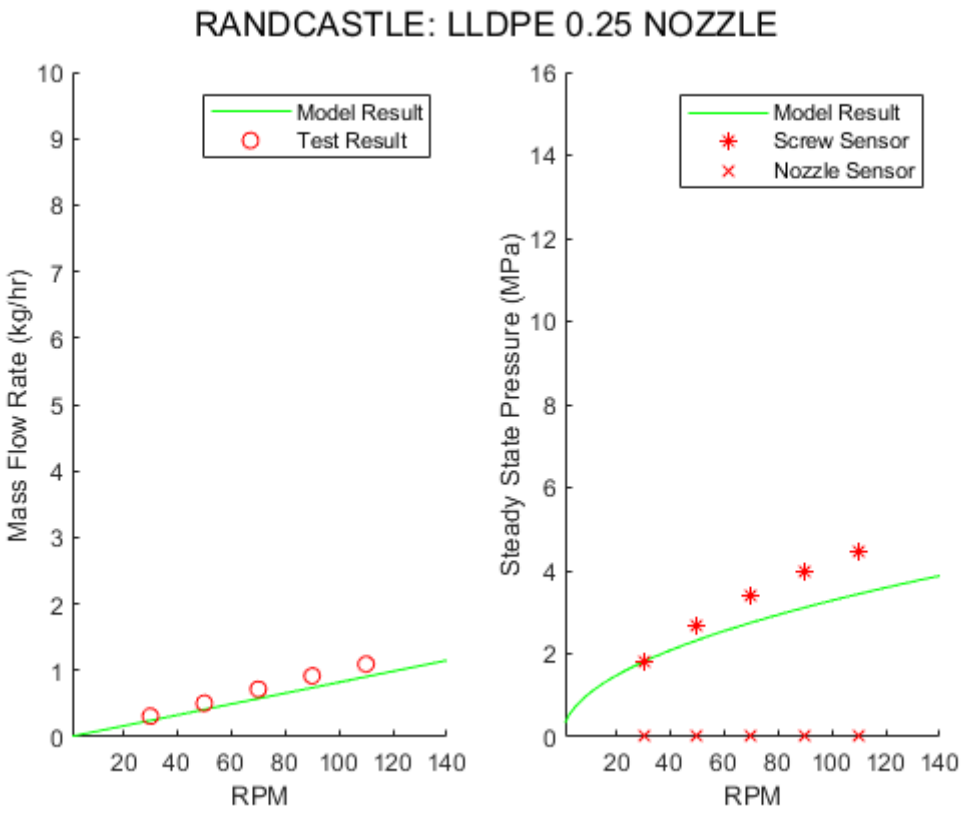

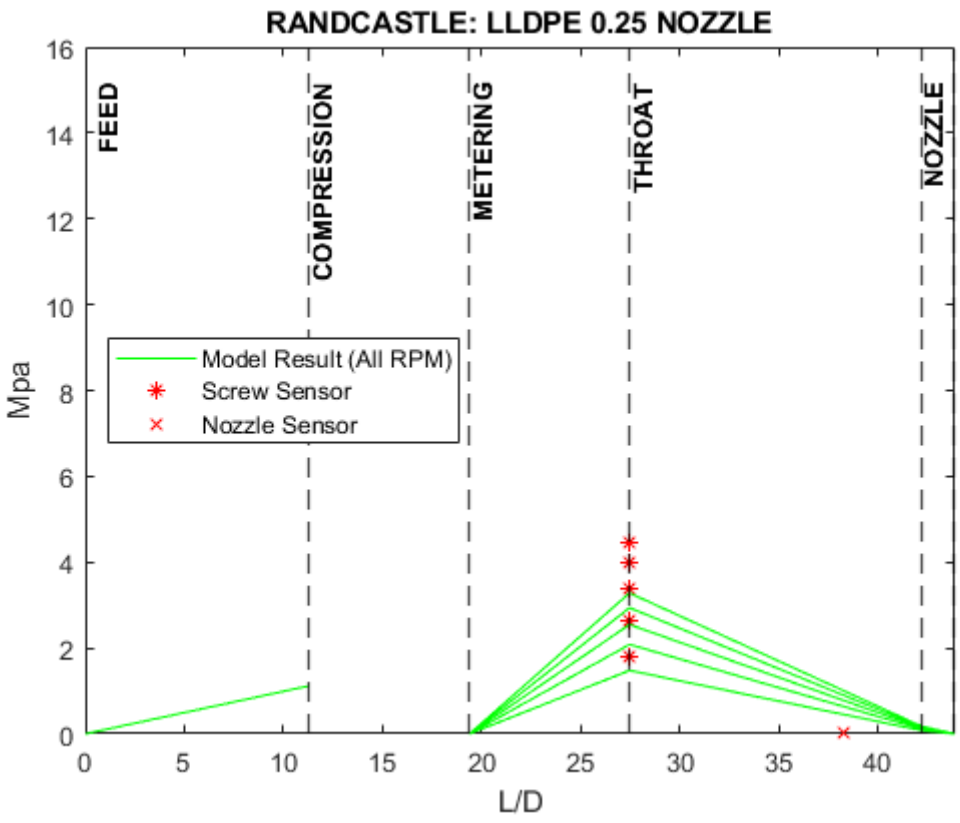
RANDCASTLE: LLDPE 0.25 NOZZLE
FEED
COMPRESSION
METERING
THROAT
NOZZLE
Model Result (All RPM)
Screw Sensor
Nozzle Sensor
Mpa
L/D

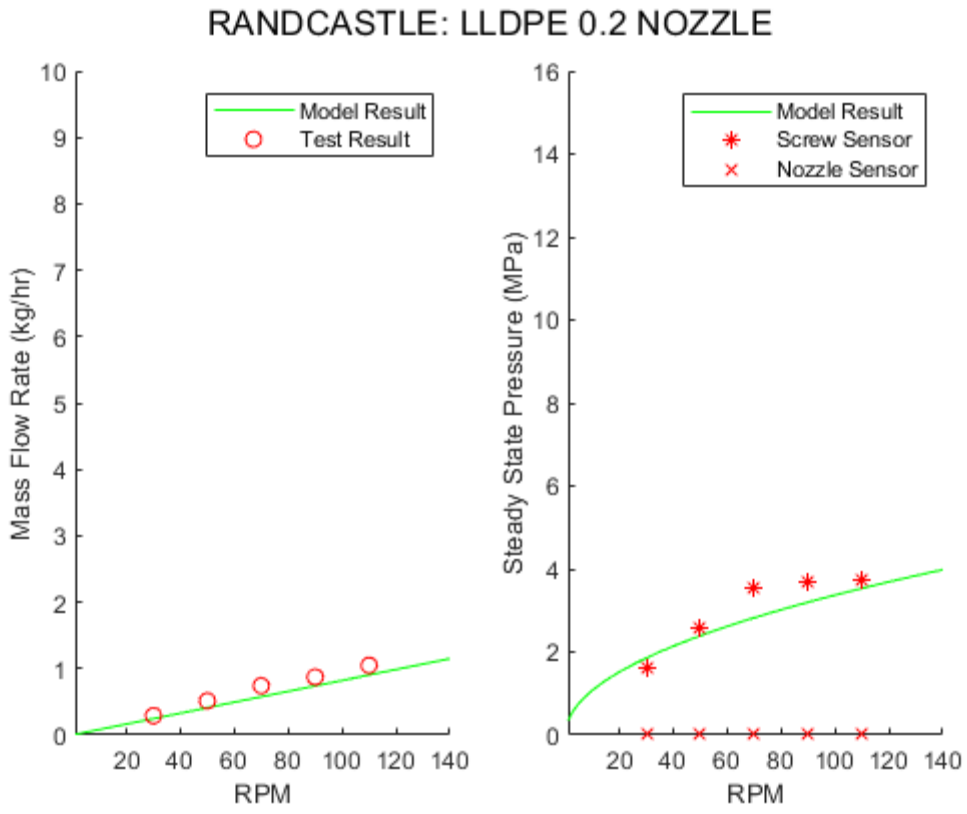
RANDCASTLE: LLDPE 0.2 NOZZLE
Model Result
Test Result
Mass Flow Rate (kg/hr)
RPM
Model Result
Screw Sensor
Nozzle Sensor
Steady State Pressure (MPa)
RPM

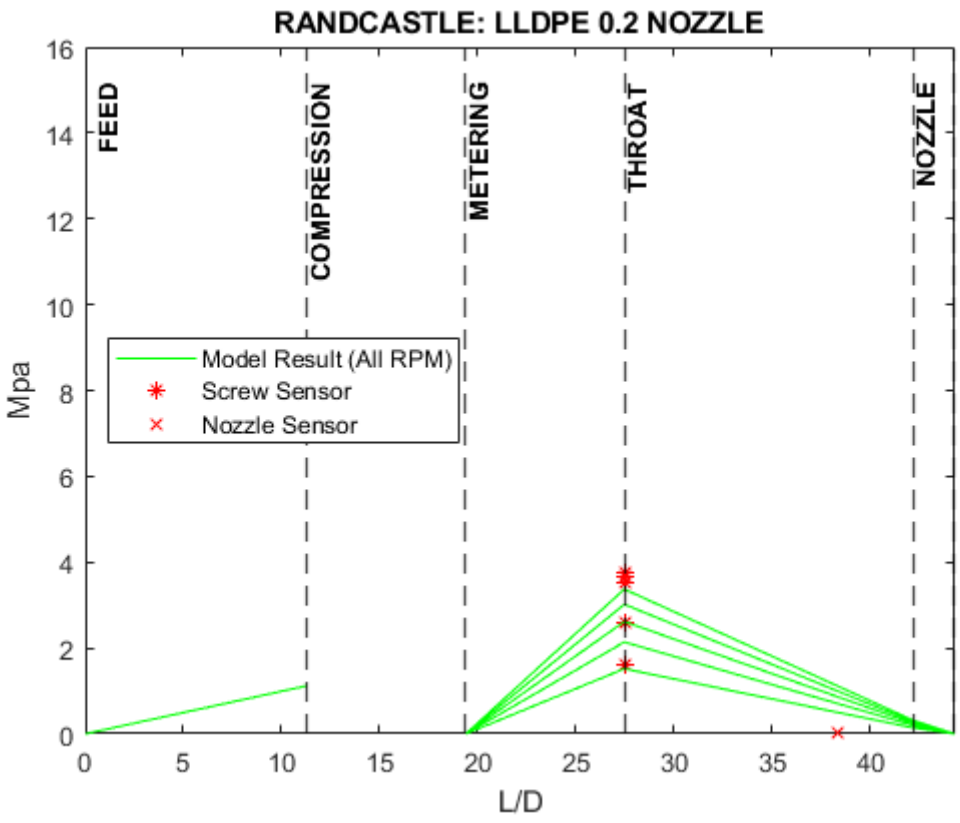
RANDCASTLE: LLDPE 0.2 NOZZLE
FEED
COMPRESSION
METERING
THROAT
NOZZLE
Model Result (All RPM)
Screw Sensor
Nozzle Sensor
Mpa
L/D

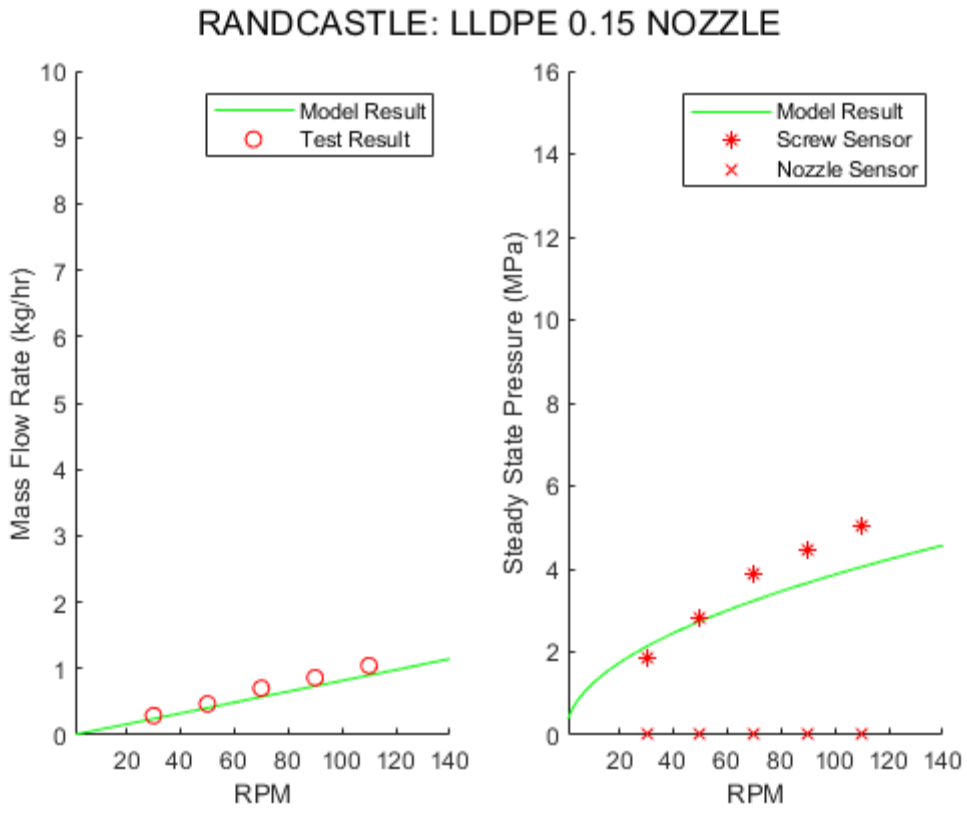
RANDCASTLE: LLDPE 0.15 NOZZLE
Model Result
Test Result
Mass Flow Rate (kg/hr)
RPM
Model Result
Screw Sensor
Nozzle Sensor
Steady State Pressure (MPa)
RPM

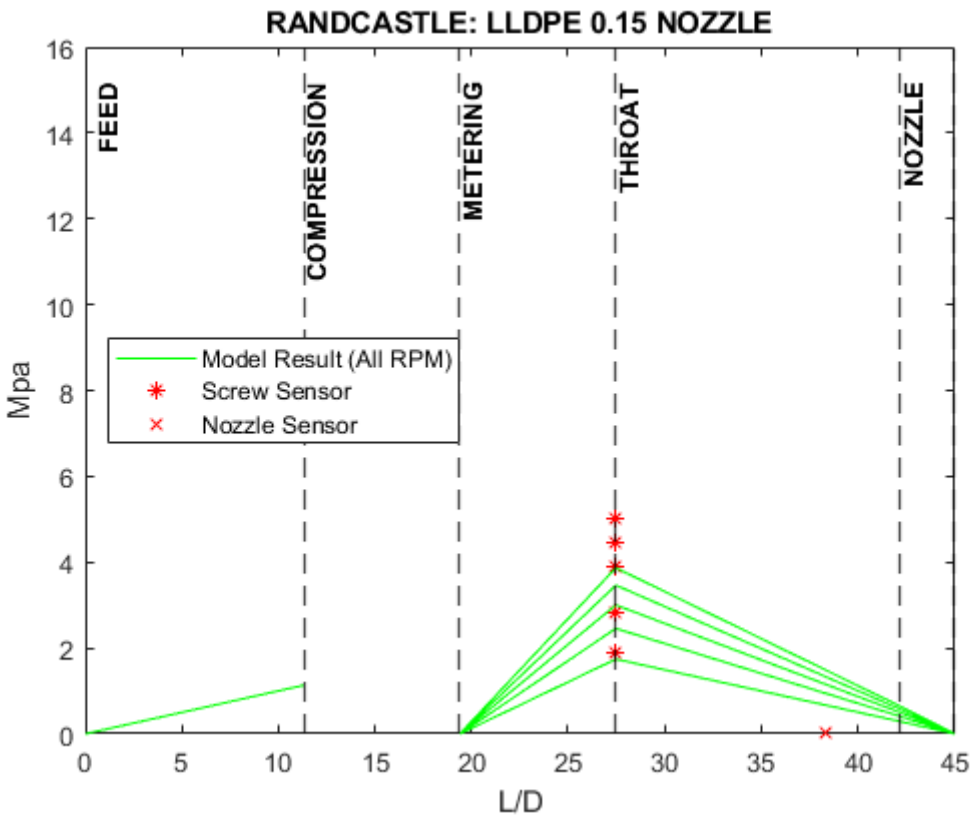
RANDCASTLE: LLDPE 0.15 NOZZLE
FEED
COMPRESSION
METERING
THROAT
NOZZLE
Model Result (All RPM)
Screw Sensor
Nozzle Sensor
Mpa
L/D

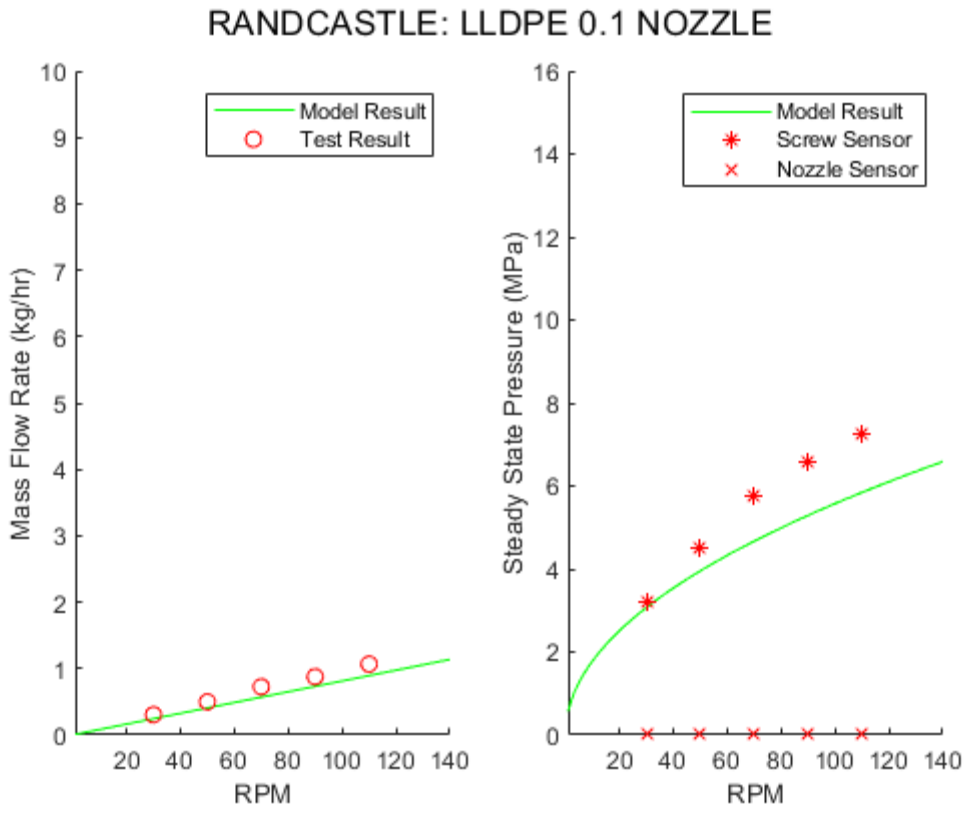
RANDCASTLE: LLDPE 0.1 NOZZLE
Model Result
Test Result
Mass Flow Rate (kg/hr)
RPM
Model Result
Screw Sensor
Nozzle Sensor
Steady State Pressure (MPa)
RPM

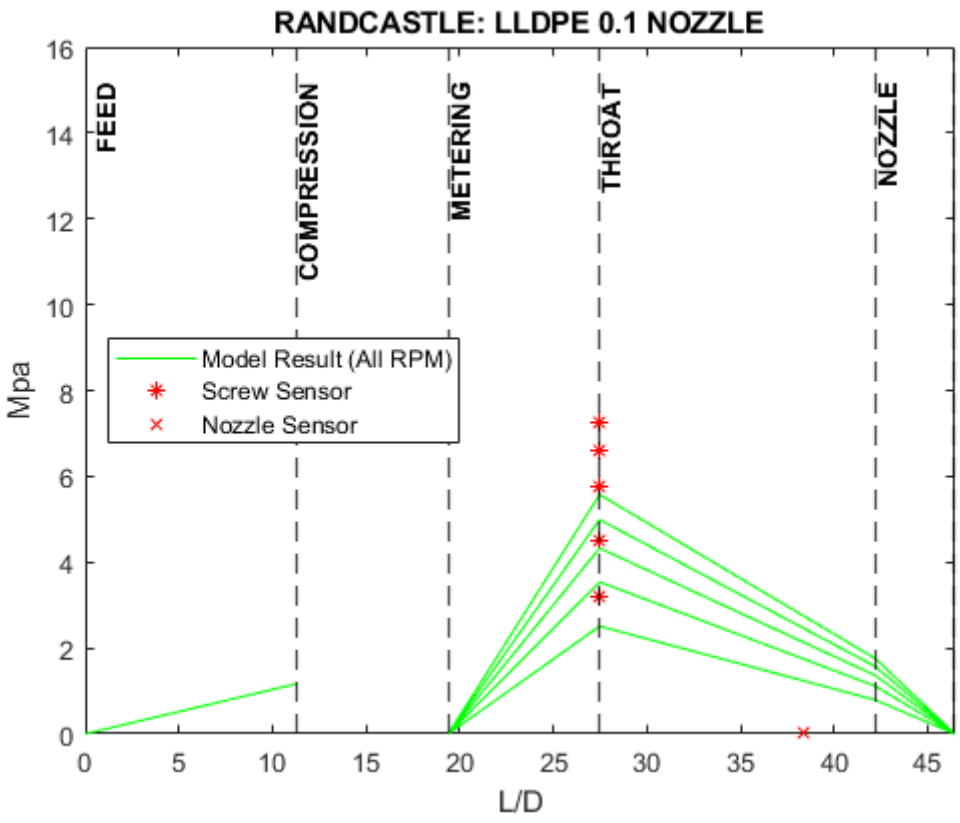
RANDCASTLE: LLDPE 0.1 NOZZLE
FEED
COMPRESSION
METERING
THROAT
NOZZLE
Model Result (All RPM)
Screw Sensor
Nozzle Sensor
Mpa
L/D

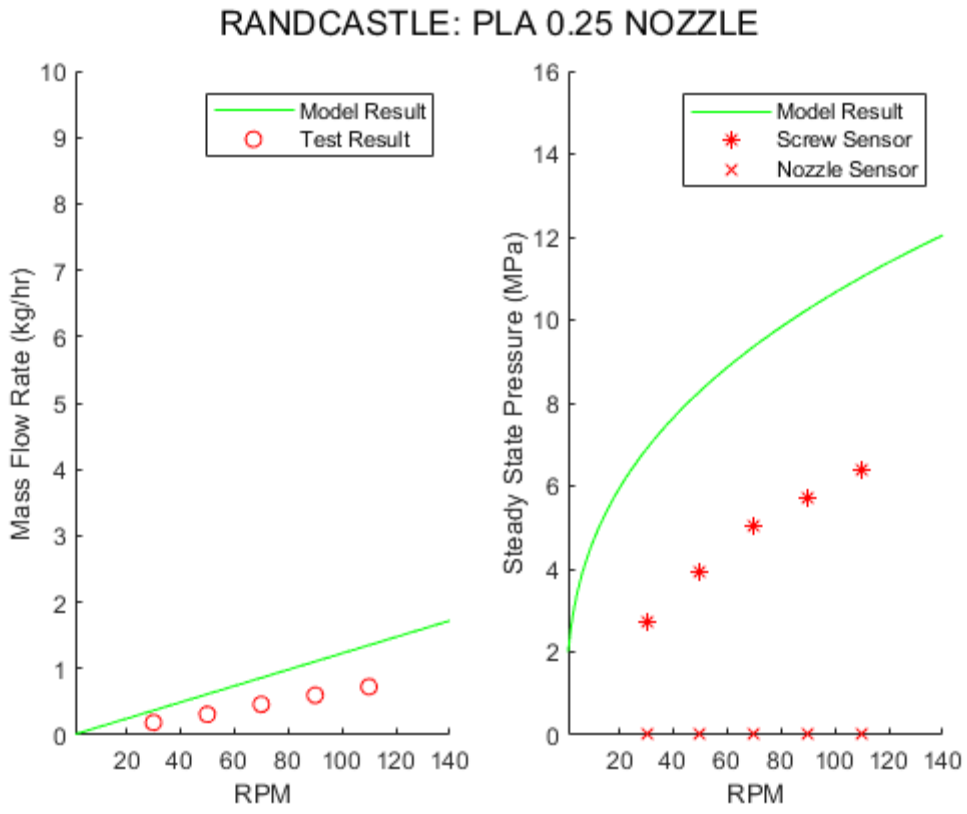
RANDCASTLE: PLA 0.25 NOZZLE
Model Result
Test Result
Mass Flow Rate (kg/hr)
RPM
Model Result
Screw Sensor
Nozzle Sensor
Steady State Pressure (MPa)
RPM

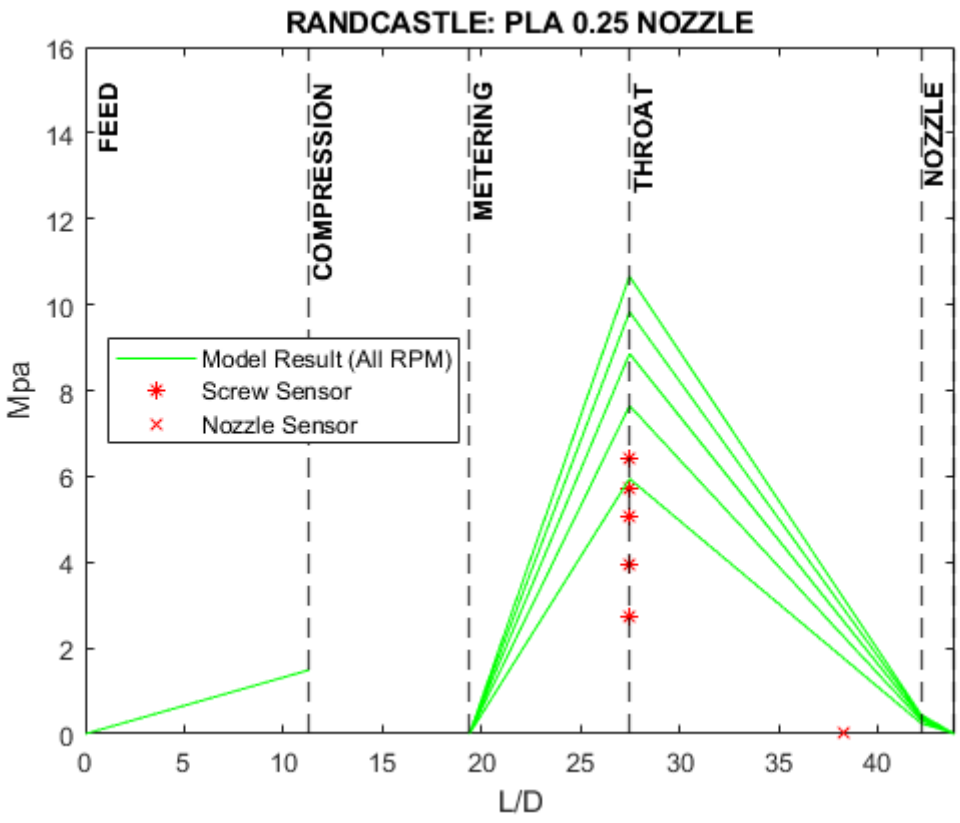
RANDCASTLE: PLA 0.25 NOZZLE
FEED
COMPRESSION
METERING
THROAT
NOZZLE
Model Result (All RPM)
Screw Sensor
Nozzle Sensor
Mpa
L/D

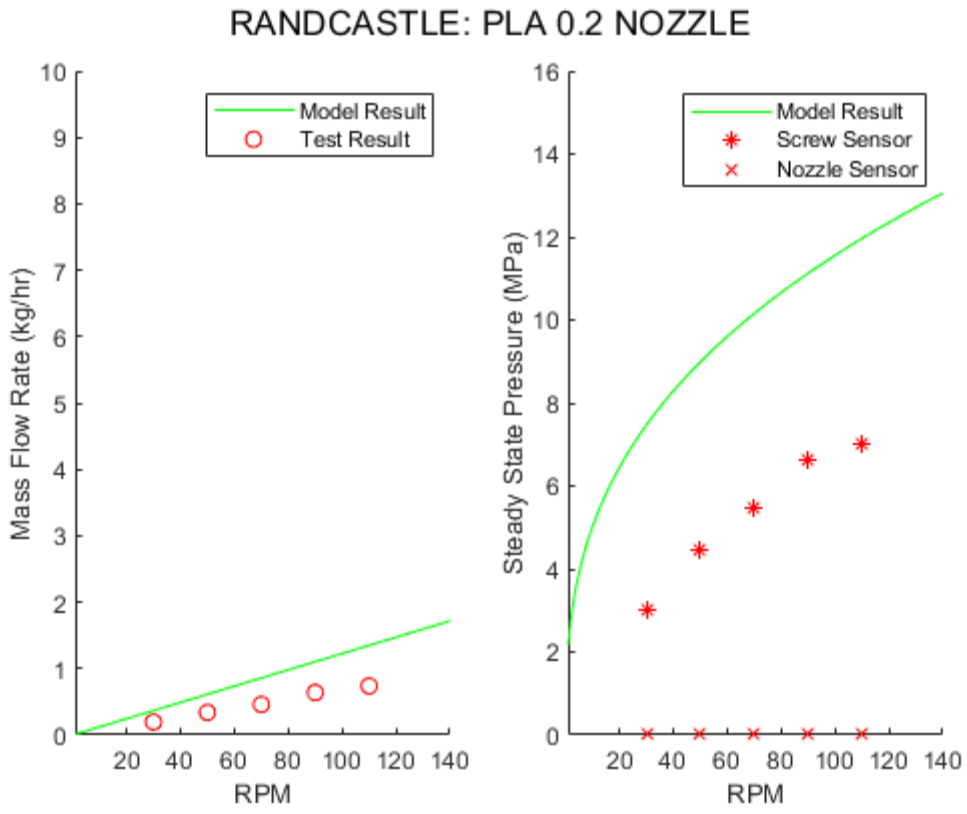
RANDCASTLE: PLA 0.2 NOZZLE
Model Result
Test Result
Mass Flow Rate (kg/hr)
RPM
Model Result
Screw Sensor
Nozzle Sensor
Steady State Pressure (MPa)
RPM

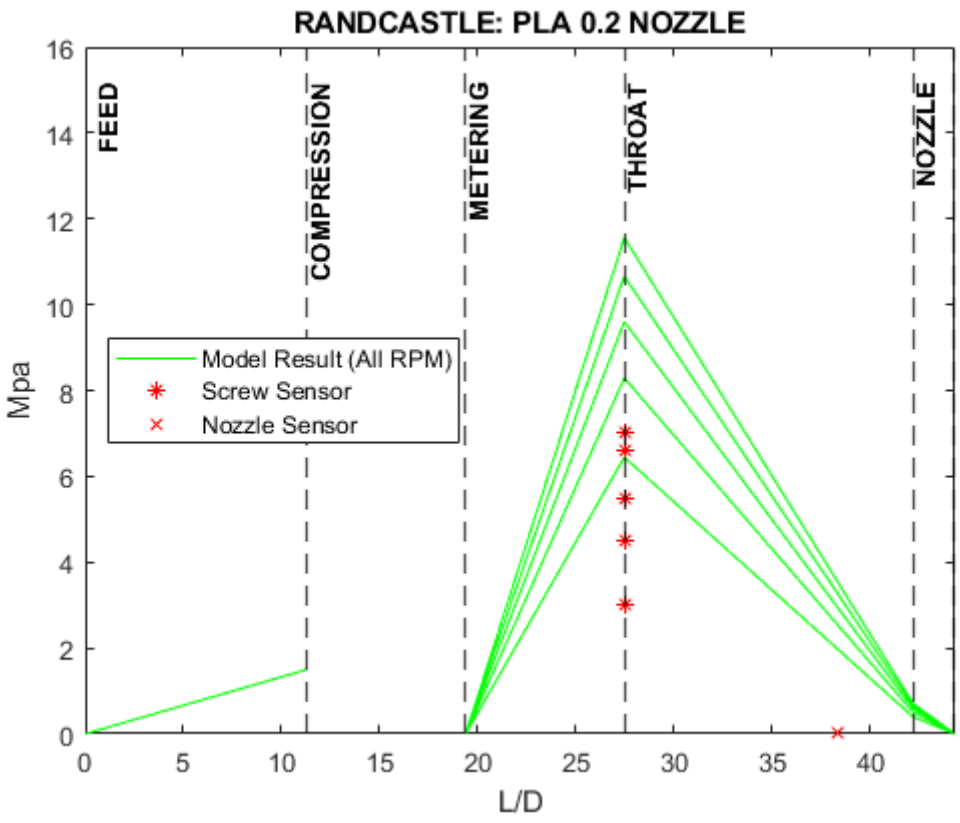
RANDCASTLE: PLA 0.2 NOZZLE
FEED
COMPRESSION
METERING
THROAT
NOZZLE
Model Result (All RPM)
Screw Sensor
Nozzle Sensor
Mpa
L/D

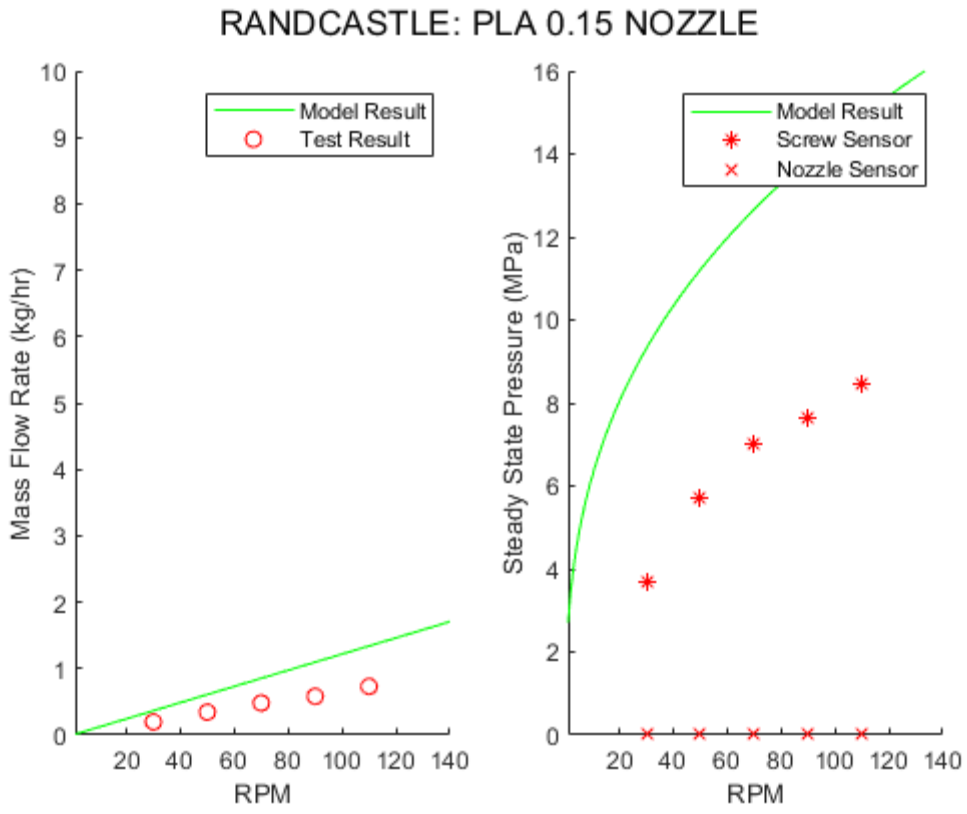
RANDCASTLE: PLA 0.15 NOZZLE
Model Result
Test Result
Mass Flow Rate (kg/hr)
RPM
Model Result
Screw Sensor
Nozzle Sensor
Steady State Pressure (MPa)
RPM

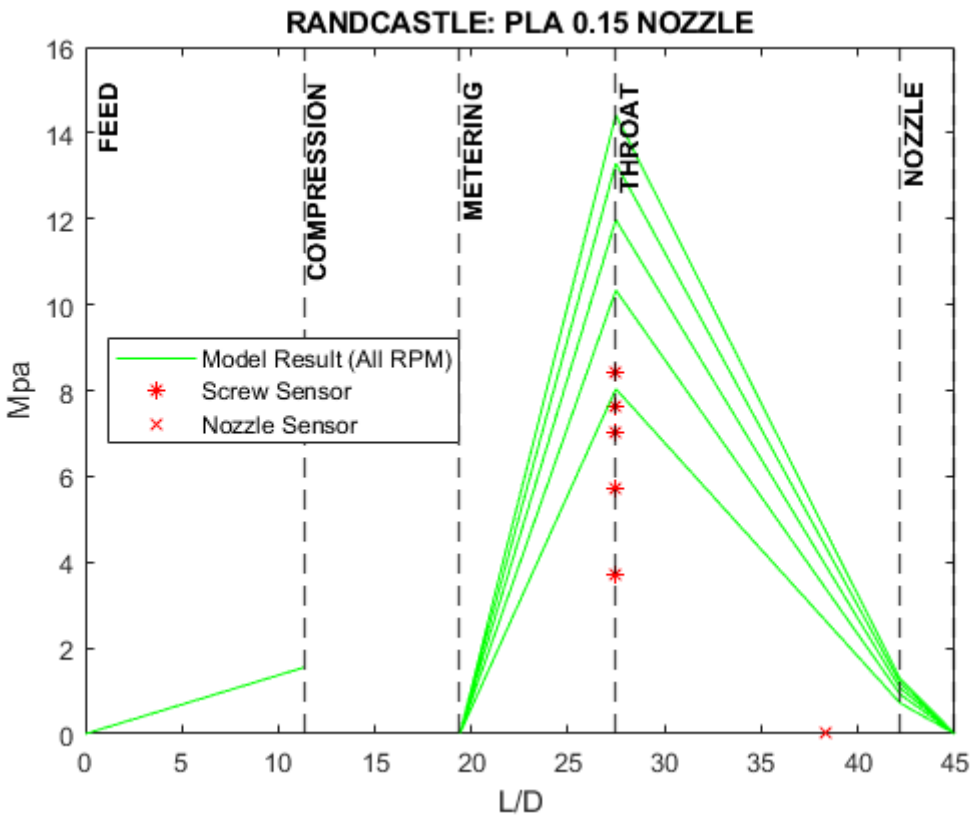
RANDCASTLE: PLA 0.15 NOZZLE
FEED
COMPRESSION
METERING
THROAT
NOZZLE
Model Result (All RPM)
Screw Sensor
Nozzle Sensor
Mpa
L/D

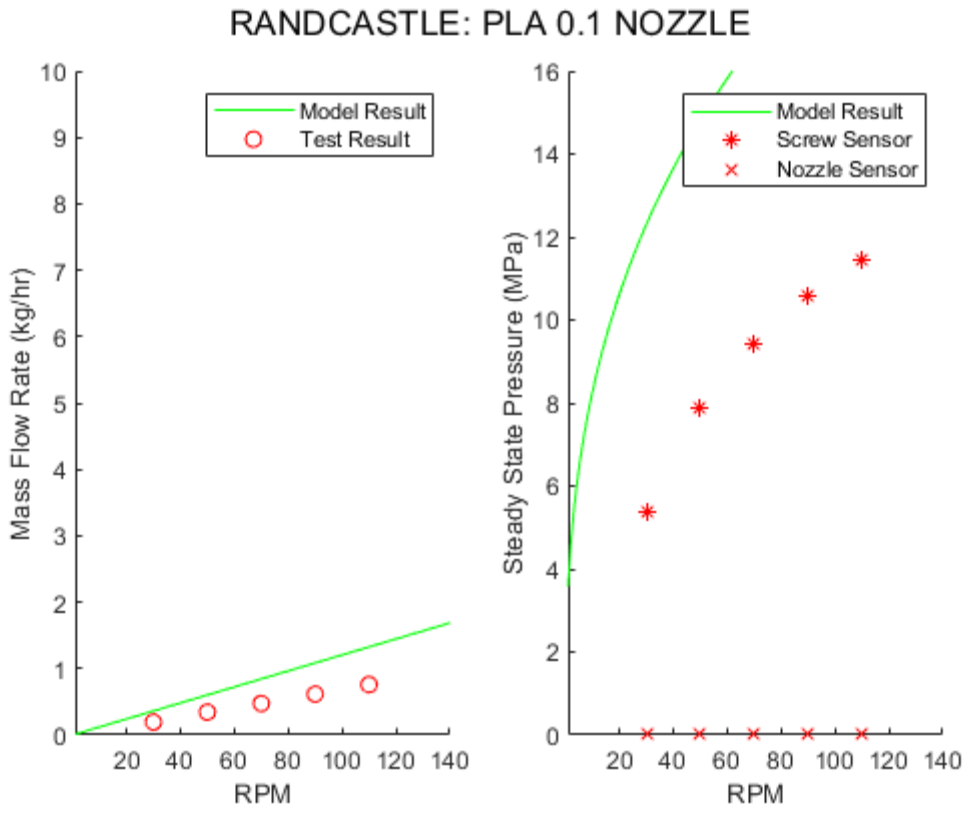
RANDCASTLE: PLA 0.1 NOZZLE
Model Result
Test Result
Mass Flow Rate (kg/hr)
RPM
Model Result
Screw Sensor
Nozzle Sensor
Steady State Pressure (MPa)
RPM

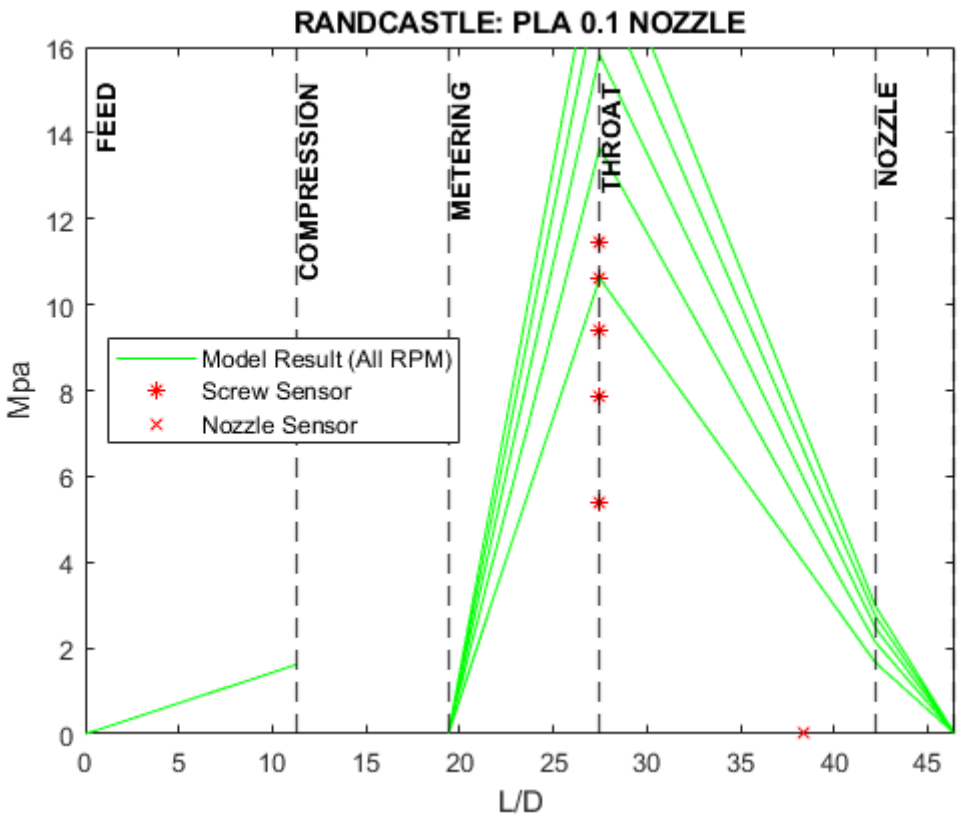
RANDCASTLE: PLA 0.1 NOZZLE
FEED
COMPRESSION
METERING
THROAT
NOZZLE
Model Result (All RPM)
Screw Sensor
Nozzle Sensor
Mpa
L/D

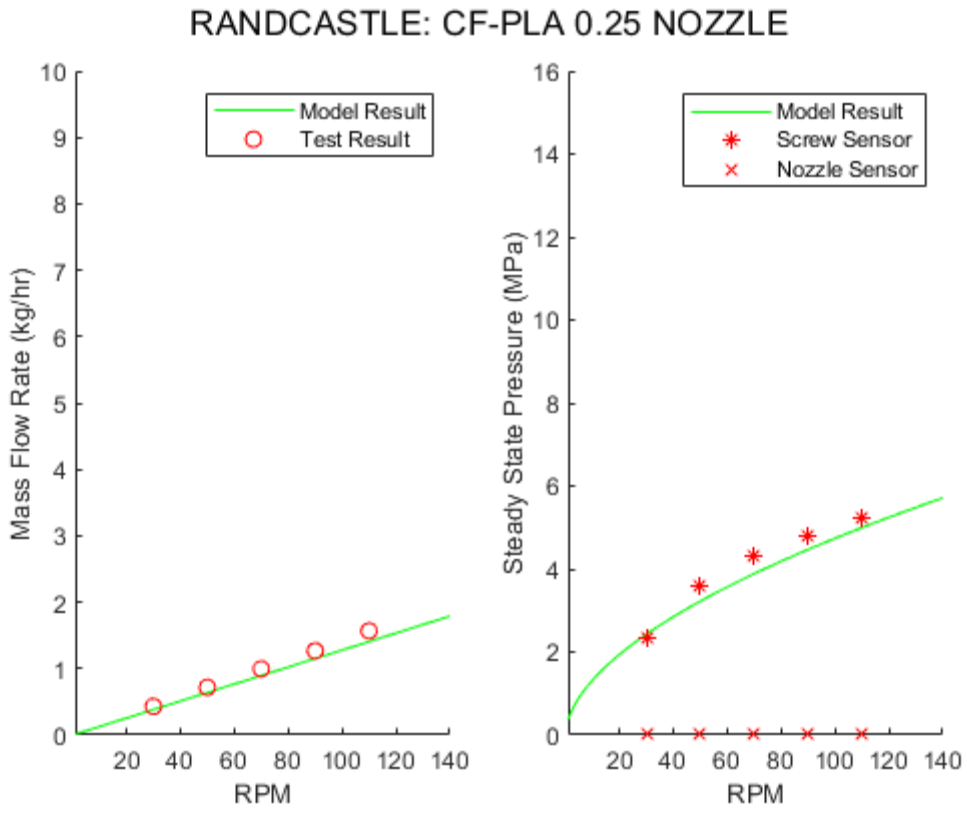
RANDCASTLE: CF-PLA 0.25 NOZZLE
Model Result
Test Result
Mass Flow Rate (kg/hr)
RPM
Model Result
Screw Sensor
Nozzle Sensor
Steady State Pressure (MPa)
RPM

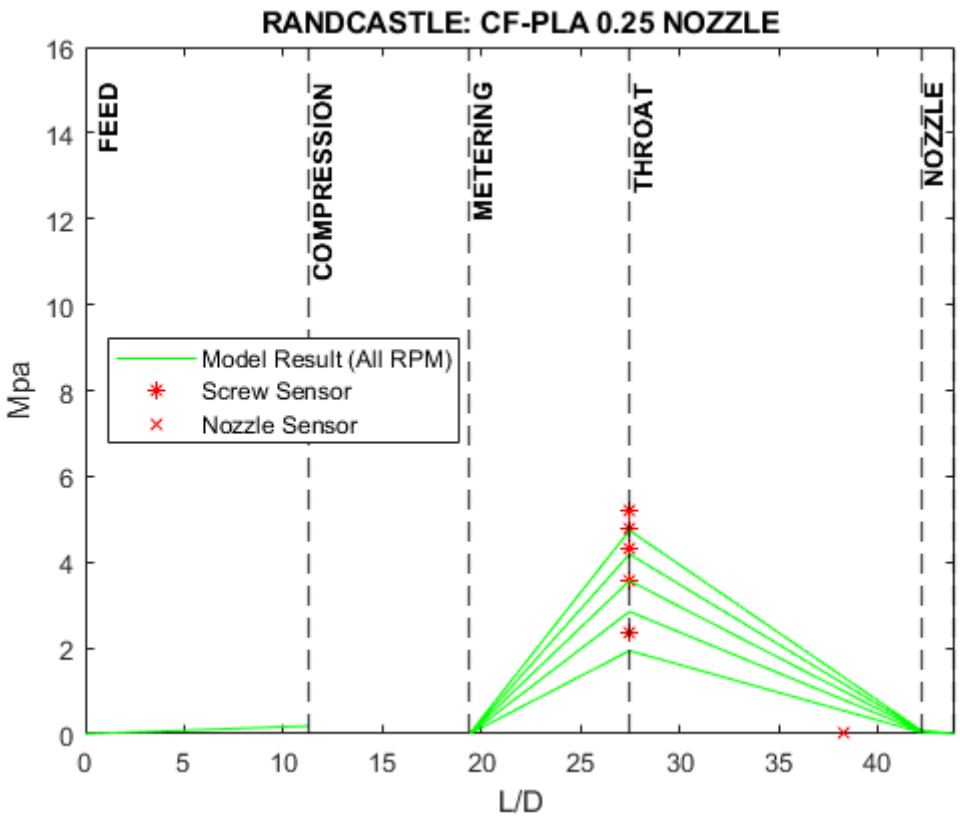
RANDCASTLE: CF-PLA 0.25 NOZZLE
FEED
COMPRESSION
METERING
THROAT
NOZZLE
Model Result (All RPM)
Screw Sensor
Nozzle Sensor
Mpa
L/D

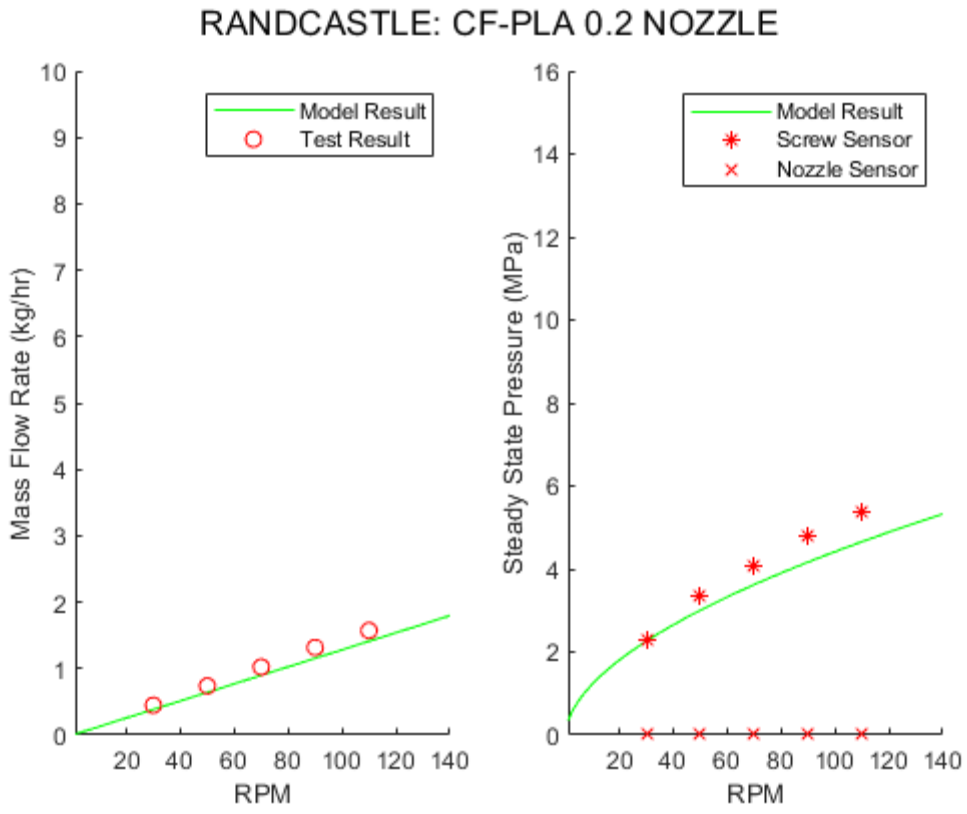
RANDCASTLE: CF-PLA 0.2 NOZZLE
Model Result
Test Result
Mass Flow Rate (kg/hr)
RPM
Model Result
Screw Sensor
Nozzle Sensor
Steady State Pressure (MPa)
RPM

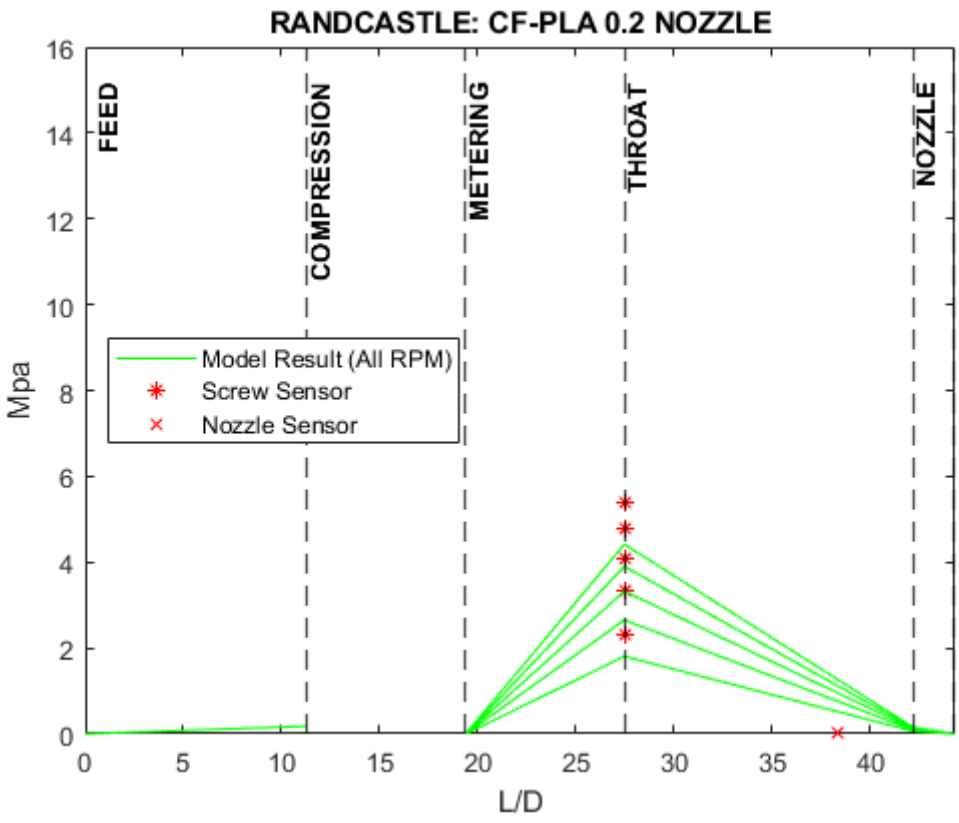
RANDCASTLE: CF-PLA 0.2 NOZZLE
FEED
COMPRESSION
METERING
THROAT
NOZZLE
Model Result (All RPM)
Screw Sensor
Nozzle Sensor
Mpa
L/D

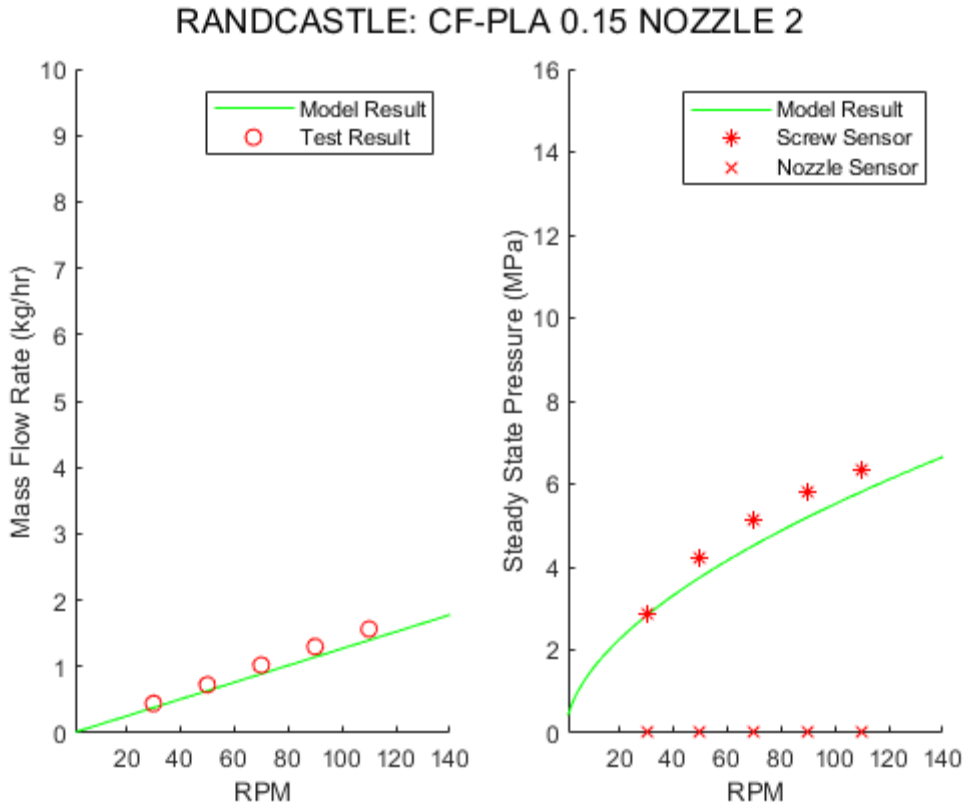
RANDCASTLE: CF-PLA 0.15 NOZZLE 2
Model Result
Test Result
Mass Flow Rate (kg/hr)
RPM
Model Result
Screw Sensor
Nozzle Sensor
Steady State Pressure (MPa)
RPM

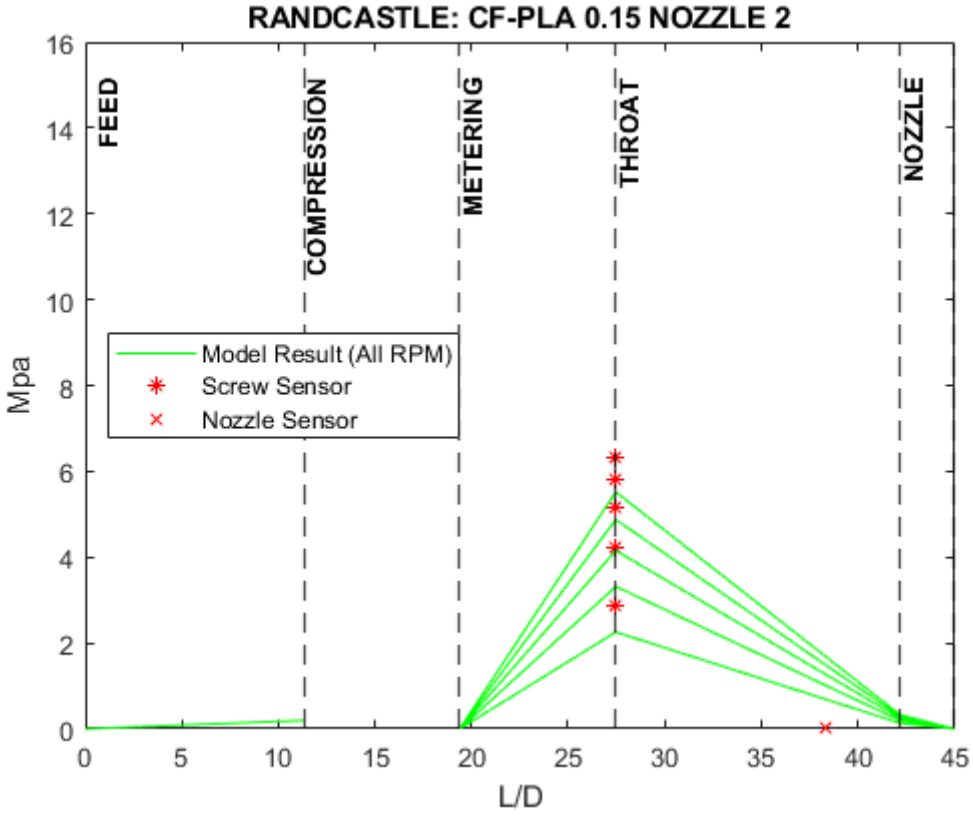
RANDCASTLE: CF-PLA 0.15 NOZZLE 2
FEED
COMPRESSION
METERING
THROAT
NOZZLE
Model Result (All RPM)
Screw Sensor
Nozzle Sensor
Mpa
L/D

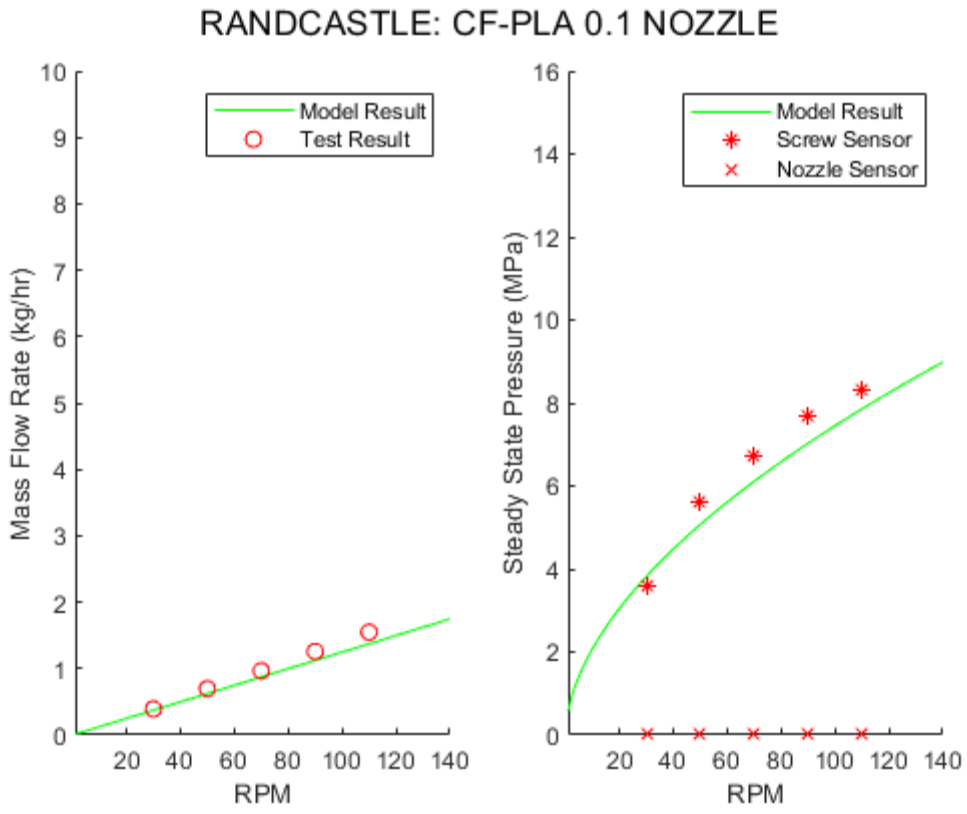
RANDCASTLE: CF-PLA 0.1 NOZZLE
Model Result
Test Result
Mass Flow Rate (kg/hr)
RPM
Model Result
Screw Sensor
Nozzle Sensor
Steady State Pressure (MPa)
RPM

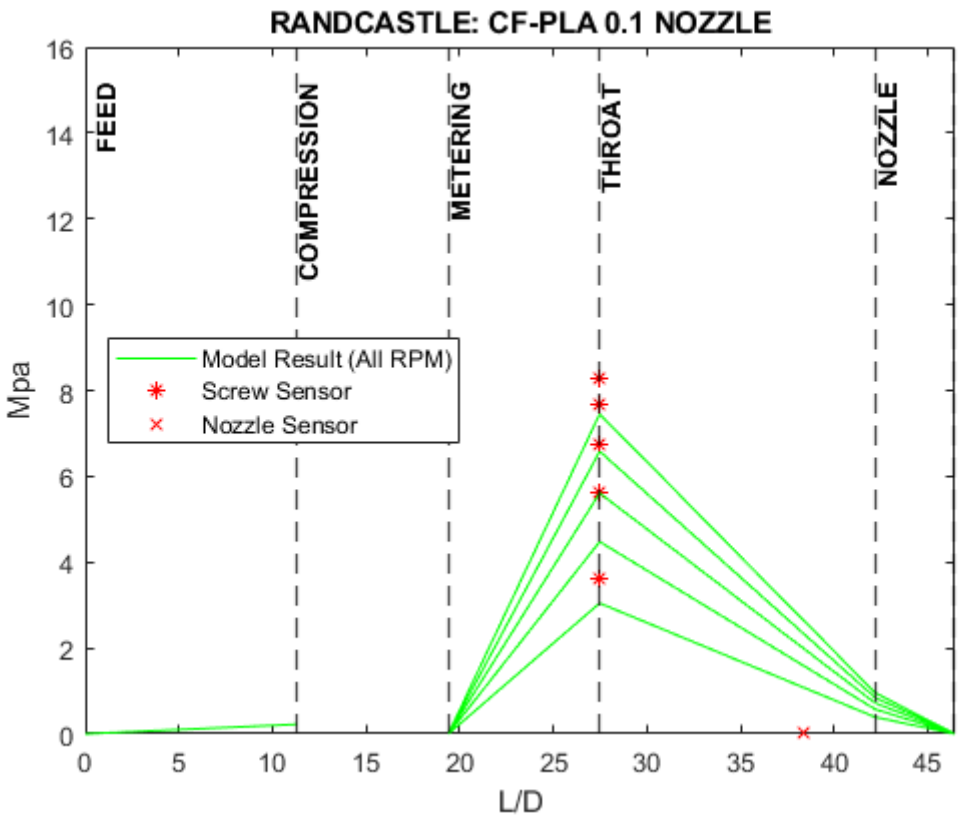
RANDCASTLE: CF-PLA 0.1 NOZZLE
FEED
COMPRESSION
METERING
THROAT
NOZZLE
Model Result (All RPM)
Screw Sensor
Nozzle Sensor
Mpa
L/D

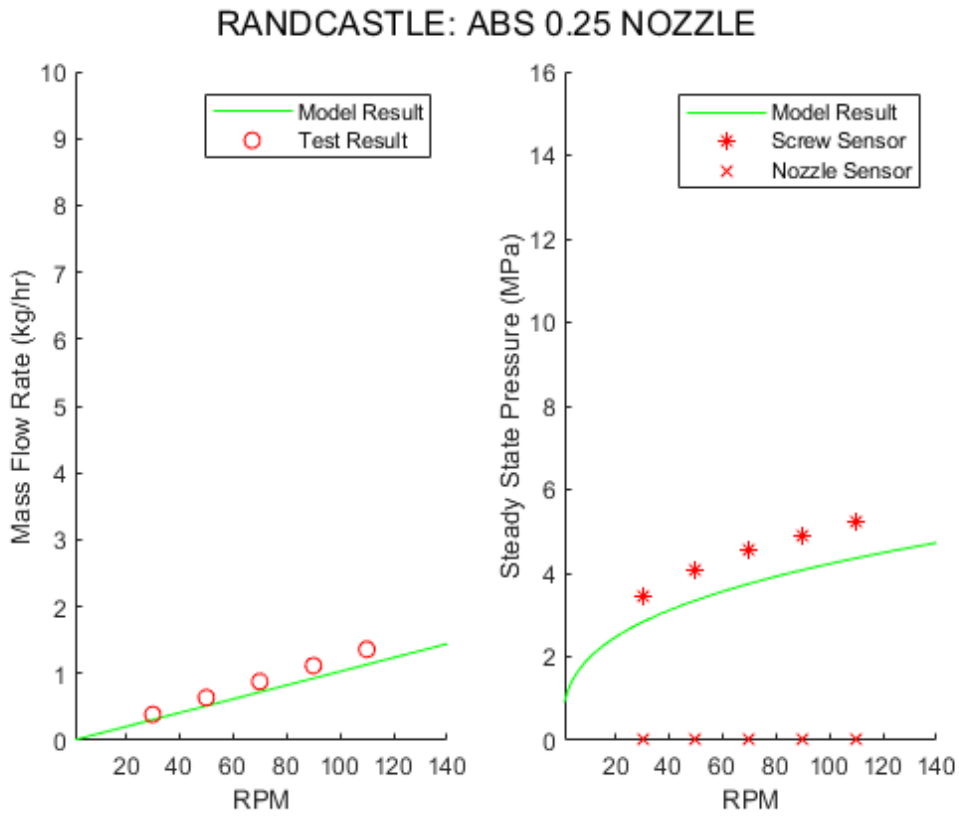
RANDCASTLE: ABS 0.25 NOZZLE
Model Result
Test Result
Mass Flow Rate (kg/hr)
RPM
Model Result
Screw Sensor
Nozzle Sensor
Steady State Pressure (MPa)
RPM

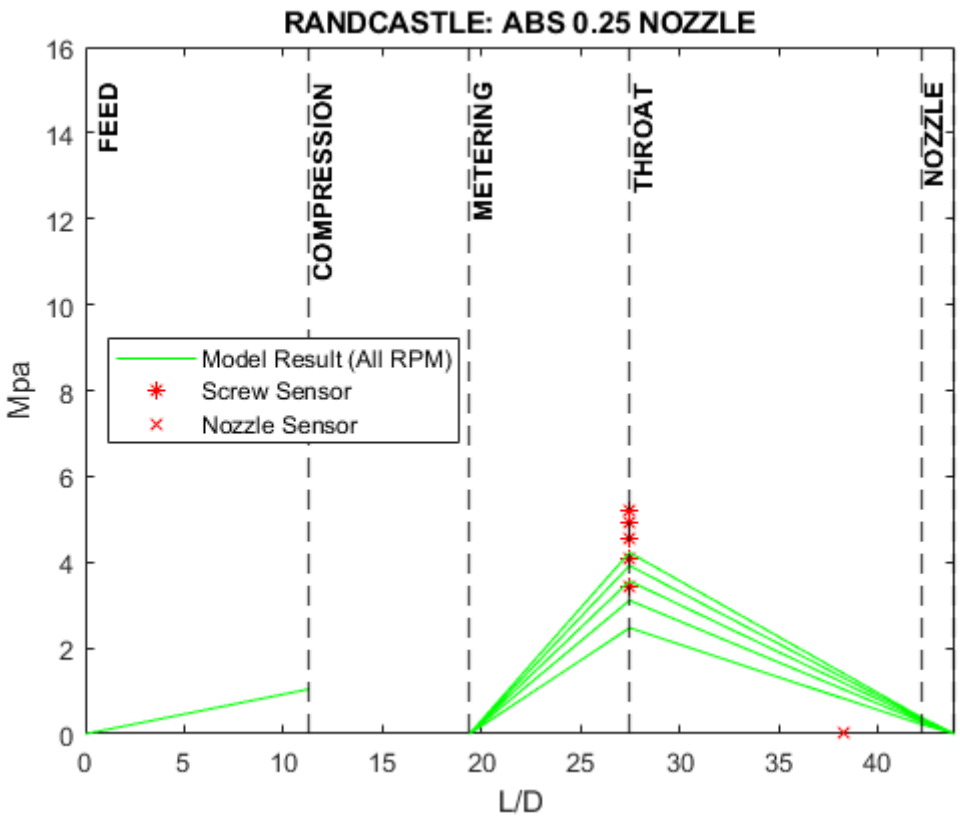
RANDCASTLE: ABS 0.25 NOZZLE
FEED
COMPRESSION
METERING
THROAT
NOZZLE
Model Result (All RPM)
Screw Sensor
Nozzle Sensor
Mpa
L/D

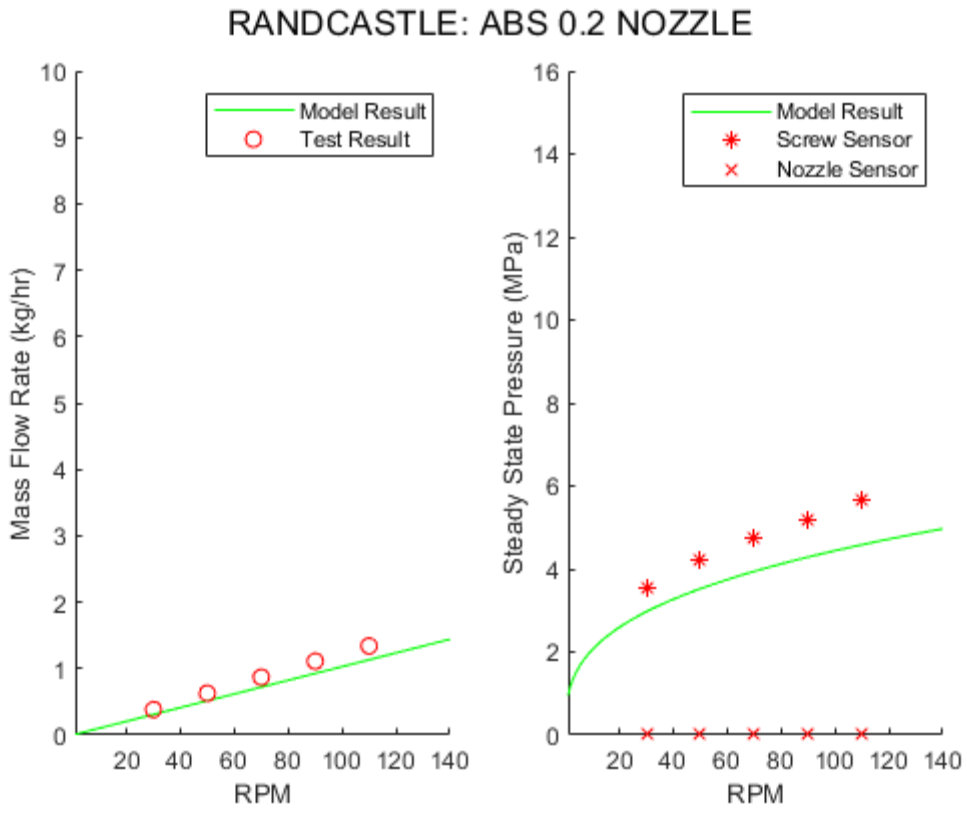
RANDCASTLE: ABS 0.2 NOZZLE
Model Result
Test Result
Mass Flow Rate (kg/hr)
RPM
Model Result
Screw Sensor
Nozzle Sensor
Steady State Pressure (MPa)
RPM

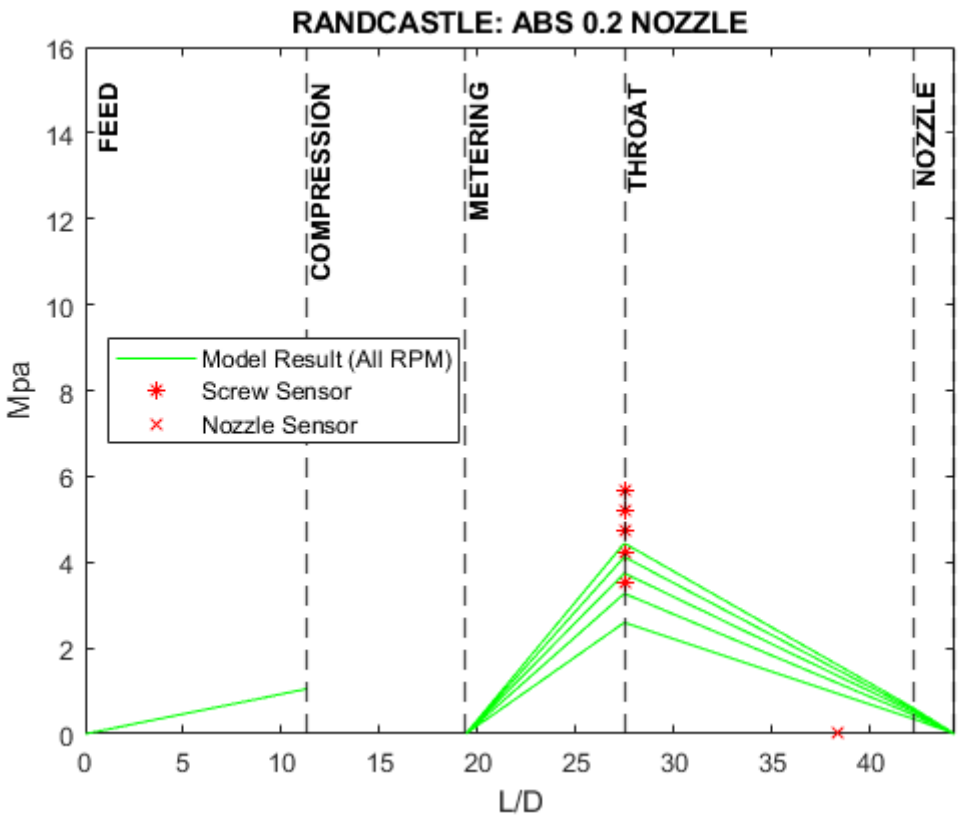
RANDCASTLE: ABS 0.2 NOZZLE
FEED
COMPRESSION
METERING
THROAT
NOZZLE
Model Result (All RPM)
Screw Sensor
Nozzle Sensor
Mpa
L/D

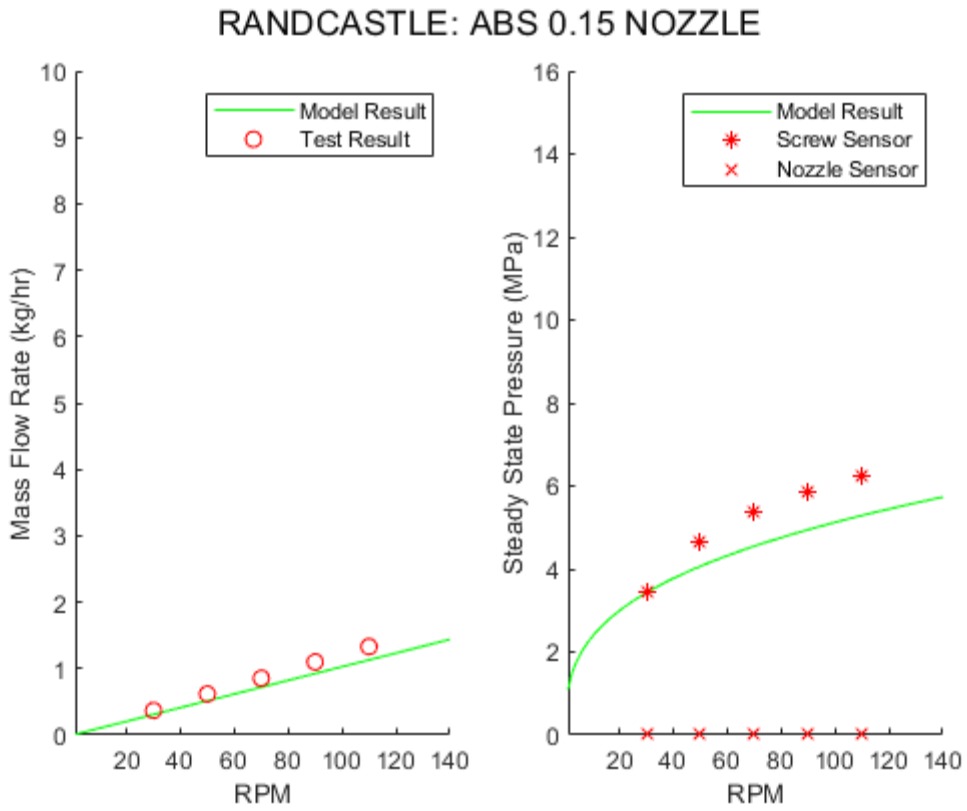
RANDCASTLE: ABS 0.15 NOZZLE
Model Result
Test Result
Mass Flow Rate (kg/hr)
RPM
Model Result
Screw Sensor
Nozzle Sensor
Steady State Pressure (MPa)
RPM

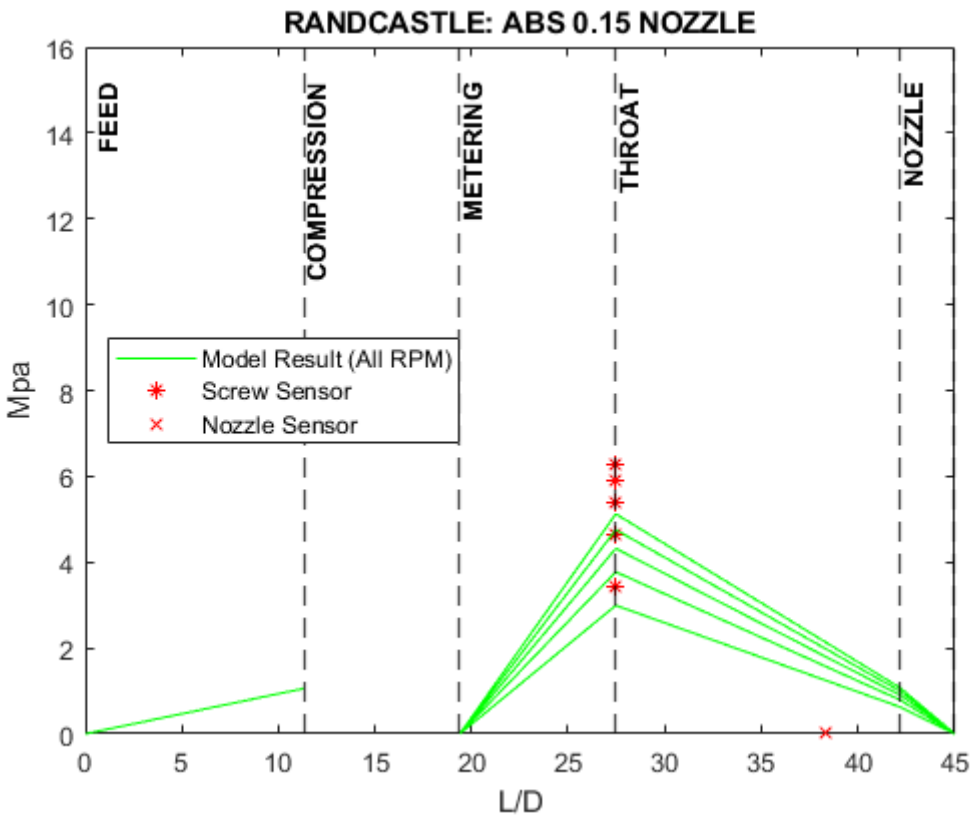
RANDCASTLE: ABS 0.15 NOZZLE
FEED
COMPRESSION
METERING
THROAT
NOZZLE
Model Result (All RPM)
Screw Sensor
Nozzle Sensor
Mpa
L/D

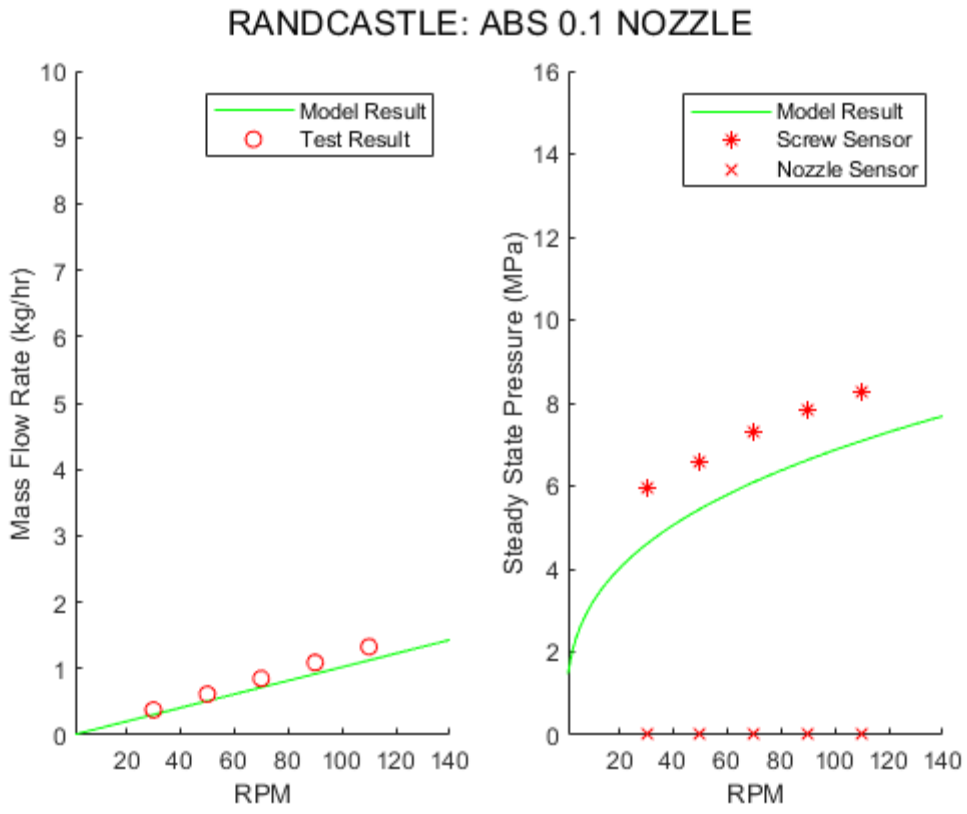
RANDCASTLE: ABS 0.1 NOZZLE
Model Result
Test Result
Mass Flow Rate (kg/hr)
RPM
Model Result
Screw Sensor
Nozzle Sensor
Steady State Pressure (MPa)
RPM

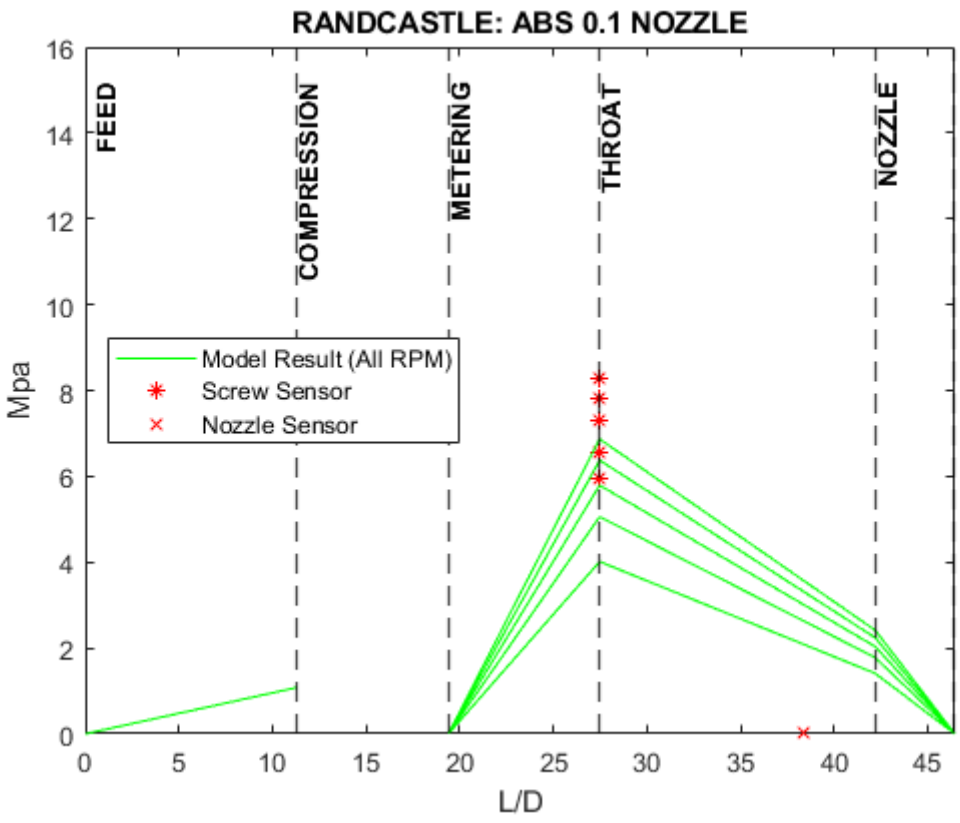
RANDCASTLE: ABS 0.1 NOZZLE
FEED
COMPRESSION
METERING
THROAT
NOZZLE
Model Result (All RPM)
Screw Sensor
Nozzle Sensor
Mpa
L/D

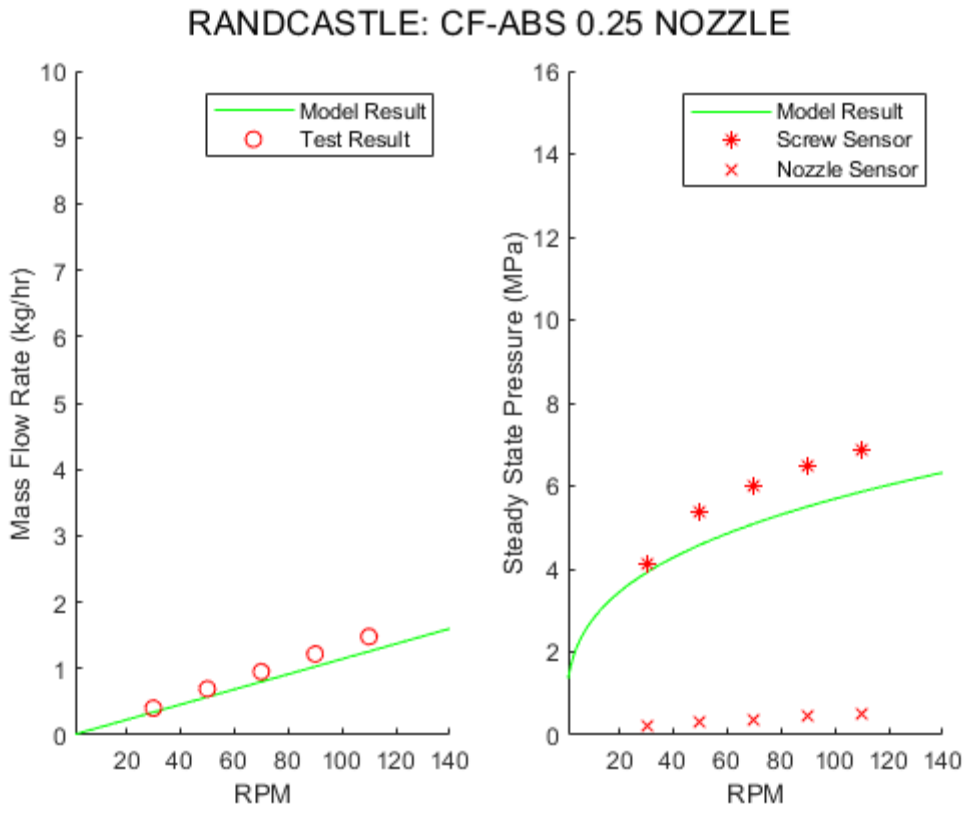
RANDCASTLE: CF-ABS 0.25 NOZZLE
Model Result
Test Result
Mass Flow Rate (kg/hr)
RPM
Model Result
Screw Sensor
Nozzle Sensor
Steady State Pressure (MPa)
RPM

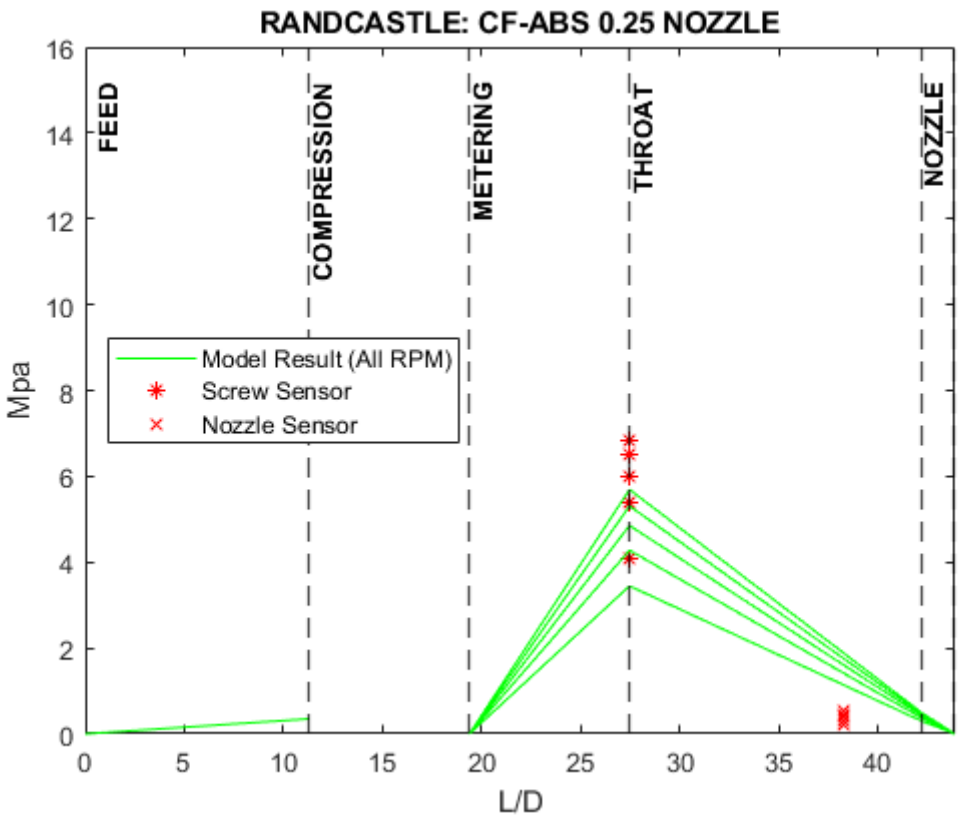
RANDCASTLE: CF-ABS 0.25 NOZZLE
FEED
COMPRESSION
METERING
THROAT
NOZZLE
Model Result (All RPM)
Screw Sensor
Nozzle Sensor
Mpa
L/D

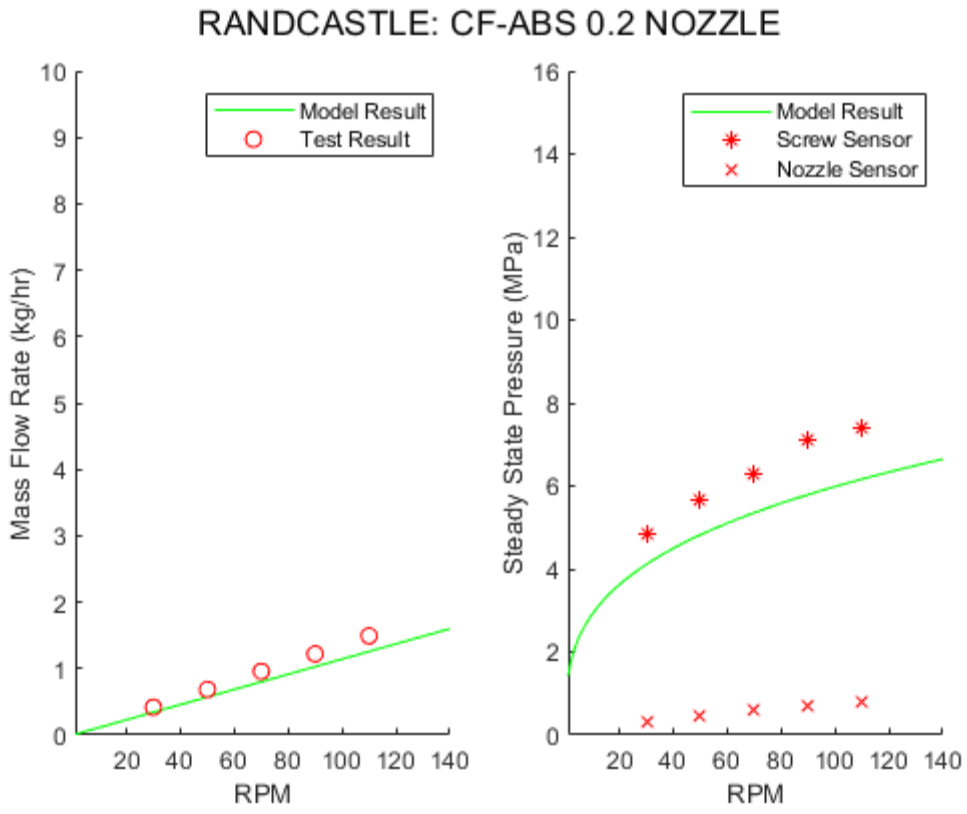
RANDCASTLE: CF-ABS 0.2 NOZZLE
Model Result
Test Result
Mass Flow Rate (kg/hr)
RPM
Model Result
Screw Sensor
Nozzle Sensor
Steady State Pressure (MPa)
RPM

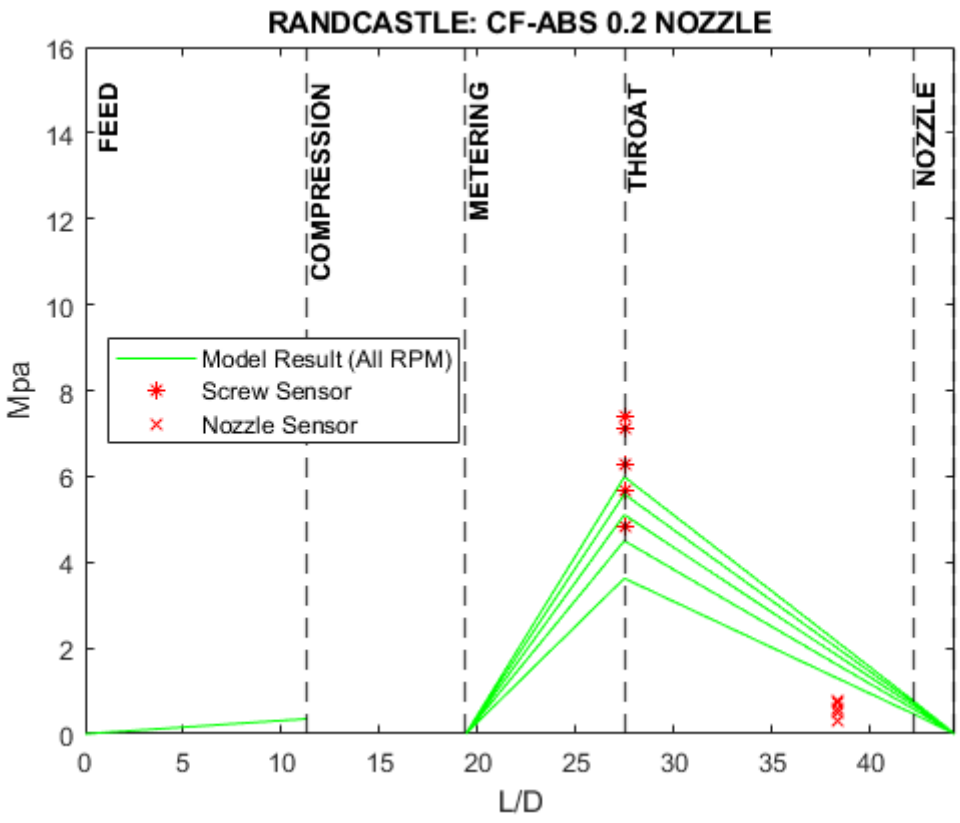
RANDCASTLE: CF-ABS 0.2 NOZZLE
FEED
COMPRESSION
METERING
THROAT
NOZZLE
Model Result (All RPM)
Screw Sensor
Nozzle Sensor
Mpa
L/D

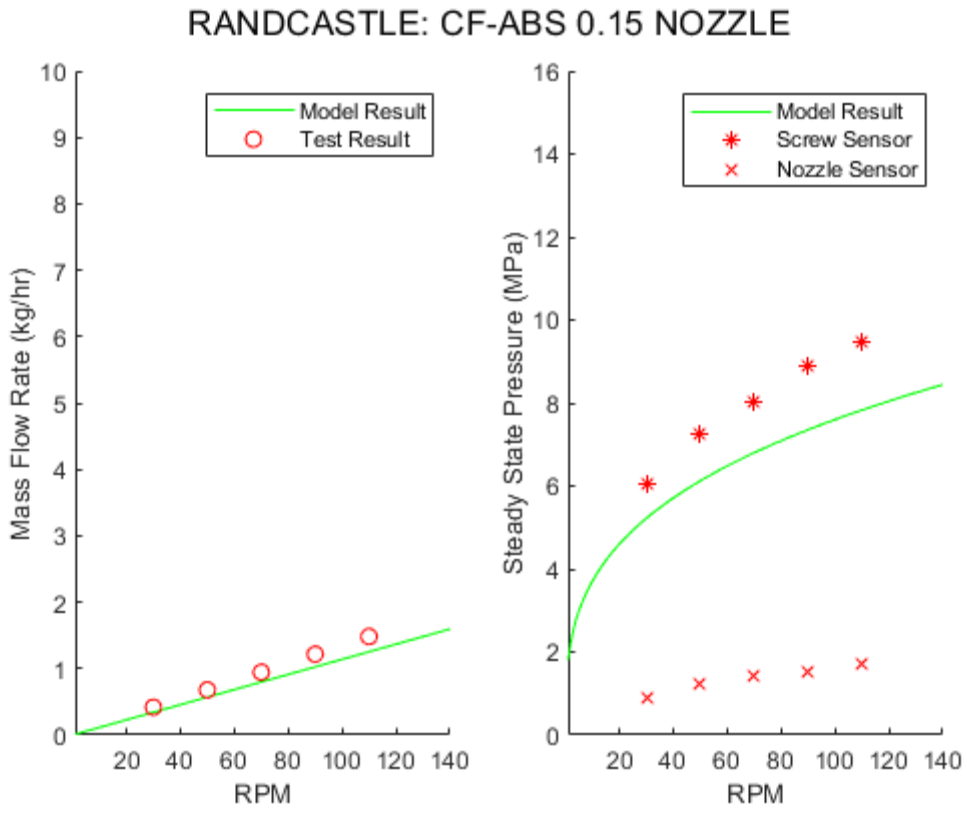
RANDCASTLE: CF-ABS 0.15 NOZZLE
Model Result
Test Result
Mass Flow Rate (kg/hr)
RPM
Model Result
Screw Sensor
Nozzle Sensor
Steady State Pressure (MPa)
RPM

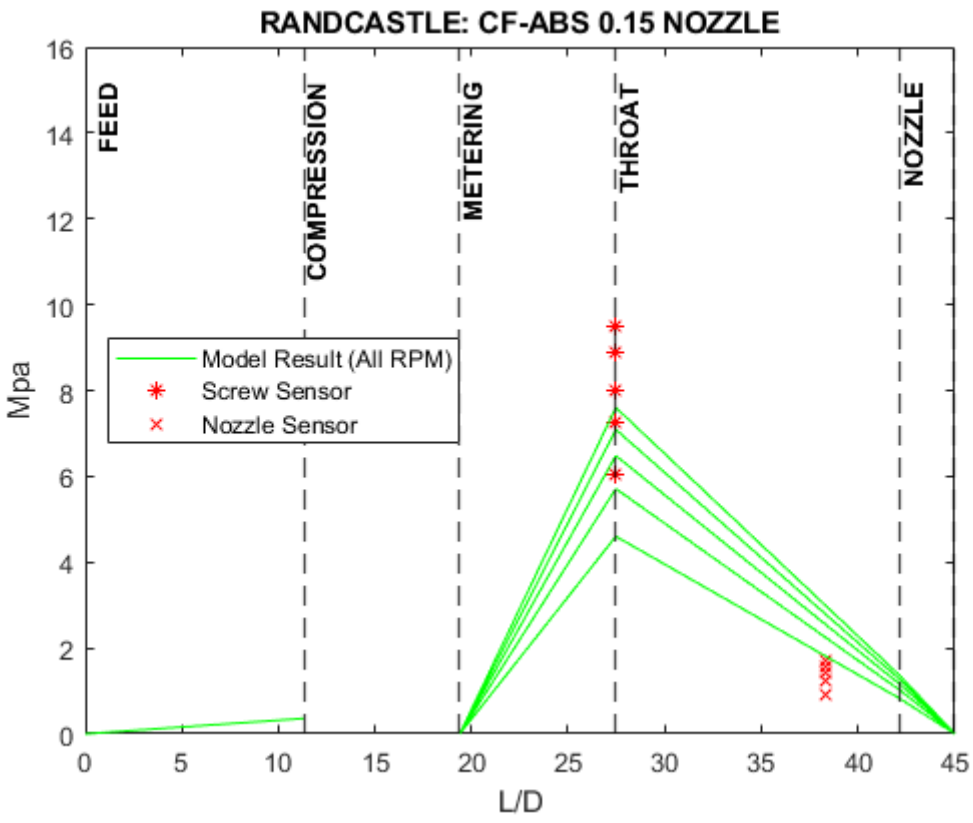
RANDCASTLE: CF-ABS 0.15 NOZZLE
FEED
COMPRESSION
METERING
THROAT
NOZZLE
Model Result (All RPM)
Screw Sensor
Nozzle Sensor
Mpa
L/D

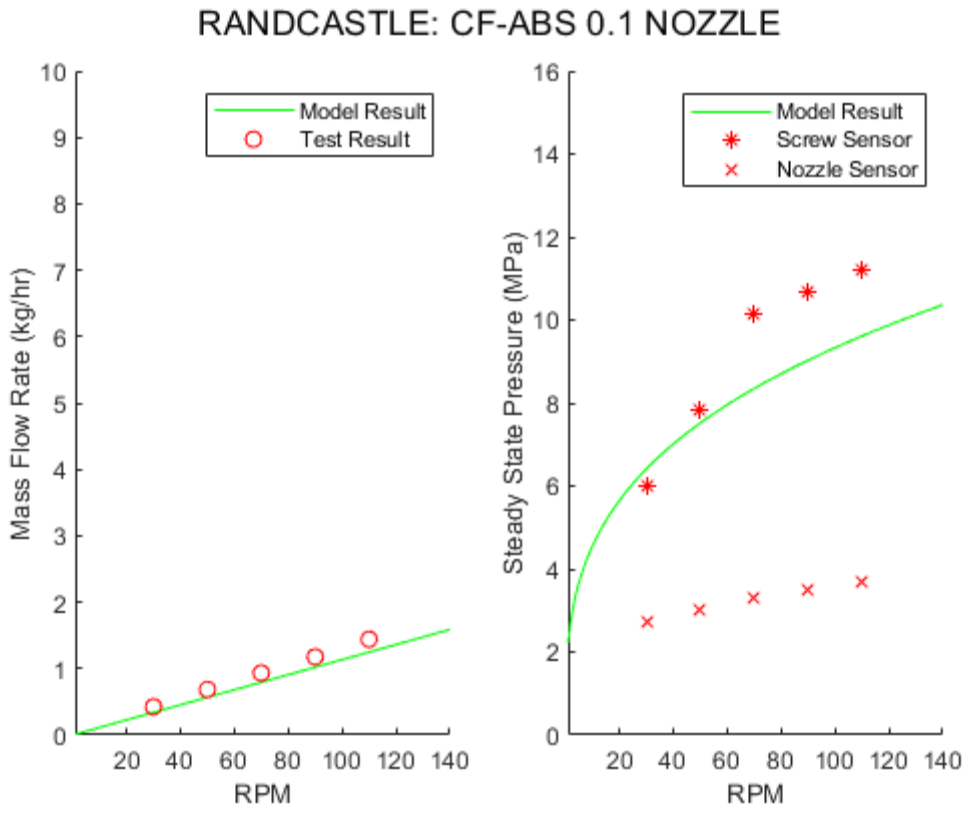
RANDCASTLE: CF-ABS 0.1 NOZZLE
Model Result
Test Result
Mass Flow Rate (kg/hr)
RPM
Model Result
Screw Sensor
Nozzle Sensor
Steady State Pressure (MPa)
RPM

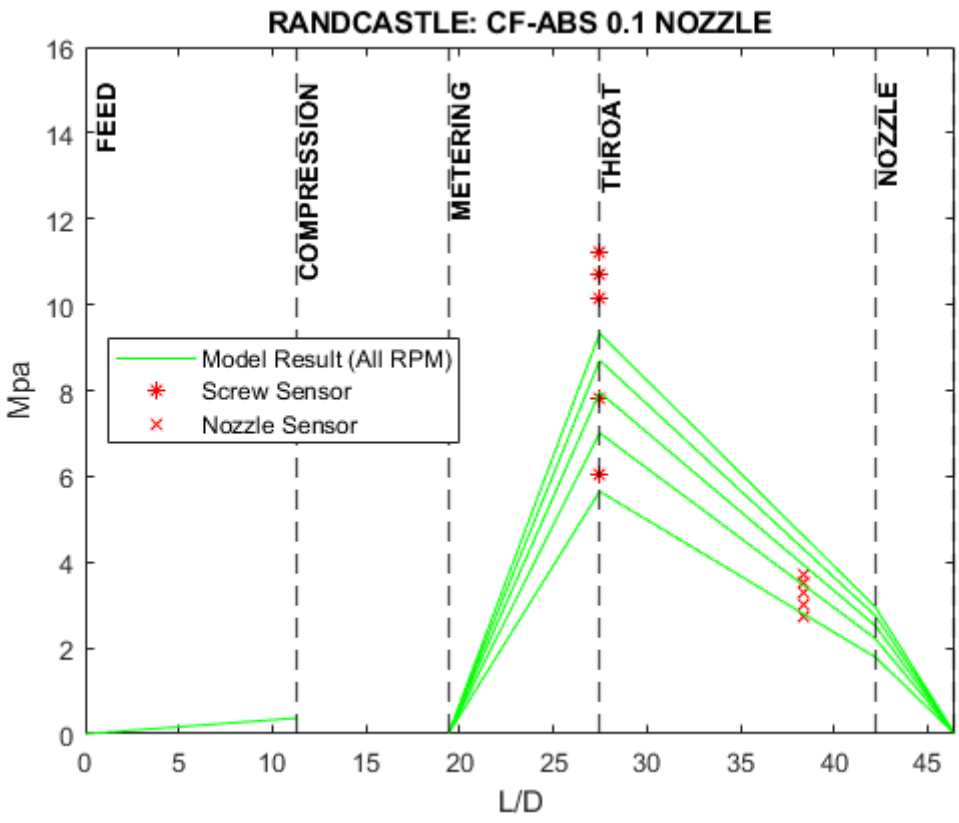
RANDCASTLE: CF-ABS 0.1 NOZZLE
FEED
COMPRESSION
METERING
THROAT
NOZZLE
Model Result (All RPM)
Screw Sensor
Nozzle Sensor
Mpa
L/D
0
2
4
6
8
10
12
14
16
0
5
10
15
20
25
30
35
40
45

A5. Microtruder Tabulated Data

Neat PLA, 0.1 Nozzle, Barrel Location							
Screw Speed (RPM)	Trial #	Mass of Extrudate (g)	Time (s)	Mass Flow Rate (kg/hr)	Average Mass Flow Rate (kg/hr)	Average Pressure (MPa)	Average Pressure for Each RPM (Mpa)
30	1	4.970	90.24	0.1983	0.1933	5.5165	5.3823
30	2	4.710	90.00	0.1884		5.2480	
50	1	8.970	90.20	0.3580	0.3441	8.0670	7.8628
50	2	8.290	90.40	0.3301		7.6586	
70	1	11.98	90.24	0.4779	0.4724	9.4875	9.4138
70	2	11.70	90.20	0.4670		9.3401	
90	1	15.19	89.84	0.6087	0.6160	10.516	10.593
90	2	15.70	90.68	0.6233		10.669	
110	1	19.28	90.24	0.7692	0.7600	11.533	11.443
110	2	18.82	90.24	0.7508		11.353	

Neat PLA, 0.15 Nozzle, Barrel Location							
Screw Speed (RPM)	Trial #	Mass of Extrudate (g)	Time (s)	Mass Flow Rate (kg/hr)	Average Mass Flow Rate (kg/hr)	Average Pressure (MPa)	Average Pressure for Each RPM (Mpa)
30	1	4.240	90.72	0.1683	0.1955	3.2973	3.6957
30	2	5.610	90.64	0.2228		4.0941	
50	1	8.150	89.72	0.3270	0.3441	5.4647	5.7013
50	2	9.020	89.92	0.3611		5.9378	
70	1	12.01	90.08	0.4800	0.4817	6.9690	7.0037
70	2	12.09	90.04	0.4834		7.0384	
90	1	14.61	91.32	0.5760	0.5822	7.5824	7.6292
90	2	14.71	90.00	0.5884		7.6760	
110	1	18.25	89.96	0.7303	0.7318	8.4557	8.4396
110	2	18.30	89.84	0.7333		8.4235	

Neat PLA, 0.2 Nozzle, Barrel Location							
Screw Speed (RPM)	Trial #	Mass of Extrudate (g)	Time (s)	Mass Flow Rate (kg/hr)	Average Mass Flow Rate (kg/hr)	Average Pressure (MPa)	Average Pressure for Each RPM (Mpa)
30	1	4.530	89.92	0.1814	0.1951	2.8875	3.0224
30	2	5.230	90.20	0.2087		3.1572	
50	1	8.430	90.00	0.3372	0.3381	4.4436	4.4814
50	2	8.470	89.96	0.3390		4.5191	
70	1	11.49	89.92	0.4600	0.4600	5.4661	5.4823
70	2	11.51	90.08	0.4600		5.4984	
90	1	15.98	89.68	0.6415	0.6395	6.5928	6.6045
90	2	15.93	89.96	0.6375		6.6162	
110	1	18.19	89.96	0.7279	0.7378	6.9324	6.9980
110	2	18.65	89.80	0.7477		7.0635	

Neat PLA, 0.25 Nozzle, Barrel Location							
Screw Speed (RPM)	Trial #	Mass of Extrudate (g)	Time (s)	Mass Flow Rate (kg/hr)	Average Mass Flow Rate (kg/hr)	Average Pressure (MPa)	Average Pressure for Each RPM (Mpa)
30	1	4.810	89.84	0.1927	0.1878	2.7898	2.7463
30	2	4.560	89.76	0.1829		2.7028	
50	1	7.640	89.76	0.3064	0.3102	3.9361	3.9248
50	2	7.840	89.88	0.3140		3.9134	
70	1	12.03	89.80	0.4823	0.4613	5.1768	5.0413
70	2	11.02	90.08	0.4404		4.9057	
90	1	14.89	90.32	0.5935	0.5990	5.6835	5.7197
90	2	15.09	89.88	0.6044		5.7559	
110	1	17.28	89.92	0.6918	0.7262	6.1868	6.4016
110	2	19.00	89.92	0.7607		6.6164	

Neat ABS, 0.1 Nozzle, Barrel Location							
Screw Speed (RPM)	Trial #	Mass of Extrudate (g)	Time (s)	Mass Flow Rate (kg/hr)	Average Mass Flow Rate (kg/hr)	Average Pressure (MPa)	Average Pressure for Each RPM (Mpa)
30	1	9.380	90.16	0.3745	0.3770	6.1507	5.9344
30	2	9.520	90.32	0.3795		5.7181	
50	1	15.44	89.96	0.6179	0.6149	6.6196	6.5696
50	2	15.32	90.12	0.6120		6.5196	
70	1	21.29	90.12	0.8505	0.8508	7.2842	7.2847
70	2	21.27	89.96	0.8512		7.2851	
90	1	27.24	89.92	1.091	1.091	7.8391	7.8358
90	2	27.30	90.00	1.092		7.8325	
110	1	33.28	90.08	1.330	1.328	8.3040	8.2873
110	2	33.17	90.00	1.327		8.2706	

Neat ABS, 0.15 Nozzle, Barrel Location							
Screw Speed (RPM)	Trial #	Mass of Extrudate (g)	Time (s)	Mass Flow Rate (kg/hr)	Average Mass Flow Rate (kg/hr)	Average Pressure (MPa)	Average Pressure for Each RPM (Mpa)
30	1	9.050	92.72	0.3514	0.3690	3.4125	3.4323
30	2	9.670	90.04	0.3866		3.4520	
50	1	15.39	90.12	0.6148	0.6179	4.6499	4.6644
50	2	15.63	90.60	0.6211		4.6788	
70	1	21.46	89.96	0.8588	0.8558	5.3881	5.3919
70	2	22.46	94.80	0.8529		5.3956	
90	1	27.48	89.92	1.100	1.100	5.8960	5.8777
90	2	27.53	90.08	1.100		5.8594	
110	1	33.23	90.08	1.328	1.332	6.2479	6.2528
110	2	33.39	90.00	1.336		6.2576	

Neat ABS, 0.2 Nozzle, Barrel Location							
Screw Speed (RPM)	Trial #	Mass of Extrudate (g)	Time (s)	Mass Flow Rate (kg/hr)	Average Mass Flow Rate (kg/hr)	Average Pressure (MPa)	Average Pressure for Each RPM (Mpa)
30	1	9.600	90.04	0.3838	0.3823	3.6190	3.5195
30	2	9.520	90.00	0.3808		3.4199	
50	1	15.58	89.84	0.6243	0.6289	4.2131	4.2089
50	2	15.83	89.96	0.6335		4.2046	
70	1	21.70	90.32	0.8649	0.8699	4.7373	4.7435
70	2	21.86	89.96	0.8748		4.7497	
90	1	27.84	90.08	1.113	1.111	5.1884	5.1821
90	2	27.78	90.08	1.110		5.1757	
110	1	33.64	90.04	1.345	1.341	5.4481	5.4646
110	2	33.43	90.08	1.336		5.4811	

Neat ABS, 0.25 Nozzle, Barrel Location							
Screw Speed (RPM)	Trial #	Mass of Extrudate (g)	Time (s)	Mass Flow Rate (kg/hr)	Average Mass Flow Rate (kg/hr)	Average Pressure (MPa)	Average Pressure for Each RPM (Mpa)
30	1	9.700	90.08	0.3877	0.3865	3.5094	3.4246
30	2	9.640	90.04	0.3854		3.3398	
50	1	15.85	90.04	0.6337	0.6386	4.0972	4.0737
50	2	15.58	87.16	0.6435		4.0501	
70	1	21.98	90.08	0.8784	0.8800	4.5645	4.5628
70	2	22.04	90.00	0.8816		4.5610	
90	1	28.05	90.00	1.122	1.117	4.9262	4.9129
90	2	27.80	90.08	1.111		4.8996	
110	1	33.97	89.96	1.359	1.361	5.2211	5.2189
110	2	34.07	90.00	1.363		5.2167	

LLDPE, 0.1 Nozzle, Barrel Location							
Screw Speed (RPM)	Trial #	Mass of Extrudate (g)	Time (s)	Mass Flow Rate (kg/hr)	Average Mass Flow Rate (kg/hr)	Average Pressure (MPa)	Average Pressure for Each RPM (Mpa)
30	1	7.730	90.24	0.3084	0.3059	3.2440	3.2060
30	2	7.580	89.96	0.3033		3.1679	
50	1	12.49	89.96	0.4998	0.4999	4.4818	4.4961
50	2	12.50	90.00	0.5000		4.5103	
70	1	18.60	89.96	0.7443	0.7268	5.9061	5.7821
70	2	17.70	89.84	0.7093		5.6581	
90	1	21.55	90.16	0.8605	0.8777	6.5320	6.5774
90	2	22.58	90.84	0.8949		6.6227	
110	1	26.60	90.20	1.062	1.068	7.2340	7.2545
110	2	26.77	89.68	1.075		7.2749	

LLDPE, 0.15 Nozzle, Barrel Location							
Screw Speed (RPM)	Trial #	Mass of Extrudate (g)	Time (s)	Mass Flow Rate (kg/hr)	Average Mass Flow Rate (kg/hr)	Average Pressure (MPa)	Average Pressure for Each RPM (Mpa)
30	1	7.520	90.16	0.3003	0.2915	1.9089	1.8670
30	2	7.090	90.28	0.2827		1.8251	
50	1	11.54	90.24	0.4604	0.4693	2.7804	2.8421
50	2	12.02	90.48	0.4783		2.9038	
70	1	17.43	90.44	0.6938	0.7054	3.8423	3.8986
70	2	18.01	90.44	0.7169		3.9548	
90	1	21.68	90.00	0.8672	0.8625	4.5162	4.4774
90	2	21.51	90.28	0.8577		4.4386	
110	1	22.23	75.64	1.058	1.045	5.0646	5.0312
110	2	25.74	89.76	1.032		4.9978	

LLDPE, 0.2 Nozzle, Barrel Location							
Screw Speed (RPM)	Trial #	Mass of Extrudate (g)	Time (s)	Mass Flow Rate (kg/hr)	Average Mass Flow Rate (kg/hr)	Average Pressure (MPa)	Average Pressure for Each RPM (Mpa)
30	1	7.220	90.52	0.2871	0.2901	1.5938	1.6010
30	2	7.300	89.68	0.2930		1.6081	
50	1	12.61	92.36	0.4915	0.5144	2.4884	2.5845
50	2	13.40	89.80	0.5372		2.6805	
70	1	19.18	90.32	0.7645	0.7416	3.5720	3.5342
70	2	17.99	90.12	0.7186		3.4963	
90	1	22.42	90.36	0.8932	0.8729	3.3852	3.3128
90	2	21.72	91.72	0.8525		3.2403	
110	1	25.83	90.08	1.032	1.049	3.6775	3.7356
110	2	26.63	90.00	1.065		3.7937	

LLDPE, 0.25 Nozzle, Barrel Location							
Screw Speed (RPM)	Trial #	Mass of Extrudate (g)	Time (s)	Mass Flow Rate (kg/hr)	Average Mass Flow Rate (kg/hr)	Average Pressure (MPa)	Average Pressure for Each RPM (Mpa)
30	1	7.960	90.00	0.3184	0.3115	1.8508	1.8124
30	2	7.620	90.08	0.3045		1.7740	
50	1	12.48	89.96	0.4994	0.5061	2.6267	2.6509
50	2	12.80	89.88	0.5127		2.6751	
70	1	18.35	89.92	0.7347	0.7156	3.4516	3.3903
70	2	17.42	90.04	0.6965		3.3289	
90	1	23.35	89.92	0.9348	0.9178	4.0455	3.9991
90	2	22.53	90.04	0.9008		3.9527	
110	1	26.88	90.04	1.075	1.095	4.4180	4.4577
110	2	27.85	89.96	1.115		4.4973	

20% CF PLA, 0.1 Nozzle, Barrel Location							
Screw Speed (RPM)	Trial #	Mass of Extrudate (g)	Time (s)	Mass Flow Rate (kg/hr)	Average Mass Flow Rate (kg/hr)	Average Pressure (MPa)	Average Pressure for Each RPM (Mpa)
30	1	10.10	89.96	0.4042	0.3921	3.7176	3.6025
30	2	9.500	90.00	0.3800		3.4874	
50	1	17.72	89.88	0.7098	0.6972	5.6315	5.5991
50	2	18.27	96.08	0.6846		5.5666	
70	1	23.86	90.00	0.9544	0.9676	6.7087	6.7232
70	2	24.52	90.00	0.9808		6.7377	
90	1	36.47	105.5	1.245	1.258	7.6460	7.6864
90	2	31.72	89.84	1.271		7.7268	
110	1	38.85	90.00	1.554	1.549	8.3257	8.3004
110	2	38.53	89.84	1.544		8.2751	

20% CF PLA, 0.15 Nozzle, Barrel Location							
Screw Speed (RPM)	Trial #	Mass of Extrudate (g)	Time (s)	Mass Flow Rate (kg/hr)	Average Mass Flow Rate (kg/hr)	Average Pressure (MPa)	Average Pressure for Each RPM (Mpa)
30	1	11.22	90.16	0.4480	0.4439	2.8894	2.8792
30	2	11.00	90.04	0.4398		2.8689	
50	1	18.46	90.12	0.7374	0.7269	4.2555	4.2115
50	2	17.90	89.96	0.7163		4.1674	
70	1	25.59	89.88	1.025	1.023	5.1625	5.1411
70	2	25.56	90.20	1.020		5.1197	
90	1	32.46	90.08	1.297	1.300	5.8051	5.8148
90	2	32.62	90.08	1.304		5.8244	
110	1	39.53	90.04	1.581	1.564	6.3751	6.3249
110	2	38.73	90.08	1.548		6.2746	

20% CF PLA, 0.2 Nozzle, Barrel Location							
Screw Speed (RPM)	Trial #	Mass of Extrudate (g)	Time (s)	Mass Flow Rate (kg/hr)	Average Mass Flow Rate (kg/hr)	Average Pressure (MPa)	Average Pressure for Each RPM (Mpa)
30	1	10.83	90.32	0.4317	0.4322	3.1166	3.1494
30	2	10.88	90.52	0.4327		3.1822	
50	1	18.02	90.48	0.7170	0.7201	4.3403	4.3645
50	2	18.13	90.24	0.7233		4.3887	
70	1	23.75	90.60	0.9437	0.9637	5.0584	5.1136
70	2	25.16	92.08	0.9837		5.1687	
90	1	32.20	90.80	1.277	1.267	5.7276	5.6772
90	2	31.68	90.64	1.258		5.6267	
110	1	39.30	90.20	1.569	1.550	6.1071	6.0313
110	2	38.55	90.56	1.532		5.9555	

20% CF PLA, 0.25 Nozzle, Barrel Location							
Screw Speed (RPM)	Trial #	Mass of Extrudate (g)	Time (s)	Mass Flow Rate (kg/hr)	Average Mass Flow Rate (kg/hr)	Average Pressure (MPa)	Average Pressure for Each RPM (Mpa)
30	1	10.82	90.00	0.4328	0.4310	2.3001	2.3359
30	2	10.74	90.08	0.4292		2.3716	
50	1	23.51	117.7	0.7192	0.7184	3.5703	3.5743
50	2	17.97	90.16	0.7175		3.5783	
70	1	25.08	90.04	1.003	0.9968	4.3290	4.3224
70	2	24.76	89.96	0.9908		4.3158	
90	1	32.59	89.96	1.304	1.267	4.9187	4.7953
90	2	30.77	90.04	1.230		4.6718	
110	1	38.94	90.04	1.557	1.568	5.1920	5.2109
110	2	39.53	90.12	1.579		5.2298	

20% CF ABS, 0.1 Nozzle, Barrel Location							
Screw Speed (RPM)	Trial #	Mass of Extrudate (g)	Time (s)	Mass Flow Rate (kg/hr)	Average Mass Flow Rate (kg/hr)	Average Pressure (MPa)	Average Pressure for Each RPM (Mpa)
30	1	10.66	90.48	0.4241	0.4239	5.9392	6.0240
30	2	10.62	90.24	0.4237		6.1088	
50	1	17.10	90.60	0.6795	0.6844	7.7318	7.8252
50	2	17.25	90.08	0.6894		7.9185	
70	1	23.33	90.24	0.9307	0.9338	10.113	10.135
70	2	23.65	90.88	0.9368		10.158	
90	1	29.26	90.08	1.169	1.177	10.671	10.690
90	2	29.64	90.12	1.184		10.709	
110	1	38.63	96.08	1.447	1.441	11.228	11.219
110	2	35.89	90.04	1.435		11.211	

20% CF ABS, 0.15 Nozzle, Barrel Location							
Screw Speed (RPM)	Trial #	Mass of Extrudate (g)	Time (s)	Mass Flow Rate (kg/hr)	Average Mass Flow Rate (kg/hr)	Average Pressure (MPa)	Average Pressure for Each RPM (Mpa)
30	1	10.62	91.40	0.4183	0.4182	6.0555	6.0594
30	2	10.52	90.60	0.4180		6.0632	
50	1	17.04	90.36	0.6789	0.6795	7.2892	7.2496
50	2	16.96	89.76	0.6802		7.2100	
70	1	23.70	90.24	0.9455	0.9467	7.9721	8.0047
70	2	23.76	90.24	0.9479		8.0373	
90	1	30.48	90.20	1.217	1.217	8.8202	8.8967
90	2	30.56	90.32	1.218		8.9731	
110	1	37.64	90.40	1.499	1.484	9.4399	9.4911
110	2	36.93	90.52	1.469		9.5422	

20% CF ABS, 0.2 Nozzle, Barrel Location							
Screw Speed (RPM)	Trial #	Mass of Extrudate (g)	Time (s)	Mass Flow Rate (kg/hr)	Average Mass Flow Rate (kg/hr)	Average Pressure (MPa)	Average Pressure for Each RPM (Mpa)
30	1	10.51	90.16	0.4197	0.4173	4.9325	4.8311
30	2	10.46	90.76	0.4149		4.7297	
50	1	17.28	90.36	0.6885	0.6843	5.7033	5.6824
50	2	16.99	89.92	0.6802		5.6614	
70	1	23.94	89.92	0.9585	0.9567	6.2962	6.2758
70	2	23.85	89.92	0.9549		6.2554	
90	1	30.81	90.96	1.219	1.221	7.1154	7.1035
90	2	30.76	90.52	1.223		7.0916	
110	1	37.49	90.40	1.493	1.492	7.3891	7.3957
110	2	37.44	90.36	1.492		7.4023	

20% CF ABS, 0.25 Nozzle, Barrel Location							
Screw Speed (RPM)	Trial #	Mass of Extrudate (g)	Time (s)	Mass Flow Rate (kg/hr)	Average Mass Flow Rate (kg/hr)	Average Pressure (MPa)	Average Pressure for Each RPM (Mpa)
30	1	9.800	90.48	0.3899	0.4036	3.9650	4.1021
30	2	10.43	90.00	0.4172		4.2392	
50	1	17.34	90.24	0.6918	0.6950	5.3625	5.3764
50	2	17.54	90.44	0.6982		5.3902	
70	1	23.96	90.52	0.9529	0.9534	5.9888	6.0031
70	2	23.88	90.12	0.9539		6.0174	
90	1	30.66	90.36	1.222	1.220	6.4920	6.4846
90	2	30.56	90.36	1.218		6.4772	
110	1	37.42	90.56	1.488	1.482	6.8446	6.8498
110	2	37.08	90.40	1.477		6.8550	

Neat ABS, 0.1 Nozzle, Nozzle Location							
Screw Speed (RPM)	Trial #	Mass of Extrudate (g)	Time (s)	Mass Flow Rate (kg/hr)	Average Mass Flow Rate (kg/hr)	Average Pressure (MPa)	Average Pressure for Each RPM (Mpa)
30	1	9.710	90.00	0.3884	0.3886	1.8912	1.9422
30	2	9.730	90.08	0.3889		1.9931	
50	1	15.96	89.92	0.6390	0.6385	2.5409	2.5560
50	2	15.98	90.16	0.6381		2.5710	
70	1	22.43	90.28	0.8944	0.8910	2.9877	3.0005
70	2	22.20	90.04	0.8876		3.0133	
90	1	27.71	90.04	1.108	1.107	3.3562	3.3253
90	2	27.71	90.12	1.107		3.2943	
110	1	34.04	90.12	1.360	1.347	3.4110	3.4393
110	2	33.45	90.24	1.334		3.4675	

Neat ABS, 0.15 Nozzle, Nozzle Location							
Screw Speed (RPM)	Trial #	Mass of Extrudate (g)	Time (s)	Mass Flow Rate (kg/hr)	Average Mass Flow Rate (kg/hr)	Average Pressure (MPa)	Average Pressure for Each RPM (Mpa)
30	1	9.640	90.12	0.3851	0.3847	1.4376	1.2949
30	2	9.630	90.20	0.3844		1.1522	
50	1	15.73	90.00	0.6292	0.6312	1.3388	1.2999
50	2	15.83	90.00	0.6332		1.2609	
70	1	21.91	90.00	0.8764	0.8782	1.4489	1.4425
70	2	22.03	90.12	0.8800		1.4361	
90	1	28.04	90.00	1.122	1.124	1.5684	1.5655
90	2	28.17	90.00	1.127		1.5625	
110	1	34.07	90.04	1.362	1.366	1.6944	1.6845
110	2	34.26	90.04	1.370		1.6746	

Neat ABS, 0.2 Nozzle, Nozzle Location							
Screw Speed (RPM)	Trial #	Mass of Extrudate (g)	Time (s)	Mass Flow Rate (kg/hr)	Average Mass Flow Rate (kg/hr)	Average Pressure (MPa)	Average Pressure for Each RPM (Mpa)
30	1	8.740	90.84	0.3464	0.3555	0.19410	0.20530
30	2	9.140	90.24	0.3646		0.21650	
50	1	15.31	90.20	0.6110	0.6099	0.36400	0.37015
50	2	15.41	91.12	0.6088		0.37630	
70	1	21.50	90.12	0.8589	0.8604	0.49960	0.49395
70	2	21.46	89.64	0.8619		0.48830	
90	1	27.47	90.28	1.095	1.096	0.58230	0.57790
90	2	27.53	90.40	1.096		0.57350	
110	1	33.54	90.44	1.335	1.342	0.65040	0.65305
110	2	33.76	90.16	1.348		0.65570	

Neat ABS, 0.25 Nozzle, Nozzle Location							
Screw Speed (RPM)	Trial #	Mass of Extrudate (g)	Time (s)	Mass Flow Rate (kg/hr)	Average Mass Flow Rate (kg/hr)	Average Pressure (MPa)	Average Pressure for Each RPM (Mpa)
30	1	9.660	90.40	0.3847	0.3865	0.29000	0.25315
30	2	9.790	90.76	0.3883		0.21630	
50	1	15.56	90.64	0.6180	0.6235	0.27430	0.26660
50	2	15.72	89.96	0.6291		0.25890	
70	1	21.83	90.48	0.8686	0.8688	0.33140	0.32900
70	2	21.91	90.76	0.8691		0.32660	
90	1	27.90	90.64	1.108	1.109	0.39580	0.39400
90	2	27.87	90.48	1.109		0.39220	
110	1	33.92	90.52	1.349	1.358	0.45430	0.45380
110	2	34.15	89.96	1.367		0.45330	

20% CF ABS, 0.1 Nozzle, Nozzle Location							
Screw Speed (RPM)	Trial #	Mass of Extrudate (g)	Time (s)	Mass Flow Rate (kg/hr)	Average Mass Flow Rate (kg/hr)	Average Pressure (MPa)	Average Pressure for Each RPM (Mpa)
30	1	10.18	90.04	0.4070	0.4096	2.7892	2.7204
30	2	10.35	90.40	0.4122		2.6515	
50	1	16.85	90.32	0.6716	0.6720	3.0377	3.0064
50	2	16.90	90.48	0.6724		2.9751	
70	1	23.33	90.24	0.9308	0.9314	3.2962	3.2899
70	2	23.27	89.88	0.9320		3.2836	
90	1	29.90	90.00	1.196	1.195	3.5102	3.5169
90	2	30.02	90.44	1.195		3.5235	
110	1	36.46	90.48	1.451	1.449	3.6986	3.6954
110	2	36.26	90.20	1.447		3.6921	

20% CF ABS, 0.15 Nozzle, Nozzle Location							
Screw Speed (RPM)	Trial #	Mass of Extrudate (g)	Time (s)	Mass Flow Rate (kg/hr)	Average Mass Flow Rate (kg/hr)	Average Pressure (MPa)	Average Pressure for Each RPM (Mpa)
30	1	10.51	90.04	0.4202	0.4210	0.89440	0.90130
30	2	10.54	89.96	0.4218		0.90820	
50	1	17.05	90.44	0.6787	0.6848	1.2223	1.2226
50	2	17.32	90.24	0.6910		1.2229	
70	1	23.62	90.16	0.9431	0.9439	1.4182	1.4124
70	2	23.67	90.20	0.9447		1.4065	
90	1	30.88	89.88	1.237	1.223	1.5441	1.5400
90	2	30.82	91.80	1.209		1.5359	
110	1	37.46	90.92	1.483	1.483	1.6992	1.6970
110	2	37.39	90.84	1.482		1.6947	

20% CF ABS, 0.2 Nozzle, Nozzle Location							
Screw Speed (RPM)	Trial #	Mass of Extrudate (g)	Time (s)	Mass Flow Rate (kg/hr)	Average Mass Flow Rate (kg/hr)	Average Pressure (MPa)	Average Pressure for Each RPM (Mpa)
30	1	10.37	89.84	0.4155	0.4158	0.29900	0.29990
30	2	10.39	89.88	0.4162		0.30080	
50	1	17.06	89.76	0.6842	0.6845	0.46610	0.46830
50	2	17.09	89.84	0.6848		0.47050	
70	1	23.75	89.88	0.9513	0.9501	0.60070	0.59790
70	2	23.67	89.80	0.9489		0.59510	
90	1	31.17	89.84	1.249	1.230	0.70630	0.70230
90	2	30.23	89.80	1.212		0.69830	
110	1	37.32	90.32	1.488	1.486	0.78440	0.78520
110	2	37.05	89.88	1.484		0.78600	

20% CF ABS, 0.25 Nozzle, Nozzle Location							
Screw Speed (RPM)	Trial #	Mass of Extrudate (g)	Time (s)	Mass Flow Rate (kg/hr)	Average Mass Flow Rate (kg/hr)	Average Pressure (MPa)	Average Pressure for Each RPM (Mpa)
30	1	10.46	89.52	0.4206	0.4229	0.22340	0.21490
30	2	10.59	89.68	0.4251		0.20640	
50	1	17.24	90.12	0.6887	0.6883	0.29470	0.29350
50	2	17.19	89.96	0.6879		0.29230	
70	1	23.79	89.88	0.9529	0.9523	0.37590	0.37495
70	2	23.74	89.80	0.9517		0.37400	
90	1	30.28	89.76	1.214	1.220	0.45350	0.45275
90	2	30.59	89.80	1.226		0.45200	
110	1	36.94	90.12	1.476	1.476	0.52130	0.51440
110	2	36.92	90.00	1.477		0.50750	

Vita

Jake Dvorak obtained his bachelor's degree in Mechanical Engineering from the University of Tennessee in 2017. He continued to do graduate work by becoming a graduate research assistant under Dr. Chad Duty and a graduate teaching assistant under Dr. Matthew Young. While working his teaching assistantship in the MABE Maker Lab he conducted research for Dr. Duty and the Manufacturing Demonstration Facility. Jake will be continuing graduate work to obtain his PhD under Dr. Tony Schmitz doing machining research and improving the University of Tennessee's machining capability and presence.